A Comprehensive Comparison of Contemporary Parameterized Model Order Reduction Techniques

by

Md Rafiul Hossain, B.Sc., M.Sc.

A thesis submitted to the Faculty of Graduate and Postdoctoral Affairs in partial fulfillment of the requirements for the degree of

Master of Applied Science

in

Electrical Engineering

Ottawa-Carleton Institute for Electrical Engineering
Department of Electronics
Carleton University
Ottawa, Ontario

Abstract

In current state-of-art complex designs, interconnects become the dominant factor affecting the performance of high speed integrated circuits. Signal integrity issues at high frequencies demand a reasonable consideration during early stages of the design cycle. The evaluation of performance of such interconnects often requires solutions to large sets of equations, the computation of which is CPU expensive. The need to improve the computational cost of large systems of equations brought about the development of model order reduction (MOR) techniques. However, MOR techniques by themselves do not consider process and parameter variations that cause inevitable changes in performance at high frequencies. To deal with such performance-accuracy issues, parameterized model order reduction (PMOR) models were introduced. However, there is no significant comparative study of these methods available till today in the literature. In this thesis, a comprehensive comparative analysis is presented for contemporary PMOR techniques considering the detail characteristics of each method.

Acknowledgements

It is a pleasure to express my gratitude to the people who provided support and encouragement for fulfilling the purpose of this thesis and made it enjoyable. In particular, I would like to convey my sincere thanks to my thesis supervisor Professor Pavan Gunupudi for his valuable time of many hours to discuss about the subject matter of this thesis and providing valuable suggestions to complete it. Without his invaluable insight, useful feedback and guided motivation, the completion of this thesis would be very difficult. Professor Gunupudi has been more that a mentor during this work and I will be always in his debt. I would also like to thank my colleagues, especially Behzad Nouri and Mina Farhan for sharing their in depth knowledge and providing me useful information and help at the time of necessity. I also appreciate my family for the contribution that helped me to dedicate my time for this work. The staffs of the Department of Electronics were helpful at the time of necessity and I convey my sincere thanks to them.

Contents

Abstract *ii*

Acknowledgement *iii*

List of Tables and Listings *vi*

List of Figures *vii*

Notations *ix*

Abbreviations *x*

1 Introduction **1**

1.1 Background and Motivation 1

1.2 Contributions 3

1.3 Organization of the Thesis 4

2 Role of Model Order Reduction in Circuit Simulation **5**

2.1 Modified Nodal Analysis 6

2.2 Interconnect Models 8

2.2.1 Lumped Models 8

2.2.2 Distributed Models 9

2.2.3 Full-wave Models 12

2.3 Model Order Reduction Algorithms 14

2.4 Explicit Moment Matching Technique 18

2.5 Implicit Moment Matching Technique 20

2.5.1 Relationship Between Poles and Eigenvalues 21

2.5.2 Computation of Leading Eigenvalues 22

2.5.3 Krylov Subspace Method for Computation of Eigenvalues 23

2.5.4 Arnoldi's Algorithm for Model Order Reduction 24

3 Parameterized Model Order Reduction 29

3.1 Multiparameter Moment Matching Based PMOR Method 29

3.2 SPARE PMOR Method 34

3.3 Leguerre-SVD Based PMOR Method 44

3.3.1 Formulation of the PEEC Method 45

3.3.2 The MNA for the PEEC 48

3.3.3 PMOR Algorithm 50

3.4 Optimization Based PMOR Method 53

3.4.1 Formulation of Fully Parameterized Response 53

3.4.2 Recursive Least Square Based Fully PMOR 55

4 Comparison of Parameterized Model Order Reduction Techniques 60

4.1 Criteria for PMOR Efficiency Evaluation 61

4.2 Leguerre-SVD Based PMOR Method 63

4.3 Optimization based PMOR Method 71

4.4 Multiparameter Moment-Matching PMOR Method 79

4.5 SPARE PMOR Method 86

4.6 Comparison Between Different Methods 92

4.7 Recommendations for Users of PMOR Techniques 95

5 Conclusions and Future Works 96

5.1 Conclusions 96

5.2 Future work 96

Bibliography 98

List of Tables and Listings

Table 4.1	Summary of results for Leguerre-SVD based PMOR method	71
Table 4.2	Summary of results for Optimization based PMOR method	77
Table 4.3	Summary of results for MMM based PMOR method	86
Table 4.4	Summary of results for SPARE PMOR method	92
Table 4.5	The selected criteria and the results obtained for different PMOR methods	93

Listing 3.1	Algorithm for MMM based PMOR method	34
Listing 3.2	Algorithm for SPARE PMOR method	43
Listing 3.3	Algorithm for projection matrix of Optimization based PMOR method	51
Listing 3.4	Algorithm for Optimization based PMOR method	56
Listing 3.5	Algorithm for computation of Vk	58
Listing 3.6	Complete algorithm for Optimization based PMOR method	59

List of Figures

Figure 2.1	Nonlinear network containing linear subnetwork	6
Figure 2.2	Variation in interconnect models with frequency	7
Figure 2.3	Lumped and distributed models (C_{wire} represents distributed capacitances)	8
Figure 2.4	A simple transmission line	10
Figure 2.5	Multiconductor discretized per unit length equivalent circuit	11
Figure 2.6	(a) Poles of the system (b) Time domain response	15
Figure 3.1	Parameterized system representation	41
Figure 3.2	PEEC electrical quantities for a conductor elementary cell	47
Figure 3.3	A simple scheme of design space	50
Figure 3.4	Block diagram of fully parameterized LTI system	54
Figure 3.5	Discretization in 2-D parameter space	58
Figure 4.1	Cross section of microstrip transmission line	64
Figure 4.2	Responses of microstrip transmission line (Laguerre-SVD method)	65
Figure 4.3	Relative errors of the responses (Laguerre-SVD method)	66
Figure 4.4	Cross section of coupled transmission lines	67
Figure 4.5	Responses of coupled transmission lines (Laguerre-SVD method)	67
Figure 4.6	Relative errors of the responses (Laguerre-SVD method)	68
Figure 4.7	Transmission lines with an arbitrary configuration	69
Figure 4.8	Responses of the system (Laguerre-SVD method)	69
Figure 4.9	Relative errors of the responses (Laguerre-SVD method)	70
Figure 4.10	Responses of the system (Optimization based method)	72

Figure 4.11	Relative errors of the responses (optimization based method)	73
Figure 4.12	Poles of the system (Optimization based method)	74
Figure 4.13	Responses of the system (Optimization based method)	75
Figure 4.14	Relative errors of the responses (Optimization based method)	75
Figure 4.15	Poles of the system (Optimization based method)	76
Figure 4.16	Responses of the system (Optimization based method)	77
Figure 4.17	Relative errors of the responses (Optimization based method)	78
Figure 4.18	Poles of the system (Optimization based method)	78
Figure 4.19	Responses of the system (MMM based method)	80
Figure 4.20	Relative errors of the responses (MMM based method)	81
Figure 4.21	Poles of the system (MMM based method)	81
Figure 4.22	Responses of the system (MMM based method)	82
Figure 4.23	Relative errors of the responses (MMM based method)	83
Figure 4.24	Poles of the system (MMM based method)	84
Figure 4.25	Responses of the system (MMM based method)	84
Figure 4.26	Relative errors of the responses (MMM based method)	85
Figure 4.27	Poles of the system (MMM based method)	86
Figure 4.28	Responses of the system (SPARE method)	87
Figure 4.29	Relative errors of the responses (SPARE method)	88
Figure 4.30	Responses of the system (SPARE method)	89
Figure 4.31	Relative errors of the responses (SPARE method)	89
Figure 4.32	Responses of the system (SPARE method)	90
Figure 4.33	Relative errors of the responses (SPARE method)	91

Notations

$\boldsymbol{A}$	Matrix $\boldsymbol{A}$
$\boldsymbol{A}^T$	Matrix $\boldsymbol{A}$ transpose
$\boldsymbol{A}^*$	Complex conjugate of Matrix $\boldsymbol{A}$
$\mathbb{R}^N$	The set of real vectors of size N
$\mathbb{R}^{N\times N}$	The set of real matrices of size $N \times N$
$\mathbb{C}^{N\times N}$	The set of complex matrices of size $N \times N$
$\boldsymbol{I}$	Identity matrix
$\boldsymbol{H_u}$	Upper-Hessenberg Matrix
$\boldsymbol{x}_\alpha$	Vector of unknown in MNA formulation of network α, as defined in equation (2.1)
$\boldsymbol{F}(\boldsymbol{x}_\alpha)$	Vector of nonlinear elements of network α, as defined in equation (2.1)
$\boldsymbol{b}_\alpha$	Source vector of network α, as defined in equation (2.1)
N_α	Total number of variables in MNA formulation of network α as in equation (2.1)
$\boldsymbol{Y}_\beta$	Y-parameter matrix of subnetwork β, as defined in equation (2.2)
$\boldsymbol{V}_\beta$	Vector of terminal voltage nodes that connect subnetwork β to network α, as defined in equation (2.2)
$\boldsymbol{I}_\beta$	Vector of currents subnetwork β, as defined in equation (2.2)
$\boldsymbol{Z}$	Transmission line per unit length impedance matrix as defined in equation (2.10)
$\boldsymbol{Y}$	Transmission line per unit length admittance matrix as defined in equation (2.10)

Abbreviations

AWE	Asymptomatic waveform evaluation
CFH	Complex frequency hopping
CPU	Central processing unit
SI	Signal integrity
IC	Integrated circuit
PCB	Printed circuit board
KCL	Kirchhoff's current law
KVL	Kirchhoff's voltage law
MNA	Modified nodal analysis
LU	Lower/upper triangular decomposition
MOR	Model order reduction
PMOR	Parameterized Model order reduction
RLC	Resistor-inductor-capacitor network
TEM	Transverse electromagnetic
PEEC	Partial element equivalent circuit
SVD	Singular value decomposition
RLS	Recursive least square
MMT	Moment matching technique
L-SVD	Leguerre-SVD parameterized MOR technique
MMM	Multi-parameter moment matching
CORE	Compact Order Reduction
SPARE	A scalable algorithm for passive, structure preserving, parameter-aware model order reduction
EFIE	Electric field integral equation
PMTBR	Poor man's truncated balanced reduction

Chapter 1

INTRODUCTION

1.1 Background and Motivation

According to Moore's law, the number of transistors in a dense integrated circuit (IC) doubles approximately in every 18 months. This large number of transistors results in reduction in feature sizes of integrated circuits and increase in operating frequencies. Such reduction, however, introduces many signal integrity (SI) issues, such as crosstalk, ringing, ground bounce, distortion, signal loss, and power supply noise that are not significant problems at lower frequencies. These adverse effects were previously ignored in circuit analyses performed at relatively low frequencies. At higher frequencies (typically greater than 100 MHz), SI analysis becomes an important activity at all levels of electronics packaging and assembly, from internal connections of an IC, through the package, the printed circuit board (PCB), the backplane, and inter-system connections. Although continuous scaling reduces the feature sizes, gate-delays and interconnect cross sections, it also drastically increases interconnect delays. Wire delays have become comparable or even greater than gate delays when feature sizes get below 0.25 μm. As such, interconnect delays have to be accurately predicted to achieve timing closure. In addition, crosstalk has become an important consideration for digital design in nanometer technologies at 0.13 μm and below. Therefore, SI related issues demand comprehensive analysis of interconnects. SI issues are discussed with greater detail in Chapter 2.

As complexity grows, interconnects need to be modeled using infinitesimal length of elements for proper analysis. This leads to large sets of equations, the simulation of which is

computationally expensive. Moreover, the models used to capture the behavior of interconnects that is generally predictable only through 3-D analysis, such as partial element equivalent circuit (PEEC), give rise to even larger sets of equations. In order to overcome the computational cost of solving a large set of equations, model order reduction (MOR) techniques have been introduced. MOR techniques utilize a set of numerical methods, which replace large order original systems with much lower order reduced models that can retain the electrical behavior of the original systems accurately. Such models can be used very efficiently for large systems where the desired degree of performance-accuracy can be achieved with much less computational cost. Examples of MOR methods that are available in the literature are: asymptotic waveform evaluation (AWE) [1], matrix Padé via Lanczos (MPVL) [2], symmetric Padé via Lanczos (syMPVL) [3], block Arnoldi [4], complex frequency hopping (CFH) [5], passive reduced order interconnect macromodeling (PRIMA) [6], Leguerre-SVD reduced order modeling [7]. Although there are significant differences in the implementations of these models, most of these algorithms use efficient subspace projection techniques to obtain a low order rational approximation of the system transfer function. It is essential that the process of reduction retain important characteristics of the original system, such as response and passivity. The theory behind MOR techniques is discussed in detail in Chapter 2.

There are several situations in the design-cycle, such as optimization and Monte Carlo analysis, where predicting the response of SI models for varying design/process parameters is crucial. Traditional MOR models are usually generated for a particular set of design/process parameters and if the response of the model has to be found for a different set of parameters a new model has to be developed. This makes the traditional MOR techniques inefficient, especially when the response of the system is sought for variations of parameters. In order to address this issue, parameterized model order reduction (PMOR) techniques [7]-[10] have been

introduced in the literature. While initial attempts to develop the parameterized models were based on perturbation techniques [11], later methods involved the use of projection based MOR techniques. These techniques can be broadly classified into two categories: multidimensional moment matching techniques, where the projection matrix is built by selecting orthogonal moments of the multidimensional transfer function and sample-based techniques, where the projection matrix is generated from the samples in the multidimensional space.

Most of the earliest PMOR methods, however, concentrate only on handling small variations of the process and design parameters and are suitable particularly for simple interconnects such as bus system and clock tree, whose parameterized responses can be easily captured by increasing the orders of the projection matrices by a few degrees than that of MOR techniques. On the other hand, attempts are continuously made to develop PMOR methods for more complex applications, especially in the field of digital and analog ICs. Although continuous improvements are taking place in this field, PMOR techniques that work for a broad variety of applications are not common yet. All techniques have their merits and demerits. One method may work well for one application while the other may be well-suited for another application. An in-depth comparison of different PMOR methods that have been proposed is not available till today in the literature. In this work, a comprehensive analysis of some widely known PMOR techniques is carried out by establishing a set of criteria to compare the existing PMOR algorithms and measuring them up against the set criteria.

1.2 Contributions

The overall contributions of this thesis can be summarized as follows:

- Establish the criteria to evaluate different PMOR algorithms.

- Comprehensive analysis and comparison of contemporary PMOR methods against the specified criteria.
- Figure out the relative merits and demerits of the PMOR methods that were studied.
- Explore the possibility to improve some of the limitations of these methods.

1.3 Organization of the Thesis

This thesis is organized as follows: Chapter 2 describes SI issues related to high-speed systems and reviews common interconnect models used in SI analysis while highlighting the computational issues generated by the use of these interconnect models. In addition, Chapter 2 also reviews MOR techniques and their use in mitigating the computational expense of performing detailed SI analysis using accurate interconnect models. In Chapter 3, contemporary PMOR techniques are reviewed, which are later compared in this thesis. Chapter 4 establishes the criteria to compare various PMOR techniques. The information presented in this chapter is then used to compare the performance of contemporary PMOR techniques using typical examples. Chapter 5 presents conclusions and possible future work that can be taken up in this area relevant to the work presented in this thesis.

Chapter 2

ROLE OF MODEL ORDER REDUCTION IN CIRCUIT SIMULATION

The trends in VLSI technology to accomplish high speed and nano-scale designs and the continual increase of integration of analog blocks with digital circuits impose numerous signal integrity (SI) issues in the design cycles. It is now an established fact that interconnects are mainly responsible for major degradation of signals in high speed integrated circuits. Moreover, such SI issues, which are related to interconnect, encompass a wide area, such as on-chip, packaging, off-chip modules, PCB and backplanes. SI issues influencing signal propagation appear in various forms such as distortion, signal delay, attenuation, ringing, reflection, cross-talk, skin effect and edge effect. These combined effects may severely affect the performance of interconnects as well as the overall circuit. The decision on whether these distortion effects should be taken into consideration depends primarily on the length and the cross section of the interconnect, signal slew-rate and clock-speed. Other factors that may influence the decision are logic levels, dielectric material and conductor resistance. When the length and the cross section of interconnect become comparable to wavelength of the applied signal, SI issues may no longer be neglected. The developers of current state-of-art circuit simulator software are very concerned about these issues and researchers are investing continuous efforts to overcome such SI problems. It is very important that the designers use realistic models of interconnects in the circuits they analyze so that the results from the simulation of circuits can be sufficiently relied. It should be noted that consideration of SI issues should be done in the early stages of design so as to avoid expensive design iterations that could be detrimental to the successful

completion of design projects. Today, successful implementation of a project significantly depends on the efficient handling of signal integrity problems mainly arising from interconnects.

2.1 Modified Nodal Analysis

The established way to formulate circuit equations for interconnects is to use the modified nodal analysis (MNA). Modified nodal analysis is an extension of classical nodal analysis, which utilizes branch currents in addition to node voltages in order to solve electrical systems. To understand the MNA formulation in the presence of interconnects, consider a general network α consisting of arbitrary number of linear and nonlinear elements. The network contains both lumped and distributed components. For simplicity, the linear components are grouped into a separate linear subnetwork β as shown in Figure 2.1. The MNA of the network can be written as given in [12]

$$\boldsymbol{C}_\alpha \dot{\boldsymbol{x}}_\alpha(t) + \boldsymbol{G}_\alpha \boldsymbol{x}_\alpha(t) + \boldsymbol{L}_\beta \boldsymbol{i}_\beta(t) + \boldsymbol{F}\big(\boldsymbol{x}_\alpha(t)\big) = \boldsymbol{b}_\alpha(t); \qquad t \in [0, T] \tag{2.1}$$

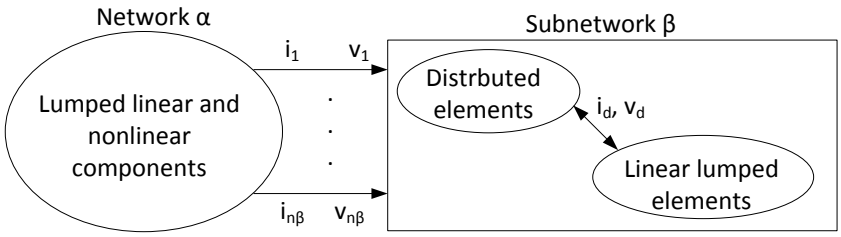

Figure 2.1: Nonlinear network containing linear subnetwork

where

- $C \in \mathbb{R}^{N_\alpha \times N_\alpha}$ and $G \in \mathbb{R}^{N_\alpha \times N_\alpha}$ are constant matrices representing lumped memory and memoryless elements of network α respectively,
- $\boldsymbol{x}_\alpha(t) \in \mathbb{R}^{N_\alpha}$ is a vector of node voltages appended by voltage source currents, linear inductor currents, nonlinear capacitor charges and nonlinear inductor fluxes,

- $\boldsymbol{L}_\alpha = [l_{i,j}]$ is a matrix with elements $l_{i,j} \in \{0, 1\}$ where $i \in \{0, \dots, N_\alpha\}$ and $j \in \{0, \dots, n_\beta\}$ with a maximum of one nonzero in each row or column, that maps $\boldsymbol{i}_\beta(t) \in \mathbb{R}^{N_\beta}$the vector of currents entering the network β, into the node space $\mathbb{R}^{N_\alpha}$ of the network α,
- $\boldsymbol{F}(\boldsymbol{x}_\alpha)$ is a function describing the nonlinear elements of the network α,
- $\boldsymbol{b}_\alpha \in \mathbb{R}^{N_\alpha}$ is a constant vector comprises of independent voltage and current sources,
- N_α is the total number of variables which include node voltages, voltage source currents and inductor currents and n_β is the total number of ports in network β.

The linear multiterminal subnetwork β can be characterized in the frequency domain by its terminal behavior as given by [12]

$$\boldsymbol{Y}_\beta(s)\boldsymbol{V}_\beta(s) = \boldsymbol{I}_\beta(s) \tag{2.2}$$

where $\boldsymbol{Y}_\beta(s)$ is the y-parameter matrix of subnetwork β, $\boldsymbol{V}_\beta(s)$ is the vector of terminal voltage nodes that connects the subnetwork β to network α and $\boldsymbol{I}_\beta(s)$ is the Laplace transform of $\boldsymbol{i}_\beta(t)$. The circuit characteristics given by (2.2) are influenced by the techniques chosen to model interconnects. Few of the commonly used interconnect models are reviewed in the following section.

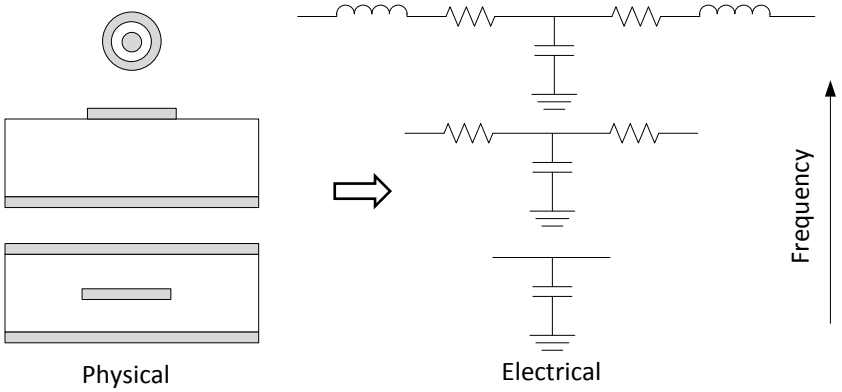

Figure 2.2: Variation in interconnect models with frequency

2.2 Interconnect Models

In current designs, different types of interconnects are used, such as striplines, microstrip lines and cables, commonly known as transmission lines. In a circuit simulator, an electrical model is required to model the behavior of interconnects. Such models should be a function of the physical properties of interconnects, such as the width of the line or the thickness of the dielectric. In addition, the nature and complexity of these models grow with the increase of the operating frequency. Figure 2.2 shows the variations of transmission line models with increasing frequency. Some of the commonly used transmission line models are reviewed below.

2.2.1 Lumped Models

For low frequency applications, interconnects are modeled using lumped RC or RLC models. Selection of lumped models can be influenced by signal integrity issues under consideration. For example, if it is necessary to incorporate the ringing effect in interconnects analysis, RLC model can be a preferable choice. Lumped RC components are usually extracted for each node of the circuit during place and route analysis of the VLSI design flow. Therefore, the layout containing a large number of nodes may make the simulation highly CPU intensive [12]. This implies that RC models work well for moderate size circuits but not a good choice for relatively large circuits. Figure 2.3 shows a simple lumped representation of a transmission line.

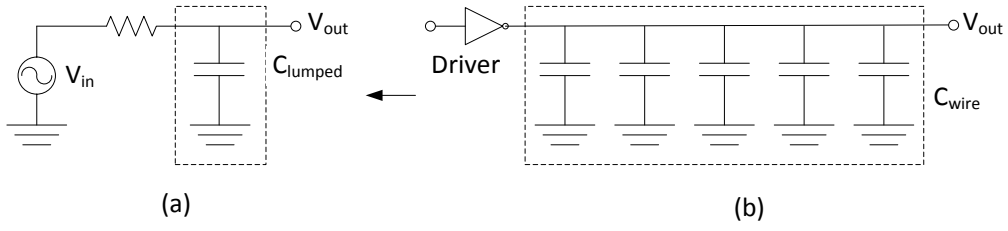

Figure 2.3: Lumped and distributed models (C_{wire} represents distributed capacitances)

2.2.2 Distributed Models

At high frequencies, the electrical length of the interconnect becomes a significant fraction of the operating wavelength. This introduces distortion effects that do not exist at low frequencies. Conventional lumped models become incapable to handle these effects and transmission lines models utilizing quasi-transverse electromagnetic mode (TEM) assumptions are required. In such case, the solution of Maxwell's equations can be obtained by assuming a quasi-TEM mode and are characterized by per unit length distributed *RLGC* parameters. A quasi-TEM mode is derived from the ideal TEM mode with an appropriate approximation that both the *E* and *H* fields are only present in the direction perpendicular to the direction of propagation. This approximation, however, is valid only if the cross section of the transmission line is much smaller than the wavelength of the applied signal. However, the inhomogeneous nature of practical interconnects gives rise to *E* and *H* fields in the direction of propagation and quasi-TEM mode may not be applicable [12].

On the contrary, at higher frequencies, this assumption is not valid because the current distribution along the cross section of the conducting line is not uniform with the variation of frequency. The current distribution has more density at the outer surface of the conductor than the center of the conductor. This is due to the Eddy current effect. The non-uniform current distribution effects are categorized into three types, namely skin effect, edge effect and proximity effect. These effects may affect the per unit parameters significantly as the frequency increases beyond certain limit. Therefore, when the performance of an application is affected much by these undesirable phenomena then models with frequency dependent parameters need to be considered [12]. Transmission line characteristics associated with such models are described by Telegrapher's equations.

Consider a simple single conductor transmission line as shown in Figure 2.4. To derive the Telegrapher's equations, we need to discretize the transmission lines into infinitesimal sections of length Δl. Assume that the total length of the line is d and the per unit length parameters of transmission line are resistance R, capacitance C, conductance G and inductance L. Therefore, the resistance, capacitance, conductance and inductance of each section are given by $R\Delta l$, $C\Delta l$, $G\Delta l$ and $L\Delta l$, respectively.

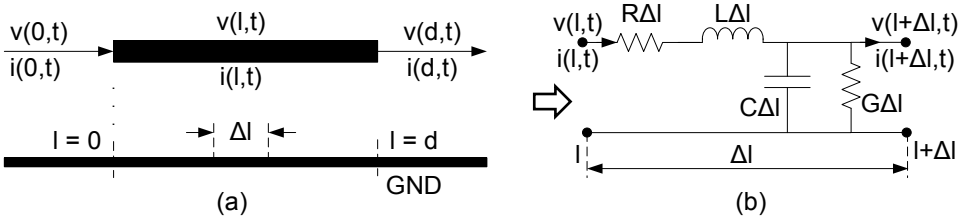

Figure 2.4: A simple transmission line

If t represents the time of propagation then using KVL and KCL into each segment of the single conductor transmission line of Figure 2.4 results in [12]

$$\frac{\partial}{\partial l}v(l,t) = -Ri(l,t) - L\frac{\partial}{\partial t}i(l,t) \tag{2.3}$$

$$\frac{\partial}{\partial l}i(l,t) = -Gv(l,t) - C\frac{\partial}{\partial t}v(l,t) \tag{2.4}$$

Taking Laplace transformation of (2.3) and (2.4) results in [12]

$$\frac{\partial}{\partial l}V(l,s) = -(R+sL)I(l,s) = -ZI(l,s) \tag{2.5}$$

$$\frac{\partial}{\partial l}I(l,s) = -(G+sC)V(l,s) = -YV(l,s) \tag{2.6}$$

where Z represents the p.u.l. series impedance and Y represents the p.u.l. parallel admittance and they are given by

$$Z = R + sL,\ Y = G + sC \tag{2.7}$$

Equations (2.3) and (2.4) are known as Telegrapher's equations in time domain and equations (2.5) and (2.6) are the corresponding frequency domain representations.

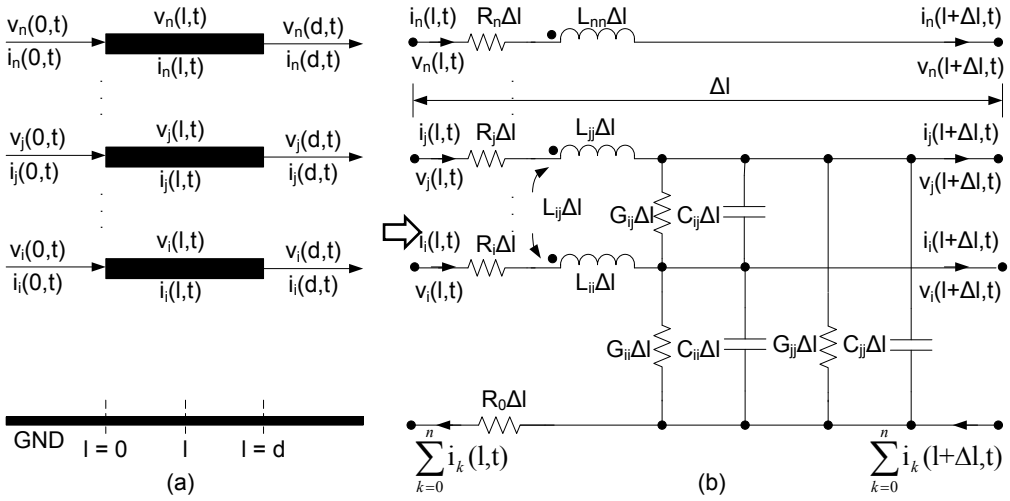

Figure 2.5: Multiconductor discretized per unit length equivalent circuit

Figure 2.5 shows the detailed discretized per unit length equivalent circuit for the derivation of multiconductor transmission line equations. By using the same concept of the single conductor transmission line, (2.5) - (2.7) can be modified for the case of multiconductor transmission lines as

$$\frac{\partial}{\partial l}\boldsymbol{V}(l,s) = -\boldsymbol{ZI}(l,s) \tag{2.8}$$

$$\frac{\partial}{\partial l}\boldsymbol{I}(l,s) = -\boldsymbol{YV}(l,s) \tag{2.9}$$

$$\boldsymbol{Z} = \boldsymbol{R} + s\boldsymbol{L},\ \boldsymbol{Y} = \boldsymbol{G} + s\boldsymbol{C} \tag{2.10}$$

The ***RLGC*** matrices can be determined by a 2-D solution of Maxwell's equations at appropriate positions along the direction of propagation. Such a solution can be obtained by using

techniques based on quasi-static or full-wave analysis depending on the nature and geometry of the structure and the desired degree of accuracy. The derivation of a multiconductor transmission line stamp can be found in [12].

However, simulation of large interconnect networks based on the concept of MNA has some drawbacks [12]. The chief problem known as the mixed time/frequency problem involves the fact that the Telegrapher's equations describing the distributed interconnects are partial differential equations and the equations governing other circuit components especially nonlinear components are described using ordinary differential equations [14]. This poses a major difficulty in simulating high frequency circuits that include distributed models of interconnects. The concurrent formulation of such equations is difficult to analyze using a traditional ordinary differential equation solver, such as SPICE [15].

2.2.3 Full-wave Models

As the operating frequency extends into gigahertz range, the cross sections of interconnects approach the same order of the wavelength of operation. In such a case, an interconnect block should be treated as a dispersive structure and the field components in the direction of propagation should not be neglected. The two 2-D models of interconnects, as described above, suffer from spatial EM effects and become inadequate. Only full-wave 3-D models can accurately describe the performance of interconnects by considering all possible field components and satisfying all boundary conditions. As mentioned earlier, the original EM solution is very expensive in terms of CPU cost. As an alternate solution, some researchers proposed the use of the partial element equivalent circuit (PEEC) model [16]. The PEEC method converts EM equations of a system into the corresponding circuit equations so that it can be simulated by computationally cheap circuit simulators like SPICE instead of using

computationally expensive 3-D EM solvers. In the PEEC model, individual R, L, C components are extracted from the geometry of the structures using a quasi-static solution of Maxwell's equations. The PEEC model taking retardation into consideration is called rPEEC [17]. Both these models provide full-wave solution with lower CPU cost than its counterpart i.e., the full-wave EM solution.

Another major bottleneck of the MNA based solution of large interconnects is computational cost. The general format of the MNA and the corresponding output equation for a lumped linear network of any size in time domain can be given as [12]

$$\begin{aligned} \boldsymbol{C}\dot{\boldsymbol{x}}(t) + \boldsymbol{G}\boldsymbol{x}(t) &= \boldsymbol{B}\boldsymbol{u}(t) \\ \boldsymbol{y}(t) &= \boldsymbol{L}^T\boldsymbol{x}(t) \end{aligned} \tag{2.11}$$

And the corresponding equations in frequency domain are given as

$$\begin{aligned} (\boldsymbol{G} + s\boldsymbol{C})X(s) &= \boldsymbol{B}\boldsymbol{U}(s) \\ \boldsymbol{Y}(s) &= \boldsymbol{L}^T\boldsymbol{X}(s) \end{aligned} \tag{2.12}$$

where

- $\boldsymbol{C} \in \mathbb{R}^{N\times N}$ and $\boldsymbol{G} \in \mathbb{R}^{N\times N}$ are constant matrices representing lumped memory and memoryless elements of the network respectively
- $\boldsymbol{B} \in \mathbb{R}^{N\times n}$ and $\boldsymbol{L} \in \mathbb{R}^{N\times n}$ are selector matrices
- N is the total number of variables which include node voltages, voltage source currents and inductor currents and n is the total number of ports

The solutions of large linear networks such as that of interconnect networks can be obtained by solving (2.11) and (2.12). However, this requires LU decompositions and forward and backward substitutions at each frequency point of the operating range of frequency.

Computational cost increases as the complexity of interconnects increases. On the other hand, for time domain analysis, different numerical integration techniques are used to convert a set of differential equations in time domain into a set of difference equations in the same domain. The solutions of such difference equations often require iterative processes, which may involve several LU decompositions. This makes the computational cost of time-domain analysis expensive. Therefore, simulation algorithms must address these problems to perform high performance analysis in terms of accuracy and CPU cost. Extensive research was undertaken for several decades to resolve interconnect issues as the speed and features of an IC evolve with time. Several algorithms were developed to address these simulation issues and they can be broadly categorized into two groups [12]: macromodel based approaches like "method of characteristics" and model order reduction (MOR) based techniques, such as AWE [1], complex frequency hopping (CFH) [5], PRIMA [6], Laguerre-SVD [18]. Furthermore, MOR techniques were extended for parametric analysis especially at high frequencies. These techniques are known as parameterized model order reduction (PMOR) techniques.

2.3 Model Order Reduction Algorithms

In general, interconnect networks contain a large number of poles which are spread over a wide frequency range. The high number of poles significantly affects the computational cost because the simulator needs to handle large equations. The poles near the imaginary axis have a significant effect on the system response and are called dominant poles, whereas the distant poles from the same axis, in general, have little effect and they are known as insignificant poles. This is valid for both time domain and frequency domain analysis. By utilizing this characteristic of interconnects, it is possible to reduce the CPU cost by retaining only the required dominant poles and ignoring the large number of insignificant poles to improve performance of the circuit simulator. Moment matching techniques (MMT) [19]-[24] were introduced to capitalize this

characteristic of interconnects. To demonstrate this fact, consider a simple system, as shown in Figure 2.6. It can be seen from this figure that the dominant pole P_1 has a significant effect on the total transient response, while the distant pole P_2 has an almost negligible effect. Therefore, the pole P_2 can be eliminated during the process of finding the response of this system. However, this reduction of poles always comes at the cost of accuracy and the reduction of the poles is limited by the desired level of accuracy. The moment matching technique and its underlying mathematics related to the poles of the system is explained below.

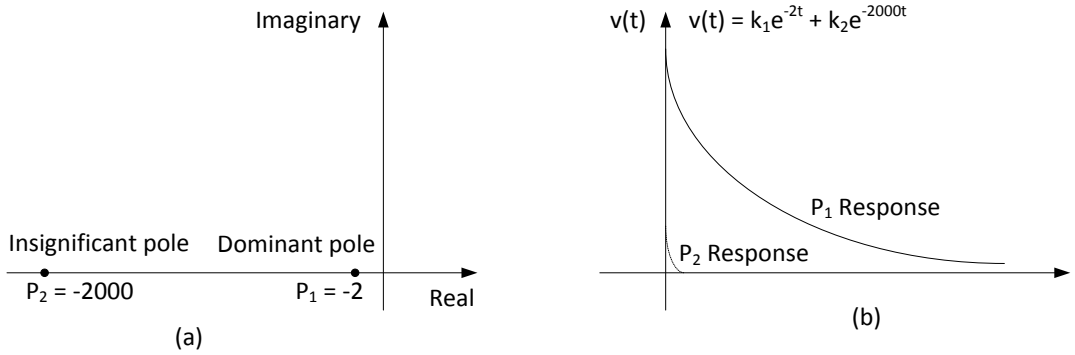

Figure 2.6: (a) Poles of the system (b) Time domain response

For simplicity, consider a simple system with a single input *u(t)* and a single output *y(t)*. The transfer function *H(s)* of the system in frequency domain can be expressed as a rational function

$$H(s) = \frac{Y(s)}{U(s)} = \frac{P(s)}{Q(s)} \tag{2.13}$$

where *P(s)* and *Q(s)* are polynomials. This can be equivalently represented by pole-residue pairs as [12]

$$H(s) = c + \sum_{i=1}^{n} \frac{k_i}{s - p_i} \tag{2.14}$$

where n is the total number of poles and p_i and k_i are the *i-th* pole-residue pair and constant c represents the direct coupling. The time domain impulse response can be obtained by taking the inverse Laplace transformation of (2.14) as [12]

$$h(t) = c\delta t + \sum_{i=1}^{n} k_i e^{p_i t} \tag{2.15}$$

Equation (2.14) provides an indication of computational cost of a system response. For a large network like interconnects, the total number of poles may easily reach the order of thousands. The computational cost may become significant even for a small system if all the poles are taken into consideration. On the other hand, for a complex interconnect system, such computational cost becomes impractical. A possible practical solution can be obtained by reducing the number of poles. This is how the concept of model order reduction (MOR) originates, which extracts only the required dominant poles, while eliminating the insignificant poles. Consider a MOR technique that requires only m dominant poles where $m << n$. Then the reduced order approximate transfer function in frequency domain $\widehat{H}(s)$ can be given as [12]

$$H(s) \approx \widehat{H}(s) = \frac{\hat{P}(s)}{\hat{Q}(s)} = \hat{c} + \sum_{i=1}^{m} \frac{\hat{k}_i}{s - \hat{p}_i} \tag{2.16}$$

And the corresponding reduced order in time domain is given by [12]

$$\hat{h}(t) = \hat{c}\delta t + \sum_{i=1}^{m} \hat{k}_i e^{\hat{p}_i t} \tag{2.17}$$

It is necessary to find a method to extract the required dominant poles from a system. An easy way to solve this problem is using Taylor series expansion. If the transfer function can be expanded as a Taylor series then the first specific number of terms that can provide the desired response can be used as the criterion to determine the required order. Therefore, their effects can be considered to be equivalent to the effects of the dominant poles. The Taylor series expansion of the transfer function *H(s)* around an expansion point *s = 0* can be given as

$$H(s) \approx \widehat{H}(s) = H(0) + \frac{s}{1!} H(0)^{(1)} + \frac{s^2}{2!} H(0)^{(2)} + \quad \ldots. \quad + \frac{s^q}{q!} H(0)^{(q)} \quad (2.18)$$

where the subscript *(q)* denotes the *q-th* derivative of the transfer function *H(0)*. This can be further simplified using simpler notation as

$$H(s) \approx \widehat{H}(s) = m_0 + m_1 s + m_2 s^2 + \quad \ldots. \quad + m_q s^q \quad (2.19)$$

$$= \sum_{i=1}^{q} s^i m_i, \qquad where, m_i = \frac{H(0)^{(i)}}{i!} \quad (2.20)$$

The coefficients m_i are identical to the time domain moments of the impulse response of the system. This is shown below

$$\begin{aligned} H(s) &= \int_0^\infty h(t) e^{-st} dt \\ &= \int_0^\infty h(t) \left[1 - st + \frac{s^2 t^2}{2!} - \ \ldots \ \right] dt \\ &= \int_0^\infty h(t) dt + s \int_0^\infty (-1) t h(t) dt + s^2 \int_0^\infty \frac{t^2}{2!} h(t) dt + \cdots \\ &= \sum_0^\infty s^i \left[\frac{(-1)^i}{i!} \int_0^\infty t^i h(t) dt \right] \end{aligned} \quad (2.21)$$

Because of this analogy, the coefficients m_i are also referred to as moments of the system. Therefore, the effects of dominant poles are related to the moments of the system. Furthermore, moments can be used to estimate the delay and the rise time associated with the response [25], [26]. The Elmore delay [25] matches only the first moment of the response which is the most basic form of approximation. However, in order to model interconnects with sufficient degree of accuracy it is necessary to match or preserve as many moments as required. Many algorithms have been developed in an effort to reduce the order of interconnect models. These algorithms can be broadly divided into two categories: Explicit moment matching techniques [19], [27], [28], which are less efficient and Implicit moment matching techniques

[2]-[6], which are proven to be more efficient. These techniques are briefly described in the following section.

2.4 Explicit Moment Matching Technique

Explicit moment matching techniques utilize Padé approximation to extract the dominant poles and residues of a given system. The transfer function $H(s)$ can be approximated by a rational function to obtain a reduced order transfer function $\widehat{H}(s)$

$$H(s) \approx \widehat{H}(s) = \frac{P_M(s)}{Q_N(s)} = \frac{a_0+a_1s+a_2s^2+\cdots+a_Ms^M}{1+b_1s+b_2s^2+\cdots+b_Ns^N} \tag{2.22}$$

where a_0, a_1, … a_M and b_0, b_1, … b_N are the unknown coefficients. In order to relate with the moments, the above rational function is equated to the corresponding Taylor series expansion

$$\frac{a_0+a_1s+a_2s^2+\cdots+a_Ms^M}{1+b_1s+b_2s^2+\cdots+b_Ns^N} = m_0 + m_1s + m_2s^2 + \quad \ldots. \quad + m_{M+N}s^{M+N} \tag{2.23}$$

Such moment matching technique is also known as Padé approximation. Using cross multiplication and equating the coefficients of similar powers of s from s^{M+1} to s^{M+N} on both sides, the coefficients of the denominator polynomial can be represented as matrix form as given below [12]

$$\begin{bmatrix} m_{M-N+1} & m_{M-N+2} & \cdots & m_M \\ m_{M-N+2} & \cdots & \cdots & m_{M+1} \\ \cdots & \cdots & \cdots & \cdots \\ m_M & m_{M+1} & \cdots & m_{M+N-1} \end{bmatrix} \begin{bmatrix} b_M \\ b_{M-1} \\ \cdots \\ b_1 \end{bmatrix} = - \begin{bmatrix} m_{M+1} \\ m_{M+2} \\ \cdots \\ m_{M+N} \end{bmatrix} \tag{2.24}$$

The coefficients of the numerator polynomial can be obtained by equating the power of s from s^0 to s^M on both sides and can be given as [12]

$$a_0 = m_0$$

$$a_1 = m_1 + b_0 m_0$$

…

$$a_1 = m_M + \sum_{i=1}^{\min(M,N)} b_i m_{M-1} \tag{2.25}$$

Therefore, if the moments of the system are known then an approximate transfer function in terms of rational polynomials can be obtained. Shown below is the method used to obtain the moments of the circuit. These moments are obtained from the time domain system representation as mentioned in (2.11) which is repeated below for convenience

$$\boldsymbol{C}\dot{\boldsymbol{x}}(t) + \boldsymbol{G}\boldsymbol{x}(t) = \boldsymbol{B}\boldsymbol{u}(t)$$

$$\boldsymbol{y}(t) = \boldsymbol{L}^T\boldsymbol{x}(t)$$

where $\boldsymbol{C}, \boldsymbol{G} \in \mathbb{R}^{n \times n}$ and $\boldsymbol{B}, \boldsymbol{L}, \boldsymbol{x} \in \mathbb{R}^n$, and *n* represents the total number of MNA variables associated with the given system. Pre-multiplying both sides of first equation of (2.11) by $\mathbf{G}^{-1}$ results in

$$\boldsymbol{G}^{-1}\boldsymbol{C}\dot{\boldsymbol{x}}(t) + \boldsymbol{x}(t) = \boldsymbol{G}^{-1}\boldsymbol{B}\boldsymbol{u}(t)$$

Let, $\boldsymbol{A} = -\boldsymbol{G}^{-1}\boldsymbol{C}$ and $\boldsymbol{R} = \boldsymbol{G}^{-1}\boldsymbol{B}$, then

$$\boldsymbol{A}\dot{\boldsymbol{x}}(t) = \boldsymbol{x}(t) - \boldsymbol{R}\boldsymbol{u}(t) \tag{2.26}$$

Taking Laplace transformation of (2.26) and second equation of (2.11) results in

$$s\boldsymbol{A}\boldsymbol{X}(s) = \boldsymbol{X}(s) - \boldsymbol{R}U(s) \tag{2.27}$$

$$Y(s) = \boldsymbol{L}^T\boldsymbol{X}(s) \tag{2.28}$$

Replacing ***X(s)*** from (2.27) in (2.28), the transfer function can be expressed as

$$H(s) = \frac{Y(s)}{U(s)} = \boldsymbol{L}^T(\boldsymbol{I} - s\boldsymbol{A})^{-1}\boldsymbol{R} \tag{2.29}$$

where $\boldsymbol{I}$ is an identity matrix of size *n* by *n*. Using the expansion of $(\boldsymbol{I} - s\boldsymbol{A})^{-1}$ results in

$$\begin{aligned} H(s) &= \boldsymbol{L}^T(\boldsymbol{I} + s\boldsymbol{A} + s^2\boldsymbol{A}^2 + \quad \dots \quad + s^q\boldsymbol{A}^q)^{-1}\boldsymbol{R} \\ &= \sum_{i=1}^{q} s^i\left(\boldsymbol{L}^T\boldsymbol{A}^i\boldsymbol{R}\right) \\ &= \sum_{i=1}^{q} s^i m_i; \qquad\qquad m_i = \boldsymbol{L}^T\boldsymbol{A}^i\boldsymbol{R} \end{aligned} \tag{2.30}$$

It may seem that by increasing the order of Padé rational approximation we would obtain a better solution as more moments are being included. But in practice, Padé approximation cannot produce better results when increasing the number of moments [6], [25]. Such a limitation of the Padé approximation can also be explained from (2.30). Note that the moments $m_i = \boldsymbol{L}^T\boldsymbol{A}^i\boldsymbol{R}$ are a function of $\boldsymbol{A}^i$. When the value of *i* is increased, the moments quickly converge to an eigenvector corresponding to the largest eigenvalue of $\boldsymbol{A}$. As a result, beyond a certain order the moments m_i cannot provide any further useful information; rather all these moments contain the information related with the largest eigenvalue. This fact makes the moment matrix prone to ill-conditioning. In addition, explicit moment techniques do not guarantee passivity of the reduced model. Therefore, interconnect circuits might be unstable even though they are only made of passive elements. In the following section techniques to overcome these problems are discussed.

2.5 Implicit Moment Matching Technique

Implicit moment matching techniques utilize the dominant eigenvalues of the system instead of dominant poles to obtain the reduced order model. This implies that there must be some relationship between poles and eigenvalues of the system. This relationship is established in the following subsection.

2.5.1 Relationship between Poles and Eigenvalues

Consider a matrix ***A*** represented by the following expression

$$\boldsymbol{A} = \boldsymbol{P}\lambda\boldsymbol{P}^{-1} \tag{2.31}$$

where ***P*** is a matrix that contains the eigenvectors of matrix ***A*** and λ is a diagonal matrix given as $\lambda = diag\,[\lambda_1\ \lambda_2\,\lambda_3\ \ldots.\ \lambda_q]$. By replacing ***A*** in (2.29), the transfer function can be expressed as

$$\begin{aligned} H(s) &= \boldsymbol{L}^T(\boldsymbol{I} - s\boldsymbol{P}\lambda\boldsymbol{P}^{-1})^{-1}\boldsymbol{R} \\ &= \boldsymbol{L}^T\boldsymbol{P}(\boldsymbol{I} - s\lambda)^{-1}\boldsymbol{P}^{-1}\boldsymbol{R} \\ &= \boldsymbol{L}^T\boldsymbol{P}\begin{bmatrix} \frac{\mathbf{1}}{\mathbf{1}-s\boldsymbol{\lambda_1}} & & \\ & \cdots & \\ & & \frac{\mathbf{1}}{\mathbf{1}-s\boldsymbol{\lambda_q}} \end{bmatrix}\boldsymbol{P}^{-1}\boldsymbol{R} \end{aligned} \tag{2.32}$$

After simplification, the transfer function takes the following form [12]

$$H(s) = \sum_i \frac{\eta_i}{1-s\lambda_i} = \sum_i \frac{-(\eta_i/\lambda_i)}{s-(1/\lambda_i)} = \sum_i \frac{k_i}{s-p_i} \tag{2.33}$$

where η is a function of the eigenvectors of matrix ***A*** and k and p represent the residues and poles, respectively. This demonstrates that the poles are reciprocals of the eigenvalues of matrix ***A***. Also note that the largest eigenvalues corresponds to the poles closer to the origin. Therefore, the transfer function can be evaluated in terms of the eigenvalues of matrix ***A*** where $\boldsymbol{A} = -\boldsymbol{G}^{-1}\boldsymbol{C}$. However, like the poles of a high speed complex interconnect, the computation of all eigenvalues of a matrix ***A*** becomes very expensive. In order to reduce the computational cost, a minimum number of leading eigenvalues need to be extracted so as to preserve the response of the system. The technique to calculate leading eigenvalues of a system is discussed below.

2.5.2 Computation of Leading Eigenvalues

The most common method to find out leading eigenvalues of a system is to approximate ***A*** with a reduced order matrix $\widehat{\boldsymbol{A}}$ such that the eigenvalues of $\widehat{\boldsymbol{A}}$ are an approximation of the leading eigenvalues of ***A*** and at the same time it can provide sufficient degree of accuracy [12]. Before presenting the technique to find out such eigenvalues, the orthogonal matrix is defined first as it is related with this method. A real matrix ***Q*** is orthogonal when it satisfies the following condition

$$\boldsymbol{Q}^T\boldsymbol{Q} = \boldsymbol{I} \tag{2.34}$$

where ***I*** is an identity matrix. This implies that if q_i and q_j represent the *i-th* and *j-th* columns of the matrix ***Q*** then for each column *I*, we have $\|q_i\|_2 = 1$ and $q_i{}^T q_j = 0$. If ***Q*** is a square matrix then $\boldsymbol{Q}^{-1} = \boldsymbol{Q}^T$. Two common methods used to find out the orthogonal matrix are given below.

QR decomposition: Suppose, ***K*** $\in R^{m\times n}$ where *m* > *n*. If ***K*** has full column rank then there exist a unique orthogonal matrix ***Q*** $\in R^{m\times n}$ and a unique upper triangular matrix ***R*** $\in R^{n\times n}$ with positive diagonals ($r_{ii} > 0$) such that ***K*** = ***QR***. The modified Gram-Schmidt method utilizes the QR decomposition to find the orthogonal matrix.

Upper-Hessenberg Matrix: A matrix ***H*** is called Upper-Hessenberg if $H_{ij} = 0$ for $i > (j + 1)$. Therefore, an Upper-Hessenberg matrix of order *n* can be represented as follows [12]

$$\boldsymbol{H}_u = \begin{bmatrix} 0 & 0 & 0 & \dots & 0 & -c_1 \\ 1 & & & \dots & & -c_2 \\ 0 & 1 & & \dots & & \dots \\ 0 & 0 & 1 & \dots & & \dots \\ \dots & \dots & \dots & \dots & \dots & \dots \\ 0 & 0 & 0 & \dots & 1 & -c_n \end{bmatrix} \tag{2.35}$$

The main advantage of such companion matrix is that its characteristic polynomial $\rho(x)$ can be analytically computed easily and given by [12]

$$\rho(x) = x^n + \sum_{i=1}^{n} c_i x^{i-1} \tag{2.36}$$

The eigenvalues of $\boldsymbol{H}_u$ are the roots of the characteristic polynomial $\rho(x)$. Consider the circuit equation (2.26) and a simple similarity transformation as given below [12]

$$\boldsymbol{AK} = \boldsymbol{KH}_u \tag{2.37}$$

where ***K*** is a transformation matrix and it is defined as [12]

$$\boldsymbol{K} = [\boldsymbol{R}\ \boldsymbol{AR}\ \boldsymbol{A}^2\boldsymbol{R}\quad \ldots\quad \boldsymbol{A}^{q-1}\boldsymbol{R}] \tag{2.38}$$

As $\boldsymbol{H}_u$ is related to ***A*** through a similarity transformation, the eigenvalues of ***A*** will be same of those of $\boldsymbol{H}_u$. Therefore, computation of eigenvalues is relatively easy using this method. However, there are some limitations of this method. Computation of $\boldsymbol{H}_u$ using (2.37) requires the evaluation of inverse of matrix ***K***. As ***K*** is a dense matrix, calculation of inverse of this matrix is rather expensive. Moreover, columns of ***K*** are prone to ill-conditioned as they are function of $\boldsymbol{A}^n$, which is explained before. Solution to such problem can be acquired by using Krylov subspace techniques, which is discuss below.

2.5.3 Krylov Subspace Method for Computation of Eigenvalues

Consider an orthogonal matrix ***Q***, which is related to a transformation matrix ***K*** in such that the leading *n* number of columns of ***K*** and ***Q*** span the same space. Such a space is called Krylov subspace of order *n* and is denoted by $\kappa(\boldsymbol{A}, \boldsymbol{R},\ n)$. So, it implies that any vector that is a linear combination of the leading *n* columns of ***K*** can be also expressed as a linear combination of *n* columns of ***Q***. Hence mathematically it can be represented as [12]

$$\kappa(\boldsymbol{A}, \boldsymbol{R},\ n) = column\ space([\boldsymbol{R}\ \boldsymbol{AR}\ \boldsymbol{A}^2\boldsymbol{R}\ \ \ldots\ \ \boldsymbol{A}^{n-1}\boldsymbol{R}]) = column\ space(\boldsymbol{Q}) \tag{2.39}$$

Therefore, one can compute as many leading columns of $\boldsymbol{Q}$ as needed to obtain sufficient degree of accuracy of the performance of a system. The advantage of such orthogonal matrix lies in the fact that it overcomes all the limitations of $\boldsymbol{K}$. Matrix $\boldsymbol{Q}$ is well conditioned and also $\boldsymbol{Q}$ is easily invertible as $\boldsymbol{Q}^{-1} = \boldsymbol{Q}^T$.

The next step is to find out the way to calculate matrix $\boldsymbol{Q}$. It can be easily determined by replacing $\boldsymbol{K}$ in the following equation by $\boldsymbol{QR}$ as in QR decomposition and relating $\boldsymbol{Q}$ with the upper Hessenberg matrix as shown below. From (2.37), we can write [12]

$$\boldsymbol{H}_u = \boldsymbol{K}^{-1}\boldsymbol{AK} = (\boldsymbol{QR})^{-1}\boldsymbol{A}(\boldsymbol{QR}) = \left(\boldsymbol{R}^{-1}\boldsymbol{Q}^T\right)\boldsymbol{A}(\boldsymbol{QR}) \tag{2.40}$$

or

$$\boldsymbol{Q}^T\boldsymbol{AQ} = \boldsymbol{RH}_u\boldsymbol{R}^{-1} = \boldsymbol{H} \tag{2.41}$$

From (2.41), it is found that the new matrix $\boldsymbol{H}$ is also an upper Hessenberg matrix. If first q columns of $\boldsymbol{Q}$ are taken into consideration, such that $q < n$, then $\boldsymbol{Q} \in \mathbb{R}^{n \times q}$ and $\boldsymbol{H} \in \mathbb{R}^{q \times q}$ while $\boldsymbol{A} \in \mathbb{R}^{n \times n}$. This implies that the matrix $\boldsymbol{A}$ of dimension $n \times n$ can be reduced into a matrix $\boldsymbol{H}$ with dimension $q \times q$ by applying orthogonal transformation. Also, the eigenvalues of the smaller system $\boldsymbol{H}$ represent the first q eigenvalues of the larger system $\boldsymbol{A}$. This is how Krylov subspace plays an important role in model order reduction. A popular Krylov subspace based MOR is known as Arnoldi's algorithm [5][6]. This algorithm is discussed in the following subsection.

2.5.4 Arnoldi's Algorithm for Model Order Reduction

Consider an orthogonal matrix $\boldsymbol{Q} = [\boldsymbol{q}_1\ \boldsymbol{q}_2\ \boldsymbol{q}_3 \ldots\ \boldsymbol{q}_m]$, where $\boldsymbol{q}_m$ is the *m-th* column vector. From (2.41), we can write [12]

$$\boldsymbol{AQ} = \boldsymbol{Q}\begin{bmatrix} h_{11} & h_{12} & h_{13} & \cdots & \cdots \\ h_{21} & h_{22} & h_{23} & \cdots & \cdots \\ 0 & h_{32} & h_{33} & \cdots & \cdots \\ \cdots & \cdots & \cdots & \cdots & \cdots \\ \cdots & \cdots & \cdots & \cdots & \cdots \end{bmatrix} \tag{2.42}$$

Using the properties of orthogonal matrix and equating both sides of (2.42), one can find out the column vectors of $\boldsymbol{Q}$. By applying the properties of orthogonal matrix, the following calculation can be made

$$\|\boldsymbol{q}_1\|_2 = 1 \; or, \boldsymbol{q}_1^T\boldsymbol{q}_1 = 1$$

or

$$\boldsymbol{q}_1 = \frac{\boldsymbol{R}}{\|\boldsymbol{R}\|_2} \tag{2.43}$$

Equating the first column of LHS and RHS of (2.43) results in

$$\boldsymbol{A}\boldsymbol{q}_1 = h_{11}\boldsymbol{q}_1 + h_{21}\boldsymbol{q}_2 \tag{2.44}$$

Pre-multiplying both side of (2.44) by $\boldsymbol{q}_1^T$ gives

$$h_{11} = \boldsymbol{q}_1^T\boldsymbol{A}\boldsymbol{q}_1 \tag{2.45}$$

Using $\|\boldsymbol{q}_2\|_2 = 1$ gives the following result

$$h_{21} = \|\boldsymbol{A}\boldsymbol{q}_1 - h_{11}\boldsymbol{q}_1\| \tag{2.46}$$

From (2.46) one can find out next column vector $\boldsymbol{q}_2$ as

$$\boldsymbol{q}_2 = \frac{\boldsymbol{A}\boldsymbol{q}_1 - h_{11}\boldsymbol{q}_1}{h_{21}} \tag{2.47}$$

The remaining column vectors of $\boldsymbol{Q}$ can be calculated in a similar fashion. The pseudo code for this algorithm is given in [12]. The advantage of Arnoldi's algorithm relies on the fact that it doesn't require evaluating of $\boldsymbol{A}^i\boldsymbol{R}$, which eliminates the possibility of ill-conditioned matrix.

There are some other alternative methods to find out the orthogonal basis of Krylov subspace [29]. Orthogonal matrix $\boldsymbol{Q}$, as obtained from Arnoldi's algorithm, can be used to map state vectors $\boldsymbol{x}$ of a system of order *n* into a smaller state vector $\hat{\boldsymbol{x}}$ of a reduced system of order *q* where *q* << *n* [29]-[34]. This mapping can be done by the following relationship [12]

$$\boldsymbol{x} = \boldsymbol{Q}\hat{\boldsymbol{x}} \tag{2.48}$$

Using this relationship, (2.27) and (2.28) can be written as follows

$$s\boldsymbol{A}\boldsymbol{Q}\hat{\boldsymbol{X}}(s) = \boldsymbol{Q}\hat{\boldsymbol{X}}(s) - \boldsymbol{R}U(s) \tag{2.49}$$

$$Y(s) = \boldsymbol{L}^T\boldsymbol{Q}\hat{\boldsymbol{X}}(s) \tag{2.50}$$

Pre-multiplying both sides of (2.49) by $\boldsymbol{Q}^T$ and substituting $\boldsymbol{Q}^T\boldsymbol{Q}$ by an identity matrix $\boldsymbol{I}$ of the same order results in

$$s\boldsymbol{Q}^T\boldsymbol{A}\boldsymbol{Q}\hat{\boldsymbol{X}}(s) = \boldsymbol{Q}^T\boldsymbol{Q}\hat{\boldsymbol{X}}(s) - \boldsymbol{Q}^T\boldsymbol{R}U(s)$$

or

$$\hat{\boldsymbol{X}}(s) = (\boldsymbol{I} - s\boldsymbol{Q}^T\boldsymbol{A}\boldsymbol{Q})^{-1}\boldsymbol{Q}^T\boldsymbol{R}U(s) \tag{2.51}$$

Replacing $\hat{\boldsymbol{X}}(s)$ in (2.50) gives

$$Y(s) = \boldsymbol{L}^T\boldsymbol{Q}(\boldsymbol{I} - s\boldsymbol{Q}^T\boldsymbol{A}\boldsymbol{Q})^{-1}\boldsymbol{Q}^T\boldsymbol{R}U(s)$$

The transfer function of the reduced system can be written as

$$\hat{H}(s) = \frac{Y(s)}{U(s)} = \boldsymbol{L}^T\boldsymbol{Q}(\boldsymbol{I} - s\boldsymbol{H})^{-1}\boldsymbol{Q}^T\boldsymbol{R} \tag{2.52}$$

where $\boldsymbol{H} = \boldsymbol{Q}^T\boldsymbol{A}\boldsymbol{Q}$. If one compares the original system transfer function $H(s)$ given in (2.29) with the reduced system transfer function $\hat{H}(s)$ as in (2.52), it is found that the eigenvalues of $\hat{H}(s)$ come from the eigenvalues of $\boldsymbol{H}$, which corresponds to the approximate leading eigenvalues of $\boldsymbol{A}$ of the original system. Eigenvalues of $\boldsymbol{A}$ in turn are related to the poles of the

original system. However, the accuracy of the reduced system depends on how well the reduced system can preserve the desired moments of the original system. It is shown in literature that a reduced order system of order *q* can preserve first *q* moments of the original system. However, the classical Arnoldi's algorithm cannot guarantee passivity of the reduced system. But if one can use the congruence transformation in conjunction with Arnoldi's algorithm, it is possible to obtain a passive reduced order system under certain conditions [6]. The congruence transformation reduces ***C*** and ***G*** matrices directly in order to obtain the reduced transfer function as discussed below.

Rewriting the original system given in (2.11) for *N* ports system

$$\boldsymbol{C}\dot{\boldsymbol{x}}(t) + \boldsymbol{G}\boldsymbol{x}(t) = \boldsymbol{B}\boldsymbol{u}(t)$$

$$\boldsymbol{y}(t) = \boldsymbol{L}^T\boldsymbol{x}(t)$$

where the dimension is defined as $\boldsymbol{B}, \boldsymbol{L} \in \mathbb{R}^{n\times N}$ instead of $\boldsymbol{B}, \boldsymbol{L} \in \mathbb{R}^{n\times 1}$. Using $\boldsymbol{x} = \boldsymbol{Q}\hat{\boldsymbol{x}}$ in the above equations and taking Laplace transformation result in

$$s\boldsymbol{C}\boldsymbol{Q}\hat{\boldsymbol{X}}(s) + \boldsymbol{G}\boldsymbol{Q}\hat{\boldsymbol{X}}(s) = \boldsymbol{B}\boldsymbol{U}(s) \tag{2.53}$$

$$\boldsymbol{Y}(s) = \boldsymbol{L}^T\boldsymbol{Q}\hat{\boldsymbol{X}}(s) \tag{2.54}$$

Pre-multiplying both sides of (2.53) by $\boldsymbol{Q}^T$

$$s\boldsymbol{Q}^T\boldsymbol{C}\boldsymbol{Q}\hat{\boldsymbol{X}}(s) + \boldsymbol{Q}^T\boldsymbol{G}\boldsymbol{Q}\hat{\boldsymbol{X}}(s) = \boldsymbol{Q}^T\boldsymbol{B}\boldsymbol{U}(s) \tag{2.55}$$

Let $\hat{\boldsymbol{C}} = \boldsymbol{Q}^T\boldsymbol{C}\boldsymbol{Q}$, $\hat{\boldsymbol{G}} = \boldsymbol{Q}^T\boldsymbol{G}\boldsymbol{Q}$, $\hat{\boldsymbol{B}} = \boldsymbol{Q}^T\boldsymbol{B}$ and $\hat{\boldsymbol{L}} = \boldsymbol{Q}^T\boldsymbol{L}$. Then (2.55) can be written as

$$\hat{\boldsymbol{X}}(s) = \left(\hat{\boldsymbol{G}} + s\hat{\boldsymbol{C}}\right)^{-1}\hat{\boldsymbol{B}}\boldsymbol{U}(s) \tag{2.56}$$

Replacing (2.56) into (2.54) gives

$$\widehat{\boldsymbol{Y}}(s) = \widehat{\boldsymbol{L}}^T\left(\widehat{\boldsymbol{G}} + s\widehat{\boldsymbol{C}}\right)^{-1}\widehat{\boldsymbol{B}}\boldsymbol{U}(s) \tag{2.57}$$

The transfer function of the reduced system can be written as

$$\widehat{\boldsymbol{H}}(s) = \widehat{\boldsymbol{L}}^T\left(\widehat{\boldsymbol{G}} + s\widehat{\boldsymbol{C}}\right)^{-1}\widehat{\boldsymbol{B}} \tag{2.58}$$

If the original ***C*** matrix is a symmetric and nonnegative definite matrix then it can be proved that the reduced order model given by (2.58) is passive. This MOR technique is commonly known as PRIMA [6]. Such condition can be achieved by modifying system matrices ***C***, ***G*** and ***x*** in the MNA formulation as given in [12]

$$\boldsymbol{C} = \begin{bmatrix} \boldsymbol{C}_a & 0 \\ 0 & \boldsymbol{C}_b \end{bmatrix},\ \boldsymbol{G} = \begin{bmatrix} \boldsymbol{F} & \boldsymbol{E} \\ -\boldsymbol{E}^T & \boldsymbol{0} \end{bmatrix},\ \boldsymbol{x} = \begin{bmatrix} \boldsymbol{v} \\ \boldsymbol{i} \end{bmatrix} \tag{2.59}$$

where the matrices $\boldsymbol{C}_a$, $\boldsymbol{C}_b$ and ***F*** contain stamps of capacitors, inductors and resistors respectively and matrix $\boldsymbol{E} \in (0, 1, -1)$ represents the current variables in a KCL formulation and ***v*** and ***i*** represent the MNA variables. Rows corresponding to the current variables are negated such that the diagonal entries of capacitor matrix contributed by inductor remain positive. $\boldsymbol{C}_a$, $\boldsymbol{C}_b$ and *F* lead to symmetric nonnegative definite matrices provided that the original system consists of passive elements. It can also be proven that the resulting ***C*** matrix in the above formulation is a symmetric nonnegative definite matrix [6].

Chapter 3

PAREMETERIZED MODEL ORDER REDUCTION

Process and geometrical variations at high operating frequencies can no longer be ignored to obtain high precision accurate models. In general, PMOR models are extended models derived from the ordinary MOR models. In such parameterized models, system responses or system descriptor matrices are functions of parameters that can show the variability in responses of systems with respect to changes in parameters. This reduces computationally expensive iterative processes of traditional MOR models in dealing with variation of parameters. Several PMOR models are available in literature that attempt to model large-scale parameterized systems. Initial attempts are based on perturbation [11][35] but the most effective methods are derived by extending projection based MOR algorithms [6][36] to deal with parametric variations. These projection based PMOR techniques can be categorized as: multidimensional moment matching techniques [8]-[10][37], where the projector matrix is built by selecting the orthonormalized moments of the multidimensional transfer function and sample-based techniques [7][38][39], where the projector matrix is generated from samples in the multidimensional space [10]. Each technique has its own advantages and limitations. Some contemporary PMOR techniques are discussed in detail in the following sections.

3.1 Multiparameter Moment Matching Based PMOR Method

PMOR techniques, based on multidimensional moment matching, are one of the earliest PMOR methods proposed in literature. Consider a linear system dependent on a single parameter as given below

$$E(\lambda)x = Bu$$

$$y = Cx \tag{3.1}$$

where *x* is a vector of the states and *u* and *y* are *m* dimensional input and output vector. *E* $\in \mathbb{R}^{n \times n}$ is a system descriptor matrix; *B* $\in \mathbb{R}^{n \times m}$ and *C* $\in \mathbb{R}^{m \times n}$ are matrices relating the input and output to the state vector *x*, respectively. The parameter is represented by λ. Using an orthogonal projection matrix *Q* $\in \mathbb{R}^{n \times q}$ *(q << n)*, the reduced system can be written as

$$[Q^T E(\lambda) Q]\hat{x} = Q^T Bu$$

$$y = CQ\hat{x} \tag{3.2}$$

where the reduced state vector $\hat{x}$ represents the projection of the original sate vector x**,** such that $x \approx Q\hat{x}$. The columns of Q are determined such that the moments of the final response of the reduced system which matches the first *q* terms of Taylor series expansion for the nominal values of the parameters. The reduced order system given by (3.2) doesn't represent a very efficient model because the explicit evaluation of $Q^T E(\lambda) Q$ requires n^2 operations if $E(\lambda)$ is a dense matrix, while it requires *nq* operations if $E(\lambda)$ is a sparse matrix [9]. In order to obtain a more efficient model one can consider using polynomial interpolation or Taylor series expansion to generate $E(\lambda)$ that can be represented by the following power series [9]

$$E(\lambda) = \sum_{i=0}^{\infty} \lambda^i E_i \tag{3.3}$$

A possible way of constructing the reduced order model is truncating the power series to an appropriate order of *p*. In addition, by introducing a new parameter, such as $\lambda_i = \lambda^i$, where *i = 1, 2, …. p,* the power series has only a linear dependency on the parameter as given below [9]

$$E(\lambda) \approx E_0 + \lambda_1 E_1 + \lambda_2 E_2 + \quad \ldots \quad + \lambda_p E_p \tag{3.4}$$

This equation can also be used for multiple parameters. However, in that case the dimension of the resulting reduced order can be very high. A more effective reduction method can be derived by converting (3.1) into a linear single parameter problem by introducing fictitious states [30]. In such a case, $\boldsymbol{E}(\lambda)$ is linearly dependent on λ and can be given as [9]

$$\left\{\begin{bmatrix} E_0 & & & \\ & I & & \\ & & I & \\ & & & \dots \end{bmatrix} - \lambda \begin{bmatrix} -E_1 & -E_2 & -E_3 & \dots \\ I & & & \\ & I & & \\ & & \dots & \dots \end{bmatrix}\right\} \times \begin{bmatrix} x \\ x_1 \\ x_2 \\ \dots \end{bmatrix} = \begin{bmatrix} B \\ 0 \\ 0 \\ \dots \end{bmatrix} \tag{3.5}$$

where the fictitious sates x_i satisfy the following relations

$$x_1 = \lambda x \quad x_2 = \lambda x_1 \quad x_3 = \lambda x_2 \quad \dots \tag{3.6}$$

The authors of [9] proved that x can be expressed in terms of λ as

$$x = \sum_{i=0}^{\infty} \lambda^i F^i \tag{3.7}$$

where

$$F^0 = E_0^{-1} B$$

$$F^i = -\sum_{j=0}^{i-1} E_0^{-1} E_{i-j} F^j, \qquad i > 0 \tag{3.8}$$

The authors of [9] also proved that the projection matrix Q of order q can be generated from the following relation

$$colspan\,(Q) \supseteq span\{F^0, F^1, \quad \dots \quad F^{q-1}\} \tag{3.9}$$

The reduced order model can be given by

$$\left(\sum_{i=0}^{p} Q^T E_i Q\, \lambda^i\right)\hat{x} = Q^T B u$$

$$y = CQ\hat{x} \tag{3.10}$$

The concept of single parameter reduced order model can be utilized in formulating a more general multiparameter model. Rewriting (3.1) as given below

$$E(\lambda_1, \lambda_2, \ \ldots \ \lambda_k)x = Bu$$
$$y = Cx \tag{3.11}$$

where $E(\lambda_1, \lambda_2, \ \ldots \ \lambda_k) \in \mathbb{R}^{n \times n}$ is a descriptor matrix and a function of *k* number of parameters. In practice, the descriptor matrix may have complex and nonlinear dependence on the given parameters. Such dependence can be represented as a power series as [9]

$$E(\lambda_1, \lambda_2, \ \ldots \ \lambda_k) = E_0 + \sum_i s_i E_{\boldsymbol{i}} + \sum_{j,k} s_j s_k E_{j,k} + \sum_{j,k,h} s_j s_k s_h E_{j,k,h} + \ \ldots \tag{3.12}$$

The easiest way to generate such a power series is to truncate Taylor series expansion as shown below [9]

$$E(\lambda_1, \lambda_2, \ \ldots \ \lambda_k) = E(\bar{\lambda}_1, \bar{\lambda}_1, \ \ldots \ \bar{\lambda}_k) + \sum_i \left(\frac{\Delta\lambda_i}{\bar{\lambda}_i}\right)\left[\bar{\lambda}_i \frac{\partial E}{\partial \lambda_i}(\bar{\lambda}_1, \bar{\lambda}_1, \ \ldots \ \bar{\lambda}_k)\right] +$$
$$\sum_{j,k} \left(\frac{\Delta\lambda_j}{\bar{\lambda}_j}\right)\left(\frac{\Delta\lambda_k}{\bar{\lambda}_k}\right)\left[\bar{\lambda}_j \bar{\lambda}_k \frac{\partial^2 E}{\partial \lambda_j \partial \lambda_k}(\bar{\lambda}_1, \bar{\lambda}_1, \ \ldots \ \bar{\lambda}_k)\right] + \tag{3.13}$$

where $\bar{\lambda}_1, \bar{\lambda}_2, \ \ldots \ \bar{\lambda}_k$ represent the expansion points that are generally extracted from the nominal values of the parameters. Also, instead of using the absolute variation $\Delta\lambda_i$, it is better to use the relative variation $\frac{\Delta\lambda_i}{\bar{\lambda}_i}$. The reduced order model can be generated by applying the congruence transformation in (3.12) [9]

$$\left[Q^T E_0 Q + \sum_i s_i Q^T E_i Q + \sum_{j,k} s_j s_k Q^T E_{j,k} Q + \sum_{j,k,h} s_j s_k s_h Q^T E_{j,k,h} Q + \cdots\right]\hat{x} = Q^T B u$$
$$y = CQ\hat{x} \tag{3.14}$$

Assuming $Q \in \mathbb{R}^{n \times q}$, a reduced order model of order *q* can be represented by (3.14), where *q* is much smaller than the size *n* of the original system.

In order to find a simplified way to obtain the columns of the projection matrix *Q*, a new set of parameters $\tilde{\lambda}_i$ and $\tilde{E}_i$ can be considered as given below [9]

$$\tilde{E}_i = \begin{cases} E_i & i = 0, 1, \quad \ldots. \quad p \\ E_{j,k} & j = 1, 2, \quad \ldots. \quad p;\ k = 1, 2 \quad \ldots. \quad p \\ E_{j,k,h} & j = 1, 2, \quad \ldots. \quad p;\ k = 1, 2 \quad \ldots. \quad p; h = 1, 2 \quad \ldots. \quad p \end{cases}$$

$$\tilde{\lambda}_i = \begin{cases} \lambda_i & i = 0, 1, \quad \ldots. \quad p \\ \lambda_{j,k} & j = 1, 2, \quad \ldots. \quad p;\ k = 1, 2 \quad \ldots. \quad p \\ \lambda_{j,k,h} & j = 1, 2, \quad \ldots. \quad p;\ k = 1, 2 \quad \ldots. \quad p; h = 1, 2 \quad \ldots. \quad p \end{cases} \tag{3.15}$$

Using the above representations the system of (3.11) can be rewritten as [9]

$$\left[\tilde{E}_0 + \tilde{\lambda}_1\tilde{E}_1 + \quad \ldots \quad + \tilde{\lambda}_p\tilde{E}_p\right]x = Bu$$

$$y = Cx \tag{3.16}$$

The corresponding reduced model is given by

$$\left[Q^T\tilde{E}_0Q + \tilde{\lambda}_1Q^T\tilde{E}_1Q + \quad \ldots \quad + \tilde{\lambda}_pQ^T\tilde{E}_pQ\right]\hat{x} = Q^TBu$$

$$y = CQ\hat{x} \tag{3.17}$$

If the power series is constructed using Taylor series, then (3.15) can be expressed as [9]

$$\tilde{E}_0 = E\left(\bar{\lambda}_1, \bar{\lambda}_1, \quad \ldots \quad \bar{\lambda}_k\right)$$

$$\tilde{E}_i = \begin{cases} \left[\bar{\lambda}_i \frac{\partial E}{\partial \lambda_i}\left(\bar{\lambda}_1, \bar{\lambda}_1, \quad \ldots \quad \bar{\lambda}_k\right)\right] & i = 0, 1, \quad \ldots. \quad p \\ \left[\bar{\lambda}_j\bar{\lambda}_k \frac{\partial^2 E}{\partial \lambda_j \partial \lambda_k}\left(\bar{\lambda}_1, \bar{\lambda}_1, \quad \ldots \quad \bar{\lambda}_k\right)\right] & j = 1, 2, \quad \ldots. \quad p;\ k = 1, 2 \quad \ldots. \quad p \\ \ldots \end{cases}$$

$$\tilde{\lambda}_i = \begin{cases} \left(\frac{\Delta\lambda_i}{\bar{\lambda}_i}\right) & i = 0, 1, \quad \ldots. \quad p \\ \left(\frac{\Delta\lambda_j}{\bar{\lambda}_j}\right)\left(\frac{\Delta\lambda_k}{\bar{\lambda}_k}\right) & j = 1, 2, \quad \ldots. \quad p;\ k = 1, 2 \quad \ldots. \quad p \\ \ldots \end{cases} \tag{3.18}$$

The column span of the projection matrix *Q* is derived in [9] as

$$colspan(Q) = span\{b_M,\ M_1 b_M,\ M_2 b_M, \dots\ ,\ M_p b_M, M_1^2 b_M, (M_1 M_2 + M_2 M_1) b_M, \dots\ ,$$

$$(M_1 M_2 + M_2 M_1) b_M, M_2^2 b_M, (M_2 M_3 + M_3 M_2) b_M,\ \dots\} \tag{3.19}$$

where

$$M_i = -\tilde{E}_0^{-1}\tilde{E}_i, \text{ for } \quad i = 1, 2, \qquad \dots . \quad p$$

$$B_M = \tilde{E}_0^{-1} B, \text{ for multiple inputs system} \tag{3.20}$$

$$b_M = B_M = \tilde{E}_0^{-1} b \in R^{n \times 1}, \text{ for a single input system}$$

As an alternative of Taylor series, a Chebyshev expansion can be used, especially for larger variation in parameters [9]. The algorithm for this method is presented in Listing 3.1.

Listing 3.1: Algorithm for MMM based PMOR method

1. From *C*, *G* and the nominal values of the parameters, find $\tilde{E}_0$, $\tilde{E}_i$ and $\tilde{\lambda}_i$.
2. Calculate M_i and B_M as given by (3.20).
3. Calculate the orthogonal matrix *Q* as given in (3.19).
4. Find the reduced form of $\tilde{E}_0$, $\tilde{E}_i$ and *B, L, x* as given in (3.17) and calculate the response.

3.2 SPARE PMOR Method

This method is a scalable, passive, structure preserving, parameter-aware model order reduction, which is commonly known as “SPARE”. This algorithm relies on the reformulation of parameterized system as a perturbation-like parallel interconnection of the nominal transfer function and the non-parameterized transfer function sensitivities with respect to the variations of the parameters [10]. The method utilizes an explicit dependence on each parameter, which is obtained by reducing each component system independently using a standard structure preserving algorithm. Therefore, the reduced system retains the structure of the original system, which plays an important role to improve system performance, such as better accuracy control and an independent adaptive order computation with respect to each parameter. In

addition, the method can be scaled efficiently with the change of the size of the system and it can preserve the passivity of the reduced system. The method is proven to be efficient for larger variation of the parameters provided that the output exhibits a smooth dependence on the parameters. However, a sharp transition in the output behavior may lead to deviation in the response of the system.

Consider a parameterized state-space representation of a system as given below

$$C(\lambda)\dot{x}(\lambda) + G(\lambda)x(\lambda) = Bu$$
$$y(\lambda) = Lx(\lambda) \tag{3.21}$$

where $C, G \in \mathbb{R}^{n \times n}$ are the dynamic and static system descriptor matrices, respectively, $B \in \mathbb{R}^{n \times m}$ relates the input vector $u \in \mathbb{R}^{m}$ to the state vector $x \in \mathbb{R}^{n}$, and $L \in \mathbb{R}^{p \times n}$ relates the states to the output vector $y \in \mathbb{R}^{p}$. The descriptor matrices *C* and *G*, and the state vector *x* depend on *k* number of parameters, such that $\lambda = [\lambda_1, \lambda_2, \dots, \lambda_k]$. It is assumed that *B* and *L* matrices are not functions of parameters. The transfer function of this system in the frequency domain can be given as

$$H(s, \lambda) = L[sC(\lambda) + G(\lambda)]^{-1}B \tag{3.22}$$

The corresponding transfer function of the reduced system can be written as

$$\hat{H}(s, \lambda) = \hat{L}\left[s\hat{C}(\lambda) + \hat{G}(\lambda)\right]^{-1}\hat{B} \tag{3.23}$$

The reduced order model exhibits similar parameter dependence as the original system. The most common way to incorporate such dependency with the reduced system is to use a projection scheme. Once the orthogonal basis of the subspace *Q* is computed, the congruence transformation can be used to obtain the reduced models as

$$\hat{C}(\lambda) = Q^T C(\lambda) Q \qquad \hat{G}(\lambda) = Q^T G(\lambda) Q \qquad x(\lambda) = Q\hat{x}(\lambda)$$

$$\hat{B}(\lambda) = Q^T B \qquad \hat{L}(\lambda) = LQ \tag{3.24}$$

The parameter dependent matrices $C(\lambda)$ and $G(\lambda)$ generally represent the discrete characterization of the physical system in terms of the electrical components. Taylor series representations of these matrices can be utilized for building a reduced order model as discussed in the previous method. In such a case, they can be represented by the following relations [10]

$$C(\lambda) = C_{0\ldots0} + \sum_{a_1 \ldots a_k} F_{a_1 \ldots a_k} C_{a_1 \ldots a_k}$$
$$G(\lambda) = G_{0\ldots0} + \sum_{a_1 \ldots a_k} F_{a_1 \ldots a_k} G_{a_1 \ldots a_k} \tag{3.25}$$

where $C_{0\ldots0}$ and $G_{0\ldots0}$ are the nominal values for matrices $C(\lambda)$ and $G(\lambda)$, respectively, $C_{a_1 \ldots a_k}$ and $G_{a_1 \ldots a_k}$ are their joint sensitivities of order $(a_1 \ldots a_k)$ with respect to k parameters and $F_{a_1 \ldots a_k} = \lambda^{a_1} \ldots \lambda^{a_k}$. Taylor series can be extended up to the required order, including the cross terms, in order to obtain sufficient accuracy. By replacing (3.25) into (3.21), it is possible to generate a state space Taylor series representation. Such representation has several advantages [10]. The most significant advantage is that the sensitivity analysis can be used to extract different matrix terms of this representation. Some examples of sensitivity analyses are given in [57] – [59]. Another important advantage is that a projection based reduction leads to a ROM of the same form as the state space Taylor series of the original system but the model uses smaller dimension matrices. The same ROM can be effectively used for different set of parameters because the parameters are explicitly represented. However, this method requires solving the system for each set of the parameter, which is a major drawback.

In general, PMOR techniques extend the moment matching techniques to the multidimensional case. As discussed in Chapter 2, either the explicit or the implicit moment matching techniques can be utilized for this purpose. However, in this case, the moment must be a function of frequency along with other parameters. Such multidimensional moments can be expressed as follows [10]

$$x(s,\lambda) = \sum_{a_s a_1 \dots a_k} s^{a_s} M_{a,a_s a_1 \dots a_k} F_{a_1 \dots a_k} \tag{3.26}$$

where $M_{a,a_s a_1 \dots a_k}$ is a *a-th* ($a = a_0 + a_1 + \dots + a_k$) order multiparameter moment corresponding to the coefficient of $s^{a_s} F_{a_1 \dots a_k}$. Using the concept of the nominal moment matching technique, the basis of the subspace *Q* can be found from the following relation [10]

$$colsapn(Q) = span(M_{0,00\dots0},\ \dots\ , M_{a,a_0 a_1 \dots a_k}) \tag{3.27}$$

The orthogonal basis *Q* can be used to obtain the reduced order model from the original system. The resulting PMOR model matches up to the *a-th* order multiparameter moment of the original system. Different techniques are available to generate the moments and find out the required number of matched moments [10]. One of the easiest ways is the technique discussed in the previous method that matches all the combinations up to a certain order [9]. Some improved methods use low-rank approximation, while the other methods use the resultant projector from an overall basis of multiple disjoint subspaces built separately for each dimension, i.e., the frequency *s* and for each parameter of λ. Some recent methods use a recursive technique to compute the frequency moments of different order approximation in the parameters [40]. However, the methods that depend on local matching may result in oversized models because the number of matched moments increases due to either a wide frequency range or a high number of parameters. A larger variation of parameters may also adversely affect as different

dynamics change significantly in different frequency ranges. Some moment matching techniques utilize sampling methods. This sampling method is used either to generate Krylov subspaces for the system at different parameter sets [7] or to find the most relevant and probable moments [40]. Another sampling based method extends the poor man's truncated balanced realization (PMTBR) algorithm [39] to incorporate the variability by means of statistical interpolation [18]. The method utilizes multidimensional sampling of the combined frequency and parameter space. It can also apply statistical information available for λ to guide the sampling or use a weighting scheme in the parameter space. In this method, the most relevant vectors of the projection matrix are selected by applying singular value decomposition (SVD). The advantages of this method are that the error bounds can be estimated from the eigenvalues obtained from SVD operation and the order of the reduced model becomes less sensitive to the number of parameters or the way the parameter dependence is modeled. But it suffers more than the corresponding MOR because it requires selecting the samples from a higher dimension of space [10].

SPARE capitalizes on the explicit moment matching with respect to the parameters as used in the compact order reduction for parameterized extraction (CORE) algorithm [42]. The system is expanded by Taylor series, where $C(\lambda)$ and $G(\lambda)$ are represented by (3.25) and the state vector $x(s,\lambda)$ is expanded with respect to the parameters but not with respect to the frequency as [10]

$$x(s,\lambda) = x_{0\ldots0}(s) + \sum_{a_1\ldots a_k} F_{a_1\ldots a_k}\, x_{a_1\ldots a_k}(s) \tag{3.28}$$

where the subscripts represent the dependency on parameters and frequency dependence is stated explicitly. An augmented system can be obtained from the state equation by equating the

coefficients of the same power. For a simple case of just two parameters, λ_1 and λ_2, with a maximum of second order expansion including one cross-term, the result can be given as [10]

$$
\begin{aligned}
x_{00}(s) &= (G_{00} + sC_{00})^{-1}Bu \\
x_{10}(s) &= -(G_{00} + sC_{00})^{-1}(G_{10} + sC_{10})x_{00}(s) \\
x_{01}(s) &= -(G_{00} + sC_{00})^{-1}(G_{01} + sC_{01})x_{00}(s) \\
x_{20}(s) &= -(G_{00} + sC_{00})^{-1}(G_{10} + sC_{10})x_{10}(s) - (G_{00} + sC_{00})^{-1}(G_{20} + sC_{20})x_{00}(s) \\
x_{02}(s) &= -(G_{00} + sC_{00})^{-1}(G_{01} + sC_{01})x_{01}(s) - (G_{00} + sC_{00})^{-1}(G_{02} + sC_{02})x_{00}(s) \\
x_{11}(s) &= -(G_{00} + sC_{00})^{-1}(G_{11} + sC_{11})x_{00}(s) - (G_{00} + sC_{00})^{-1}(G_{10} + sC_{10})x_{01}(s) \\
&\quad -(G_{00} + sC_{00})^{-1}(G_{01} + sC_{01})x_{10}(s)
\end{aligned}
\tag{3.29}
$$

A non-parameterized frequency-dependent augmented system can be produced by using the state vector $\boldsymbol{x} = [x_{00}^T\ x_{10}^T\ x_{01}^T\ x_{20}^T\ x_{02}^T\ x_{11}^T]^T$, where the states are no longer functions of the parameters. The dependence on the parameters, on the other hand, is shifted to the output matrix. CORE utilizes this system for the initial formulation of the parameterized model. It uses such a model to generate a basis *Q* of order *q* by applying the nominal moment matching technique. The reduced order model is obtained by using the orthogonal projection, such as $x = Q\hat{x}$. The advantage of this model relies on that the states depend only on the frequency, which allows the application of any nominal MOR. However, there are some disadvantages of this method. The projection technique leads to a full matrix of reduced order, where the structure of the original system is lost. Since the parameter dependence is shifted to the output, such dependency is also lost after the reduction due to the projection. These effects make the model computationally expensive for different parameter sets and result in lesser flexibility. Moreover, the model is not scalable as the order of the expansion with respect to the parameters is *a priori*. The most critical drawback of this method is that it does not provide any guarantee of passivity because the condition $B = L^T$ is not valid anymore.

Using the same concept as used in CORE, the transfer function can be written as [10]

$$H(s,\lambda) = H_{0\ldots0}(s) + \sum_{a_1\ldots a_k} F_{a_1\ldots a_k} H_{a_1\ldots a_k}(s) \tag{3.30}$$

where $H_{a_1\ldots a_k} = Lx_{a_1\ldots a_k}$, which makes the parameter dependence explicit. Therefore, the parameterized transfer function can be written as a linear combination of the nominal transfer function and non-parameterized transfer function sensitivities with respect to the parameters. For simplicity, only two parameters, λ_1 and λ_2, are considered to derive a compact formulation of the overall transfer function from the individual transfer functions as given below [10]

$$\boldsymbol{H}(s) = \boldsymbol{L}[s\boldsymbol{C} + \boldsymbol{G}]^{-1}\boldsymbol{B} \tag{3.31}$$

$$H(s,\lambda) = [1 \quad \lambda_1 \quad \lambda_1^2 \quad \lambda_{21} \quad \lambda_1^2 \quad \lambda_1\,\lambda_2]\boldsymbol{H}(s) \tag{3.32}$$

where

$$\boldsymbol{B} = diag\{B,B,B,B,B,B\}$$

$$\boldsymbol{L} = diag\{L,L,L,L,L,L\}$$

$$C = \begin{bmatrix} C_{00} & & & & & \\ C_{10} & C_{00} & & & & \\ C_{20} & C_{10} & C_{00} & & & \\ C_{01} & & & C_{00} & & \\ C_{02} & & & C_{01} & C_{00} & \\ C_{11} & C_{01} & & C_{10} & & C_{00} \end{bmatrix},\ G = \begin{bmatrix} G_{00} & & & & & \\ G_{10} & G_{00} & & & & \\ G_{20} & G_{10} & G_{00} & & & \\ G_{01} & & & G_{00} & & \\ G_{02} & & & G_{01} & G_{00} & \\ G_{11} & G_{01} & & G_{10} & & G_{00} \end{bmatrix}$$

$$\boldsymbol{x} = [x_{00}^T\ x_{10}^T\ x_{01}^T\ x_{20}^T\ x_{02}^T\ x_{11}^T]^T$$

$$\boldsymbol{u} = [u^T \quad 0 \quad 0 \quad 0 \quad 0 \quad 0]^T$$

$$\boldsymbol{y} = [y_{00}^T\ y_{10}^T\ y_{01}^T\ y_{20}^T\ y_{02}^T\ y_{11}^T]^T \tag{3.33}$$

The choice of $\boldsymbol{B}$ along with its effect on the definition of $\boldsymbol{u}$ may appear strange but it implies that $\boldsymbol{B} = \boldsymbol{L}^T$ in the special and relevant case that $B = L^T$. This has some important implications over CORE, such as passivity preservation, scalability and flexibility [10].

The concept of SPARE method is graphically shown in Figure 3.1, which is a hierarchical representation generated for different orders. It is important to note that the nominal states only depend on the inputs. The first level (first order) sensitivities depend on its inputs and the nominal states. The second order (pure second order and also the cross term) depends on its inputs, the nominal states and also the first order states. Therefore, each level depends on its inputs and the previous states. Only the nominal states are excited by the inputs while the other states are independent of the inputs [10].

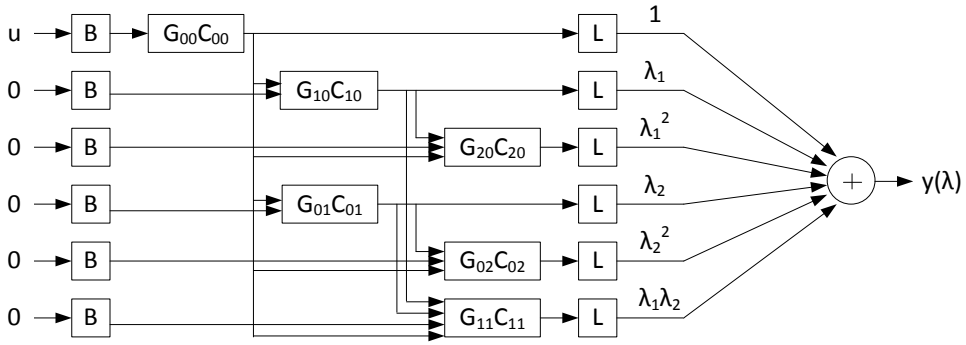

Figure 3.1: Parameterized system representation

SPARE method provides several important advantages. The system descriptor matrices in (3.33) can be stored block-wise and can be easily assembled for computation. Moreover, if one needs to work with only a subset of the parameters, it is not required to build the complete system, rather it only needs the structures related to the desired parameters. Also, the block lower triangular structure enables the possibility of using recursive procedures to evaluate the model for individual responses. Then the global response can be obtained from the linear combination of these responses. Additionally, parallel computations can be used at each level because each response depends only on the previous levels. The model evaluations for different

sets of parameters do not require extra iterations because the effect of changing the parameters can be efficiently addressed by the weighted sum associated with the terms.

Structure preservation has its own benefit [43][44] and in case of SPARE it can provide some additional advantages in terms of reduction and simulation [10]. Such preservation is required to maintain the explicit parameter dependence while keeping the computational cost at an acceptable level. It is possible to apply a block structure preserving (BSP) technique [44] due to the special structure of this representation, which ensures the block structure of the entire system. BSP technique first computes a projector for the complete system. Then the projector is split and expanded according to the block sizes into a block diagonal projector. This projector spans the same subspace as the original system but it is capable of maintaining the block structure even after reduction. The expanded basis leads to a larger reduced model. However, such reduction has additional benefits related to the accuracy [44] and sparsity. BSP projector can be built block wise in a recursive manner as each level depends only on the previous levels. Each block spans a basis such that it should capture the most relevant behavior of each block of states after the projection. This ensures that the complete reduced system will capture the most relevant behavior for any variation in the parameters.

The application of reduction technique to multiple interconnected systems can become very expensive due to the sample effort required. But careful consideration of the structure of the system matrices and of the calculation required can lead to considerable saving. Consider the following transfer function component [10]

$$H_{10} = -L(G_{00} + sC_{00})^{-1}(G_{10} + sC_{10})(G_{00} + sC_{00})^{-1}B \tag{3.34}$$

The following sample vectors have to be evaluated in order to sample the above transfer function using PMTBR scheme [52]

$$z_{10_k} = -(G_{00} + s_k C_{00})^{-1}(G_{10} + s_k C_{10})(G_{00} + s_k C_{00})^{-1} B \tag{3.35}$$

The term $(G_{00} + s_k C_{00})^{-1}$ is common to the nominal and all the other sensitivities of the transfer function. Therefore, it is evaluated once for each sample and then it can be reused in the successive computation. This computation, however, requires careful attention to ensure numerical stability. A single LU factorization at each sample point is sufficient in calculating the sample vectors of all the transfer functions given in (3.30), which reduces the CPU cost. Once the samples are obtained for each transfer function, an SVD can be applied to get the orthonormal vectors. The vectors whose associated singular value falls below a specified tolerance are not considered for the reduced system. The remaining dominant vectors produce an orthonormal projector Q_{ab}. A BSP type projector Q can be obtained as given below [10]

$$Q = diag\{Q_{00}\ Q_{10} \ldots\ Q_{ab}\} \tag{3.36}$$

Utilizing this Q, the reduced model can be obtained from (3.33). The reduced model thus has the same block sparsity pattern as the projector. Each block can be individually reduced as

$$\hat{G}_{ij} = Q_i^T G_{ij} Q \qquad \hat{B}_i = Q_i^T B$$
$$\hat{C}_{ij} = Q_i^T C_{ij} Q \qquad \hat{L}_i = LQ \tag{3.37}$$

where index *I, j* indicate the block position instead of sensitivity index. Listing 3.2 provides the algorithm for this method [10].

Listing 3.2: Algorithm for SPARE PMOR method

1. Obtain the matrices G_{00}, C_{00}, B, L, G_{ab}, C_{ab}.
2. Select m number of points in the frequency space, and for each frequency point s_m:
3. Compute LU decomposition as $LU = (G_{00} + s_k C_{00})$.
4. For each transfer function, obtain the sample vector

$$z_{00_k} = U^{-1}L^{-1}B$$
$$z_{10_k} = -U^{-1}L^{-1}(G_{10} + s_k C_{10}) z_{00_k}$$

$$z_{20_k} = -U^{-1}L^{-1}[(G_{20} + s_k C_{20})z_{00_k} + (G_{10} + s_k C_{10})z_{00_k}$$

…

5. Compose the matrices for each transfer function and apply SVD on each of them

$$Z_{ab} = [z_{ab_1} \dots z_{ab_k}]$$

$$Z_{ab} = Q_{ab} S_{ab} P_{ab}$$

6. Drop the columns for each matrix Q_{ab} whose singular value fall below a specified tolerance.
7. Build a BSP projector from the remaining columns as

$$Q = diag\{Q_{00}\ Q_{10} \dots\ Q_{ab}\}$$

8. Apply congruence transformation on the augmented system as

$$\hat{G} = Q^T G Q, \hat{C} = Q^T C Q, \hat{B} = Q^T B, \hat{L} = LQ$$

3.3 Leguerre-SVD based PMOR Method

In this sampling based PMOR method, the authors utilized the PEEC model due to the advantage of computational cost. The PEEC technique transforms an EM system into a passive RLC equivalent circuit. PEEC uses a circuit interpretation of the electric field integral equation (EFIE) [34]. Therefore, it allows the analysis of complex problems involving EM fields and circuits [2], [40], [45]-[48]. In practice, the nonlinear devices, such as drivers and receivers, are connected with PEEC circuits using a time domain circuit simulator, such as SPICE. However, such direct inclusion of PEEC model into a circuit simulator may become practically impossible for complex systems because the number of circuit elements can grow to tens of thousands. As mentioned earlier, MOR techniques can be used to reduce the size of the PEEC model [16], [41]. However, these traditional MOR techniques perform model order reduction only as a function of frequency. But for a high speed IC, the response with respect to the design parameters, such as geometrical and substrate features may be affected substantially. A typical circuit synthesis includes design space exploration and optimization, which requires repeated simulations for different values of the design parameters. Therefore, in this case, PMOR methods can be used

effectively as they can reduce large systems of equations with respect to frequency and other design parameters, and thus improve the computational time significantly. The authors of [7] proposed a PMOR method applicable to PEEC model. It is based on a parameterization process of the matrices generated by the PEEC method and the projection subspace is calculated using a suitable passivity-preserving MOR method. The Leguerre-SVD MOR method [18] is used, which guarantees passivity of PMOR method over the design space of interest. However, any other passivity-preserving MOR method, such as PRIMA [6] is equally applicable to this PMOR technique. A brief discussion of the PEEC method is presented in the following subsection because of its growing importance in circuit simulation.

3.3.1 Formulation of the PEEC method

The PEEC method is based on the integral equation forms of Maxwell's equations [38]. The main difference between the PEEC method and other integral equation based methods, such as the method of moments [37], relies on the fact that the PEEC provides a circuit representation in terms of partial elements, such as partial inductance and coefficient of potential associated with the capacitance. Therefore, the resultant equivalent circuit can be analyzed in both time and frequency domains using a SPICE-like circuit simulator [49]. In a PEEC method, the volumes and surfaces of a conductor are discretized into elementary regions, hexahedra and patches, respectively [47], over which the currents and charge densities are expanded into a series of basis functions. Pulse basis functions are commonly used as expansion and weight functions. These basis functions correspond to assuming constant current density and charge density over the elementary volume (inductive) and surface (capacitive) cells, respectively [7]. Topological elements, such as nodes and braches, are generated using the standard Galerkin's procedure and electrical lumped elements are considered modeling both the magnetic and electrical field couplings. In addition, conductors are modeled by ohmic resistance and dielectrics are modeled

by using the excess charge due to the dielectric polarization [50]. Electric and magnetic field couplings are modeled as coefficients of potential and partial inductances, respectively.

The electric field coupling between two capacitive surface cells α and β is modeled by the coefficient of potential as follows [7]

$$P_{\alpha\beta} = \frac{1}{4\pi\varepsilon}\frac{1}{S_\alpha S_\beta}\int_{S_\alpha}\int_{S_\beta}\frac{1}{R_{\alpha\beta}}dS_\alpha dS_\beta \tag{3.38}$$

where $R_{\alpha\beta}$ is the distance between any two points on surfaces α and β, and S_α and S_β represent their corresponding surface areas. On the other hand, the magnetic field coupling between two inductive volume cells γ and δ is modeled by the partial inductances as [7]

$$L_{p_{\gamma\delta}} = \frac{\mu}{4\pi}\frac{1}{a_\gamma a_\delta}\int_{u_\gamma}\int_{u_\delta}\frac{1}{R_{\gamma\delta}}du_\gamma du_\delta \tag{3.39}$$

where $R_{\gamma\delta}$ is the distance between any two points on volumes u_γ and u_δ, and a_γ and a_δ represent their corresponding cross sections. Kirchhoff's current and voltage laws for conductors can be written as [7]

$$\begin{aligned}\boldsymbol{P}^{-1}\frac{d\boldsymbol{v}(t)}{dt} - \boldsymbol{A}^T\boldsymbol{i}(t) + \boldsymbol{i}_e(t) = 0\\ -\boldsymbol{A}\boldsymbol{v}(t) - \boldsymbol{L}_p\frac{d\boldsymbol{i}(t)}{dt} - \boldsymbol{R}\boldsymbol{i}(t) = 0\end{aligned} \tag{3.40}$$

where ***A*** is the connectivity matrix, ***v(t)*** represents the node potentials to infinity, ***i(t)*** represents the currents flowing in volume cells and $\boldsymbol{i}_e(t)$ denotes the external currents. However, when dielectrics are considered, the resistive voltage drop should be replaced by the excess capacitive voltage drop, which is related to the excess charge by $\boldsymbol{v}_d(t) = \boldsymbol{C}_d^{-1}\boldsymbol{q}_d(t)$ [50]. Therefore, (3.40) can be rewritten as [7]

$$\boldsymbol{P}^{-1}\frac{d\boldsymbol{v}(t)}{dt} - \boldsymbol{A}^T\boldsymbol{i}(t) + \boldsymbol{i}_e(t) = 0$$

$$-\boldsymbol{A}\boldsymbol{v}(t) - \boldsymbol{L}_p\frac{d\boldsymbol{i}(t)}{dt} - \boldsymbol{v}_d(t) = 0$$

$$\boldsymbol{i}(t) = \boldsymbol{C}_d\frac{d\boldsymbol{v}_d(t)}{dt} \tag{3.41}$$

A selection matrix ***K*** can be introduced to define the port voltages by selecting node potentials. This matrix is also used to obtain the external currents $\boldsymbol{i}_e(t)$ from the currents $\boldsymbol{i}_s(t)$, which flow in the opposite direction of the n_p port currents $\boldsymbol{i}_p(t)$. Therefore, the voltages and currents can be expressed as [7]

$$\boldsymbol{v}_p(t) = \boldsymbol{K}\boldsymbol{v}(t)$$

$$\boldsymbol{i}_e(t) = \boldsymbol{K}^T\boldsymbol{i}_s(t) \tag{3.42}$$

Figure 3.2 shows an example PEEC circuit and its corresponding circuit elements for a conductor. The current controlled voltage sources $sL_{pij}I_j$ model the magnetic field couplings and the current controlled current sources I_{cci} model the electric field couplings.

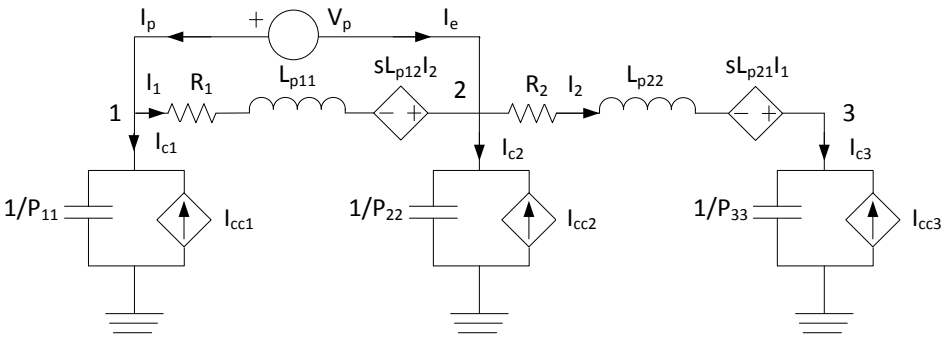

Figure 3.2: PEEC electrical quantities for a conductor elementary cell

3.3.2 The MNA for the PEEC

Consider a system consisting of both conductors and dielectrics. The current and charge density are defined in volumes and surfaces of conductors and dielectrics, respectively. The continuous EM problem described by the EFIE is converted into a discrete problem in terms of electrical quantities (currents and potentials) using a Galerkin's approach. Consider that n_n is the number of nodes and n_i is the number of branches where currents flow. The numbers of branches of conductors and dielectrics are given by n_c and n_d, respectively. An admittance representation, having n_p output currents $\boldsymbol{i}_p(t)$ in response to voltage excitations $\boldsymbol{v}_p(t)$, can be established. Since dielectrics require excess capacitance in modeling the polarization charge [51], extra n_d unknowns are needed in addition to currents. According to the MNA approach given in [52], the global number of unknown is given by $n_u = n_n + n_i + n_d + n_p$. Using equations (3.40) – (3.42), the MNA is given in [7] as

$$\underbrace{\begin{bmatrix} I_{n_n,n_n} & 0_{n_n,n_i} & 0_{n_n,n_d} & 0_{n_n,n_p} \\ 0_{n_i,n_n} & L_p & 0_{n_i,n_d} & 0_{n_i,n_p} \\ 0_{n_d,n_n} & 0_{n_d,n_i} & C_d & 0_{n_d,n_p} \\ 0_{n_p,n_n} & 0_{n_p,n_i} & 0_{n_p,n_d} & 0_{n_p,n_p} \end{bmatrix}}_{C} \frac{d}{dt} \underbrace{\begin{bmatrix} v(t) \\ i(t) \\ v_d(t) \\ i_s(t) \end{bmatrix}}_{x(t)}$$

$$= -\underbrace{\begin{bmatrix} 0_{n_n,n_n} & -PA^T & 0_{n_n,n_d} & PK^T \\ A & R & \Phi & 0_{n_i,n_p} \\ 0_{n_d,n_n} & -\Phi^T & 0_{n_d,n_d} & 0_{n_d,n_p} \\ -K & 0_{n_p,n_i} & 0_{n_p,n_d} & 0_{n_p,n_p} \end{bmatrix}}_{G} \underbrace{\begin{bmatrix} v(t) \\ i(t) \\ v_d(t) \\ i_s(t) \end{bmatrix}}_{x(t)} + \underbrace{\begin{bmatrix} 0_{n_n+n_i+n_d,n_p} \\ I_{n_p,n_p} \end{bmatrix}}_{B} \underbrace{\begin{bmatrix} v_p(t) \end{bmatrix}}_{u(t)} \qquad (3.43)$$

where I_{n_p,n_p} is the identity matrix having dimension equal to the number of ports. Matrix Φ is given by [7]

$$\Phi = \begin{bmatrix} 0_{n_c,n_d} \\ I_{n_d,n_d} \end{bmatrix} \tag{3.44}$$

Potentials ***v(t)*** can be represented in terms of charges as [7]

$$\boldsymbol{v}(t) = \boldsymbol{P}\boldsymbol{q}(t) \tag{3.45}$$

Then, (3.43) can be rewritten as [7]

$$\underbrace{\begin{bmatrix} P & 0_{n_n,n_i} & 0_{n_n,n_d} & 0_{n_n,n_p} \\ 0_{n_i,n_n} & L_p & 0_{n_i,n_d} & 0_{n_i,n_p} \\ 0_{n_d,n_n} & 0_{n_d,n_i} & C_d & 0_{n_d,n_p} \\ 0_{n_p,n_n} & 0_{n_p,n_i} & 0_{n_p,n_d} & 0_{n_p,n_p} \end{bmatrix}}_{C} \frac{d}{dt} \underbrace{\begin{bmatrix} q(t) \\ i(t) \\ v_d(t) \\ i_s(t) \end{bmatrix}}_{x(t)}$$

$$= -\underbrace{\begin{bmatrix} 0_{n_n,n_n} & -PA^T & 0_{n_n,n_d} & PK^T \\ AP & R & \Phi & 0_{n_i,n_p} \\ 0_{n_d,n_n} & -\Phi^T & 0_{n_d,n_d} & 0_{n_d,n_p} \\ -KP & 0_{n_p,n_i} & 0_{n_p,n_d} & 0_{n_p,n_p} \end{bmatrix}}_{G} \underbrace{\begin{bmatrix} q(t) \\ i(t) \\ v_d(t) \\ i_s(t) \end{bmatrix}}_{x(t)} + \underbrace{\begin{bmatrix} 0_{n_n+n_i+n_d,n_p} \\ I_{n_p,n_p} \end{bmatrix}}_{B} \underbrace{\begin{bmatrix} v_p(t) \end{bmatrix}}_{u(t)} \tag{3.46}$$

Rewriting (3.46) in a more compact form as [7]

$$\boldsymbol{C}\frac{dx(t)}{dt} = -\boldsymbol{G}x(t) + \boldsymbol{B}u(t)$$

$$\boldsymbol{i}_p(t) = \boldsymbol{L}^T x(t) \tag{3.47}$$

where $\boldsymbol{x}(t) = [\boldsymbol{q}(t) \quad \boldsymbol{i}(t) \quad \boldsymbol{v_d}(t) \quad \boldsymbol{i_s}(t)]^T$. Here $\boldsymbol{B} = \boldsymbol{L}$ and $\boldsymbol{B} \in \mathbb{R}^{n_u \times n_p}$ because voltage sources are applied only at n_p-port nodes in an n_p-port formulation. The system of (3.46) is, in general, ill-conditioned because charges are usually much smaller than voltages and currents. The entries of ***P*** are typically larger than other elements of ***C*** and ***G*** by several orders of magnitude. A scaling scheme can be used to avoid such problem [7].

3.3.3 PMOR Algorithm

A PMOR algorithm can be devised for the above system for *N* numbers of parameters, which are given as $\boldsymbol{g} = \left(g^{(1)}, \ldots, g^{(N)}\right)$ in addition to frequency. The objective of such a PMOR method is to accurately approximate the original scalable system having a high complexity with a much reduced scalable system having much lower complexity. This can be achieved only if the reduced system can capture the behavior of the original system with respect to frequency and other design parameters. The design space is designated by *D(g)* while the parameter space is represented by *P(s, g)*, which includes frequency in addition to other parameters. Two different data grids are used for this model: an estimation grid and a validation grid. The estimation grid is used to build the PMOR model and the validation grid is used to evaluate the performance of the model using only the points in design space that are not used for construction of the model [7]. A simple possible scheme of such design grids is shown in Figure 3.3 for only two design parameters $\boldsymbol{g} = \left(g^{(1)},\ g^{(2)}\right)$.

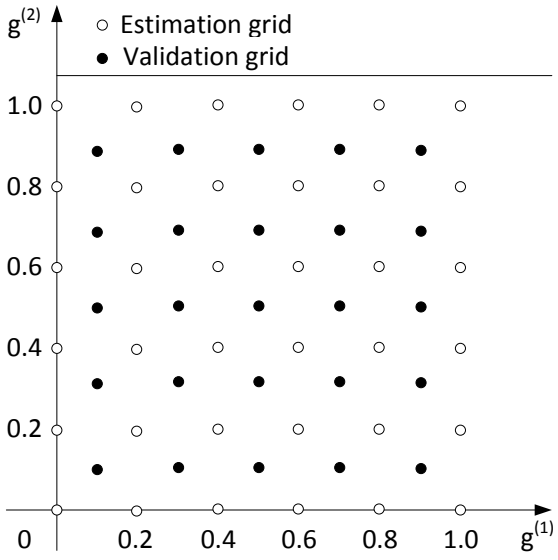

Figure 3.3: A simple scheme of design space

For *N* number of parameters, the MNA of (3.47) can be rewritten as [7]

$$\boldsymbol{C}(g)\frac{dx(t,\ g)}{dt} = -\boldsymbol{G}(g)x(t,g) + \boldsymbol{B}u(t,g)$$

$$\boldsymbol{i}_p(t,g) = \boldsymbol{L}^T x(t,g) \tag{3.48}$$

In the above formulation, a topologically fixed discretization is assumed, which is independent of the values of the specific design parameter. Therefore, it preserves the size of the system matrices along with the numbering of the mesh nodes and mesh edges. In other words, the mesh is only locally stretched or shrunk when the values of the related parameters are modified. The global coordinates of the nodes as well as the orientation and length of the edges of the topologically fixed mesh change when the related parameters vary. However, such change does not change the number of state variables. Also, matrices ***B*** and ***L*** are uniquely determined by the topology of the circuit and remain constant. On the other hand, ***C*** and ***G*** vary as they are functions of the design parameters. This implies that in the MNA representation, ***P(g)***, $\boldsymbol{L}_p(g)$, $\boldsymbol{C}_d(g)$ and ***R(g)*** are functions of the parameters while ***A***, ***Φ*** and ***K*** are constants. The formulation of this PMOR method requires computing the multivariate models of $\overline{\boldsymbol{P}}(g), \overline{\boldsymbol{L}}_P(g), \overline{\boldsymbol{C}}_d(g)$ and $\overline{\boldsymbol{R}}(g)$. However, instead of assembling a PEEC model and performing a MOR step in each point of interest $\hat{\boldsymbol{g}} = \left(g_{k_1}^{(1)}, \dots, g_{k_N}^{(N)}\right)$ in the design space, the Laguerre-SVD MOR method [18] is applied to each PEEC model related to the estimation design space grid as given in Listing 3.3 [7].

Listing 3.3: Algorithm for projection matrix of Optimization based PMOR method

1) Choose a value for scaling parameter α and the reduced order *q*.
2) Solve $(\boldsymbol{G} + \alpha\boldsymbol{C})\boldsymbol{Q}_0 = \boldsymbol{B}$.
3) For, *k = 1, 2, … , q-1* solve $(\boldsymbol{G} + \alpha\boldsymbol{C})\boldsymbol{Q}_k = (\boldsymbol{G} - \alpha\boldsymbol{C})\boldsymbol{Q}_{k-1}$.
4) $\boldsymbol{K}_r = [\boldsymbol{Q}_0, \dots, \boldsymbol{Q}_{q-1}]$.

where $\boldsymbol{K}_r$ represents a set of Krylov matrices. This set of Krylov matrices is interpolated and modeled as $\overline{\boldsymbol{K}}_r(g)$. It is important to note that the sampling density of the estimation design space grid is a critical factor in order to accurately describe the parameterized behavior of the original system over the entire design space. A technique to get suitable number of points in the estimation design space grid can be found in [52]. After completion of building the multivariate models $\overline{\boldsymbol{P}}(g), \overline{\boldsymbol{L}}_P(g), \overline{\boldsymbol{C}}_d(g), \overline{\boldsymbol{R}}(g)$, and $\overline{\boldsymbol{K}}_r(g)$, a PEEC model can be assembled as [7]

$$\boldsymbol{Y}(s, \hat{g}) = \boldsymbol{L}^T[s\boldsymbol{C}(\hat{g}) + \boldsymbol{G}(\hat{g})]^{-1}\boldsymbol{B} \tag{3.49}$$

A projection matrix $\boldsymbol{U}(\hat{g})$ can be computed using SVD [53] of $\overline{\boldsymbol{K}}_r(\hat{g})$ for any point of interest $\hat{\boldsymbol{g}} = \left(g_{k_1}^{(1)}, \ldots, g_{k_N}^{(N)}\right)$ as follows [7]

$$\boldsymbol{U}(\hat{g})\boldsymbol{S}(\hat{g})\boldsymbol{V}(\hat{g})^T = SVD[\overline{\boldsymbol{K}}_r(\hat{g})] \tag{3.50}$$

A congruence transformation can be used in order to generate the corresponding reduced order matrices as given below [7]

$$\begin{aligned} \boldsymbol{C_r}(\hat{g}) &= \boldsymbol{U}(\hat{g})^T\boldsymbol{C}(\hat{g})\boldsymbol{U}(\hat{g}) \\ \boldsymbol{G_r}(\hat{g}) &= \boldsymbol{U}(\hat{g})^T\boldsymbol{G}(\hat{g})\boldsymbol{U}(\hat{g}) \\ \boldsymbol{B_r}(\hat{g}) &= \boldsymbol{U}(\hat{g})^T\boldsymbol{B} \\ \boldsymbol{L_r}(\hat{g}) &= \boldsymbol{U}(\hat{g})^T\boldsymbol{L} \end{aligned} \tag{3.51}$$

Substitution of (3.51) into (3.49) results in the desired parameterized reduced order model. The order of the model can be increased until a specified root mean square (RMS) error is satisfied for a data point in the validation grid.

3.4 Optimization Based PMOR Method

The PMOR methods, as described in the previous sections, used conventional moment matching method or the truncated balanced reduction (TBR) technique. However, this optimization based PMOR method uses "optimal (block) vectors" to construct the projection matrix. A recursive least square (RLS) technique is used for this purpose, which minimizes the error in the whole parameter space. Such a minimization process can ensure a high degree of accuracy in appropriate cases. Also, comparatively small reduced order models can be obtained for a multi-parameter system because the size of the ROM is independent of the number of parameters. It can be used when the closed form expressions of parameterized circuit equations are not available. Moreover, the positive semi-definite structures of some systems are preserved as Taylor expansion is not used in approximating the parameterized system matrices. This implies that passivity is preserved for the parameterized RLC interconnect model [54].

3.4.1 Formulation of Fully Parameterized Response

Consider a multi-parameter linear time invariant (LTI) fully parameterized dynamic system as given by the following relations [54]

$$C(\lambda)\dot{x}(t) = G(\lambda)x(t) + B(\lambda)u(t)$$
$$y(t) = L(\lambda)x(t) \tag{3.52}$$

where the descriptor matrices are $C(\lambda), G(\lambda) \in \mathbb{R}^{n \times n}$, the matrices related to the input and output are $B(\lambda) \in \mathbb{R}^{n \times m}$ and $L(\lambda) \in \mathbb{R}^{m \times n}$, respectively. The parameters are represented by the vector $\lambda \in \mathbb{R}^{p}$, where *p* is the total number of design and process parameters. A distinct feature of this technique is that *B* and *L* matrices are also parameterized. That is why this method is referred as fully parameterized. A simplified working principle of this method is shown in Figure 3.4. The input signal $u(t)$ is first converted to $\hat{u}(t) \in \mathbb{R}^{n}$ with the aid of a

transformer matrix $B(\lambda)$ before injecting into the network. Some examples of parameter dependent matrix $B(\lambda)$ are: a voltage controlled current source and a MEMS sensor that converts optical and chemical signals to electrical signals [54].

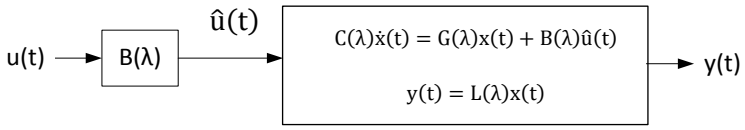

Figure 3.4: Block diagram of fully parameterized LTI system

The objective of this method is to find a fully parameterized reduced order model of order *q* where *q* << *n*, which approximates the characteristics of the original system with a high degree of accuracy. The reduced order model can be given by the following set of equations [54]

$$C_r(\lambda)\dot{z}(t) = G_r(\lambda)z(t) + B_r(\lambda)u(t)$$
$$y(t) = L_r(\lambda)z(t) \tag{3.53}$$

As mentioned in the earlier sections, this can be achieved if an appropriate projection matrix *Q* can be computed such that the reduced matrices are related to the original matrices as [54]

$$C_r(\lambda) = Q^T C(\lambda)Q,\ G_r(\lambda) = Q^T G(\lambda)Q,\ B_r(\lambda) = Q^T B(\lambda),\ L_r(\lambda) = L(\lambda)Q \tag{3.54}$$

The response of the reduced system can be obtained from the following transfer function [54]

$$H_r(s,\lambda) = L_r(\lambda)[sC_r(\lambda) - G_r(\lambda)]^{-1}B_r(\lambda) \tag{3.55}$$

The important properties of this method are summarized below

- It is valid even when *B* and *L* matrices are parameterized.
- It generates a reduced model whose size is independent of the number of parameters.

- It is useful when the close form expressions of the system matrices are unknown, which is usually the case when (3.52) is extracted from transistor level SPICE netlist and λ are some parameters of the complex semiconductor device models, or when the parameter dependence is shown by a measurement data sheet or by a look-up table.
- It preserves passivity of the systems with positive semi-definite structure.

3.4.2 Recursive Least Square Based Fully PMOR

Consider that the parameterized system matrices are continuous function of λ. Rewriting (3.52) in the frequency domain as [54]

$$sC(\lambda)x(s,\lambda) = G(\lambda)x(s,\lambda) + B(\lambda)u(s)$$
$$y(s,\lambda) = L(\lambda)x(s,\lambda) \tag{3.56}$$

If the transfer function from $u(s)$ to the state variable $x(s,\lambda)$ is denoted by $X(s,\lambda)$ then it can be computed from the following linear equation [54]

$$[sC(\lambda) - G(\lambda)]X(s,\lambda) = B(\lambda) \tag{3.57}$$

Based on the concept of rational Krylov subspace method [55] for MOR of non-parameterized systems, it can be inferred that if $X(s,\lambda)$'s are known at a set of frequency points, and a projection matrix *Q* can be obtained as given below to construct a MOR [54].

$$colspan\left\{X(s_1,\lambda), X(s_2,\lambda), \dots, X\left(s_p,\lambda\right)\right\} \subseteq Q \tag{3.58}$$

However, it is not possible to compute the closed forms of the parameterized (block) vectors $X(s_i,\lambda)$. Moreover, it is quite impossible to orthonormalize these vectors even if it is possible to compute $X(s_i,\lambda)$ for some specially structured parameterized systems. Therefore, as an alternate option, a set of non-parameterized (block) vectors $X(s_i)$ can be obtained that are

close to $X(s_i, \lambda)$'s using the constraints of some accuracy criteria. If such non-parameterized vectors $X(s_i) \in \mathbb{C}^{n \times m}$ are substituted in (3.57), a parameter dependent residual (block) vector can be obtained as given by the following expression [54]

$$E(s_i, \lambda) = [sC(\lambda) - G(\lambda)]X(s_i) - B(\lambda) \tag{3.59}$$

This residual vector can be used for estimation of error. A non-parameterized (block) vector $\hat{X}(s_i)$ can be estimated that is close to (s_i, λ), when $\hat{X}(s_i)$ is an optimizer to the following problem [54]

$$\min_{X(s_i)} \int_S \left\| [s_i C(\lambda) - G(\lambda)]X(s_i) - B(\lambda) \right\|_F^2 d\lambda(1) \ \ldots \ d\lambda(p), subject\ to\ X(s_i) \in C^{n \times m} \tag{3.60}$$

where $S \in \mathbb{R}^p$ is the parameter space, $\lambda(i)$ is the *i-th* coordinate of λ, and $\|M\|_F$ denotes the Frobenius norm of a matrix $M \in \mathbb{C}^{m_1 \times m_2}$, such that [54]

$$\|M\|_F \triangleq \left(\sum_{j=1}^{m_2} \sum_{i=1}^{m_1} |M(i,j)|^2 \right)^{1/2} \tag{3.61}$$

The optimization problem of equation (3.60) implies that $\hat{X}(s_i)$ is a non-parameterized (block) vector that is the closest to the corresponding parameterized (block) vector $X(s_i, \lambda)$, if $\hat{X}(s_i)$ is selected such that the error is minimized in the entire parameter space. The simple steps of this PMOR are summarized in Listing 3.4.

Listing 3.4: Algorithm for Optimization based PMOR method

1. Solve the optimization problem of (3.60) at different frequency points s_i to obtain $\hat{X}(s_i)$ for i = 1, 2, … , p.
2. Construct the projection matrix *Q* such that
   $$range(Q) = colspan\left\{\hat{X}(s_1), \hat{X}(s_2), \ldots, \hat{X}(s_p)\right\}$$
3. Construct the fully PMOR using (3.54).

The key feature of this algorithm is that the projection matrix *Q* is obtained by solving an error optimization problem instead of using conventional moment matching, balanced truncation or sampling techniques. However, the major problem with this algorithm is the numerical solution of the optimization problem given in (3.60). The following modification can be made in order to obtain an easier solution for this problem.

If the parameterized system matrices are assumed to be continuous functions of λ then the integration of (3.60) can be determined after discretizing the parameter space. If the variation of each element of λ can be characterized by its lower and upper bound then the entire parameter space can be discretized as in [54]

1. The entire parameter space is represented by two vectors *a* and *b* of length *p*, such that $S = \{\lambda | a(i) \leq \lambda(i) \leq b(i), for\ i = 1, 2, \dots, p\}$.
2. For each parameter $\lambda(i)$, its variation range can be segmented into m_i uniform intervals and the length of each interval is given by

$$\Delta_i = \frac{b(i) - a(i)}{m_i} \tag{3.62}$$

3. The above segmentation technique would divide the entire parameter space *S* into $N = m_1 m_2 \dots m_p$ boxes, each of which has a dimension of *p*. For each integer $k \in [1, N]$, there is a companion vector $V_k = [k_1, k_2, \dots, k_p]$, based on the following rules
   a) $k_1 + k_2 m_1 + k_3 m_2 m_1 + \cdots + k_p m_{p-1} m_{p-2} \dots m_1 = k - 1$
   b) $k_i \in \mathbb{Z}\ and\ 0 \leq k_i \leq m_i - 1$

   The pseudo code to calculate V_k is given in Listing 3.5 [54].

4. The volume of each box is given by

$$\Delta = \Delta_1 \Delta_2 \dots \Delta_p \tag{3.63}$$

5. The geometric center of the *k-th* box *B(V_k)* is a point $\bar{\lambda}(V_k)$ in the p-dimensional space whose *i-th* coordinate is given by $a(i) + (k_i + 0.5)\Delta_i$.

Using the above information, the integral of (3.60) can be rewritten as [54]

$$\begin{aligned}&\int_S \left\|[s_i C(\lambda) - G(\lambda)]X(s_i) - B(\lambda)\right\|_F^2 d\lambda(1) \ \ldots \ d\lambda(p) \\ &\approx \sum_{k=1}^{N} \Delta \left\|[s_i C(\bar{\lambda}(V_k)) - G(\bar{\lambda}(V_k))]X(s_i) - B(\bar{\lambda}(V_k))\right\|_F^2\end{aligned} \tag{3.64}$$

Since Δ is a positive constant, therefore, the original optimization problem can be reformulated in a much easier and solvable form as in [54] and given as

$$\min_{X(s_i)} \sum_{k=1}^{N} \left\|[s_i C(\bar{\lambda}(V_k)) - G(\bar{\lambda}(V_k))]X(s_i) - B(\bar{\lambda}(V_k))\right\|_F^2, \text{ subject to } X(s_i) \in C^{n\times m} \tag{3.65}$$

Listing 3.5: Algorithm for computation of V_k

---

1. Initialize $\bar{m} \in \mathbb{Z}^p: \bar{m} = 1, \bar{m}(i+1) = m_i \bar{m}(i) for\ i = 1, 2, \ldots, p-1.$
2. Initialize $V_k \in \mathbb{Z}^p: V_k = [0, \ldots, 0]\ and\ set\ \bar{k} = k - 1.$
3. for $\bar{p} = p, p-1, \ldots, 1\ do$
   $V_k(\bar{p}) = floor\left(\frac{\bar{k}}{\bar{m}(\bar{p})}\right), \bar{k} = \bar{k} - V_k(\bar{p})\bar{m}(\bar{p})$

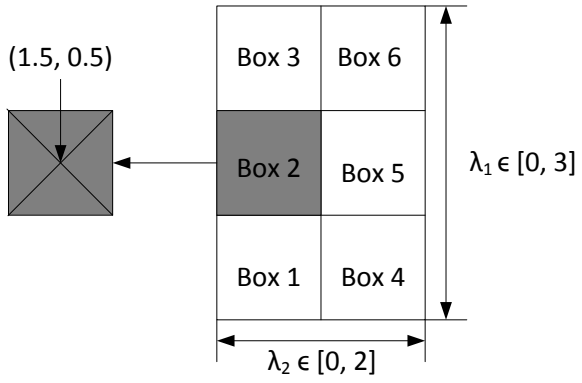

Figure 3.5: Discretization in 2-D parameter space

The discretization technique is shown in Figure 3.5 using a 2-D parameter space. The concept can be extended to higher dimension parameter spaces. The solution of (3.65) with the aid of RLS optimization technique is provided in [54] and given as

$$\hat{X}(s_i) = \left[\sum_{k=1}^{N} M_i(\bar{\lambda}(V_k))^H M_i(\bar{\lambda}(V_k)) \right]^{-1} \times \sum_{k=1}^{N} M_i(\bar{\lambda}(V_k))^H B(\bar{\lambda}(V_k)) \qquad (3.66)$$

where $M_i(\bar{\lambda}(V_k)) = s_i C(\bar{\lambda}(V_k)) - G(\bar{\lambda}(V_k))$.

The complete algorithm of this PMOR method is given in Listing 3.6 with an assumption that the original system is of order *n* and it has *p* parameters. A total number of *q* frequency points $s = s_1, s_2, \ldots, s_q$ are used to derive this algorithm [54].

Listing 3.6: Complete algorithm for optimization based PMOR method

1. initialize $V \leftarrow [\,]$,
2. for $i = 1,2, \ldots, q\ do$
3. M = 0, B = 0,
4. for $k = 1, 2, \ldots, N\ do$
5. calculate the companion vector V_k of k,
6. decide $\bar{\lambda}(V_k)$,
7. update $M = M + M_i(\bar{\lambda}(V_k))^H M_i(\bar{\lambda}(V_k))$,
8. update $B = B + M_i(\bar{\lambda}(V_k))^H B(\bar{\lambda}(V_k))$,
9. end for
10. compute $\hat{X}(s_i) = M^{-1}B$,
11. update $V : V \leftarrow [V, \hat{X}(s_i)]$,
12. end for
13. orthonormalize the column vector of V, such that range*(Q)* = colspan *{V}*,
14. construct the fully PMOR using (3.54).

Chapter 4

COMPARISON OF PARAMETERIZED MODEL ORDER REDUCTION TECHNIQUES

In this chapter, a comprehensive analysis of different PMOR techniques discussed in Chapter 3 is carried out. Each method is individually analyzed to figure out its pros and cons. A conclusive comparison between different methods is presented after analyzing all these techniques. The efficiency of a PMOR technique depends on several criteria. However, the selection of these criteria may vary in different applications. The effectiveness of any method depends on how well it satisfies the desired criteria required for a particular application. In this thesis, the following criteria are chosen to evaluate and compare PMOR techniques. These criteria represent the chief characteristics that a user of PMOR techniques would evaluate before choosing a particular technique for use in an application.

- Computational or CPU cost to generate the response,
- Accuracy or error in performance,
- Stability and passivity of the system,
- Ill-conditioning associated with a model.

In addition to the above criteria, some additional features, such as scalability of the model, preservation of the structure of the original system may become handy as additional advantages of a particular technique. In the following section, a brief discussion of each of these criteria is presented.

4.1 Criteria for PMOR Efficiency Evaluation

Computational or CPU Cost to generate the response: Computational cost, in general, involves time to build the model and the time to find out the response. However, since the time taken to build the model can be performed off-line, for the sake of comparing the different PMOR techniques, the time to evaluate the response of the reduced order model is used for this criterion. This cost depends on the type of analysis and the method involved to evaluate the desired response. In general, in frequency domain, the response can be obtained by solving the following MNA equations as given in (2.12)

$$\boldsymbol{X}(s) = (\boldsymbol{G} + s\boldsymbol{C})^{-1}\boldsymbol{B}\boldsymbol{U}(s)$$

$$\boldsymbol{Y}(s) = \boldsymbol{L}^T\boldsymbol{X}(s)$$

Accuracy or error in performance: Accuracy of the generated PMOR model can be calculated by evaluating the difference between the responses of the original system and the reduced system. Although there is no standard method for calculating error, mean squares error (MSE) is a common estimator of error for many applications. If the transfer function of the original system is $H(s)$ and the transfer function of the reduced system is $\widehat{H}(s)$, the MSE for *n* number of samples can be given as

$$MSE = \frac{1}{n}\sum_{i=1}^{n}\left(H(s) - \widehat{H}(s)\right)^2 \tag{4.1}$$

Since the magnitude of the response may vary between a wide range of values for different applications, the relative error with respect to the original response provides a better picture of the error. Therefore, the relative error is used as the metric to represent accuracy in this thesis. For a PMOR technique, in general, the order of the model can increased to get a better accuracy but it often comes with additional CPU cost.

Stability and Passivity of the system: If the output of a network is bounded for all bounded inputs then the network is stable. For a stable network with a transfer function $H(s) = \frac{P(s)}{Q(s)}$, the poles p_i of $H(s)$ should have the following properties

- $Re(p_i) \leq 0$,
- If $Re(p_i) = 0$, it must be a simple pole.

A passive network doesn't generate energy. Passivity is an important property because a stable but non-passive macromodel can lead to an unstable system when connected to another passive system. Therefore, it is essential that the ROM must be passive. A network with admittance matrix $Y(s)$ is passive if and only if [56]

- $Y(s^*) = Y^*(s)$ where * represents complex conjugate.
- $Y(s)$ is a positive real matrix which implies that $z^{*t}[Y(s^*) + Y(s)]z \geq 0$ for all complex values of *s* with $Re(s) > 0$ and any arbitrary vector *z.*

It should be noted that a passive network is stable but a stable network is not necessarily passive. Interconnects with passive elements are always passive. This criterion assesses whether or not the models produced by the technique are passive.

Ill-conditioning associated with a model: Ill-conditioning occurs when the machine precision of the computer used to solve numerical problems becomes inadequate to find an accurate solution. When ill-conditioning occurs during solving a system of equations, solutions obtained from the computational devices cannot be relied on. As such, it is imperative to avoid ill-conditioning issues while developing new numerical algorithms. Results obtained from the algorithms that suffer from ill-conditioning issues should be carefully scrutinized before using

them for other applications. This criterion assesses if the technique suffers from ill-conditioning issues.

Structure preservation in the model: If an explicit structural dependence on a parameter can be maintained in the reduced system then re-evaluation of the model for different parameter values becomes efficient. Methods that are designed to preserve structures use block structure preserving techniques for system reduction [10]. This criterion assesses whether or not the technique under consideration preserves structural dependence on its parameters.

Scalability of the model: A model is scalable if terms can be added or removed at any stage to modify the order, depending on the required accuracy, utilizing reuse of data [10]. This criterion assess whether or not the given algorithm is scalable.

To analyze each PMOR method, we use three simple applications: (a) Microstrip transmission line, (b) Coupled transmission lines and (c) Transmission lines of an arbitrary configuration. The simulations of these applications are performed for the minimum, nominal, and maximum values of a set of chosen parameters. The analyses of different methods are presented in the following sections.

4.2 Leguerre-SVD Based PMOR Method

A PMOR method utilizing PEEC analysis is proposed in [7]. This method is based on a parameterization process of matrices generated by the PEEC method and a projection subspace obtained from the passivity-preserving Laguerre-SVD MOR technique. However, for implementation of this method for this thesis, instead of using the PEEC analysis, a standard discretization technique for interconnects was used to obtain the system matrices. This PMOR technique was applied to transmission lines of different configurations and simulation results

obtained from different configurations are presented below. A summary of the results is provided at the end of this section.

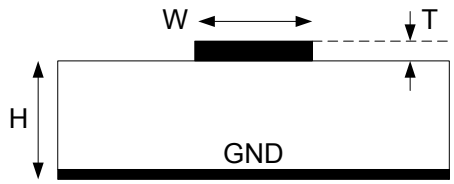

Figure 4.1: Cross section of microstrip transmission line

Figure 4.1 shows the cross section of a microstrip transmission line. The parameters that are varied for this case are the width and thickness of the conductor. The width *W* is varied from *0.5* mm to *2.5* mm and the thickness *T* is varied from *50* um to *150* um. A total of 25 data points are considered for the design grid. For the estimation grid, 9 data points are used and the remaining 16 data points are used for the validation grid. A similar parametric variation and design grid distribution are considered for other applications used for this method, unless specified otherwise. A two-port system is assumed and the transfer function $H_{12}(s)$ is considered as the output. The responses for the minimum, nominal and maximum parameter values are shown in Figure 4.2.

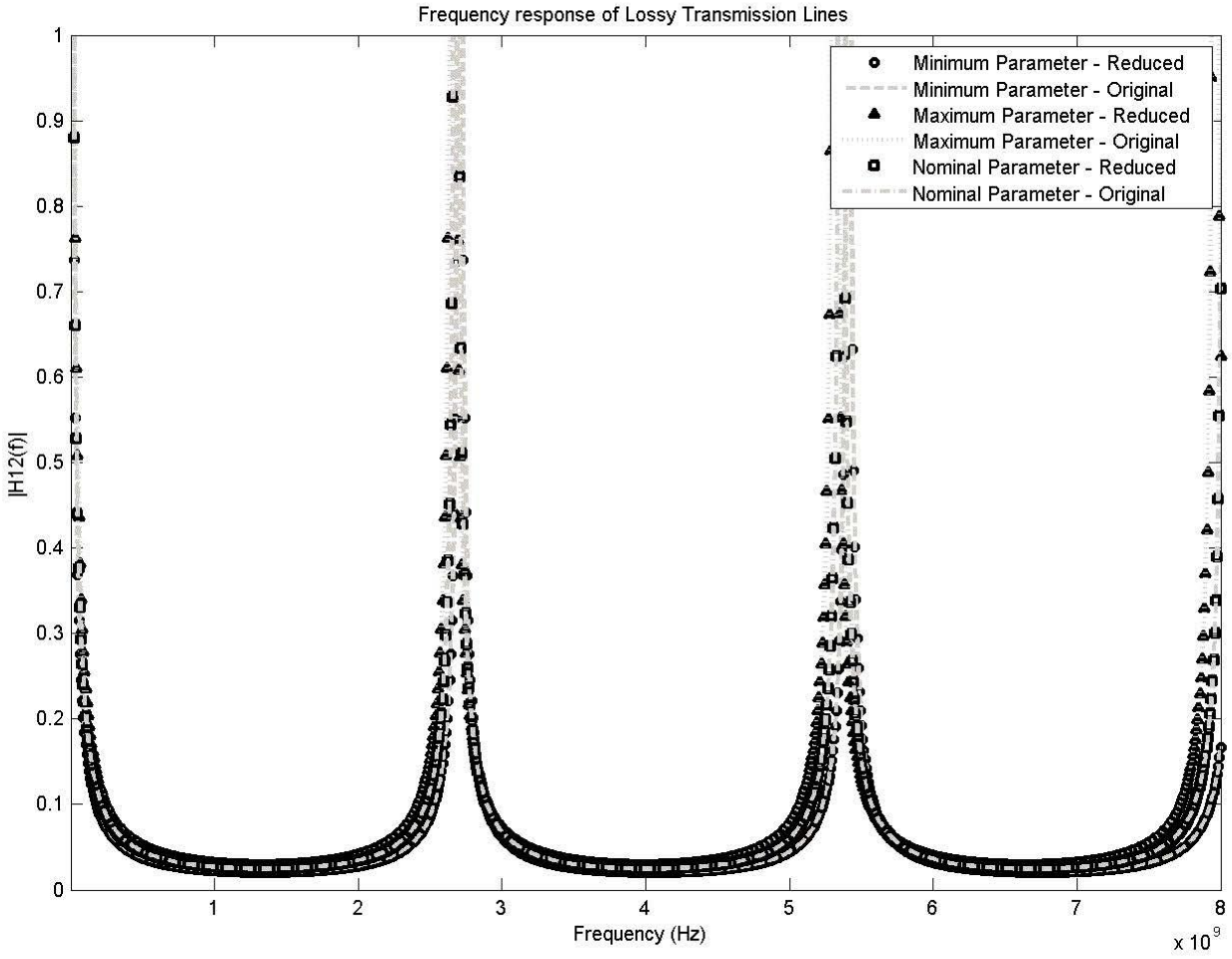

Figure 4.2: Responses of microstrip transmission line (Laguerre-SVD method)

From Figure 4.2, it is found that the responses of the reduced system match closely with the responses of the original system for the minimum (*W = 0.5* mm and *T = 50* um), nominal (*W = 1.5* mm and *T = 100* um) and maximum (*W = 2.5* mm and *T = 150* um) values of the parameter sets. To obtain a quantitative measure of the performance, the relative error between the response of the original system and the reduced system is used. Figure 4.3 shows the relative errors measured for the minimum and maximum sets of the parameters. From this figure, it is noticeable that at lower frequencies the errors are significantly low but the errors increase as frequency increases, which are the general tendency of most PMOR techniques. However, the average error for the entire range of operating frequency is approximately in the order of 10^{-6}; this might be acceptable for several practical applications.

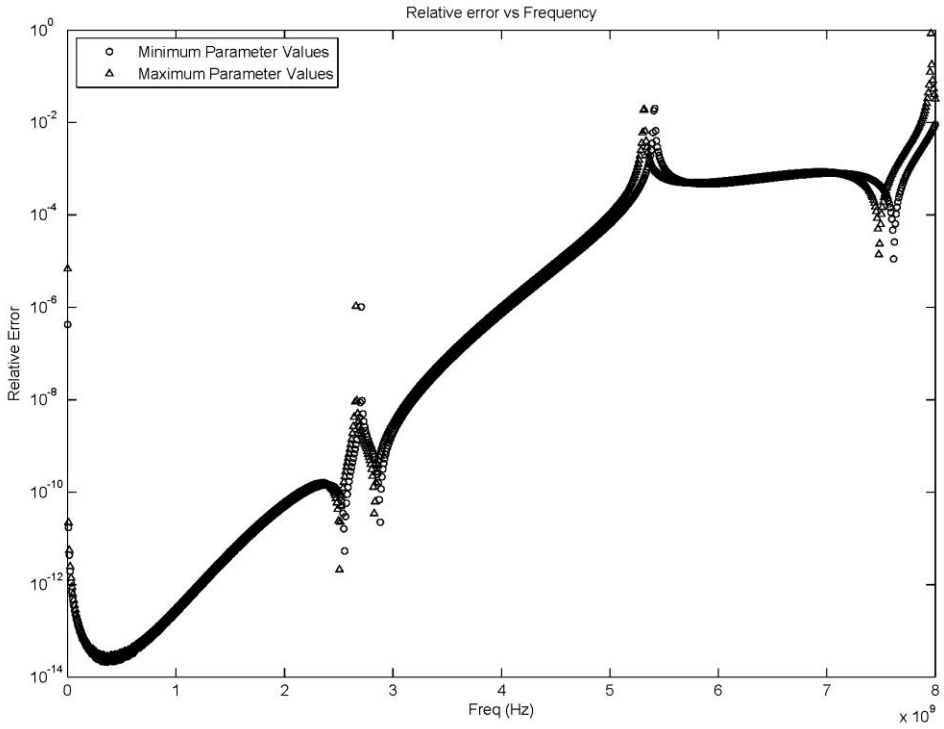

Figure 4.3: Relative errors of the responses (Laguerre-SVD method)

The cross section of coupled transmission lines is shown in Figure 4.4. A similar analysis is performed as in the case of the micro-strip transmission line. The spacing between lines is considered as the second parameter instead of the thickness of the conductor. The spacing *S* is varied from 1 mm to 3 mm. The responses of the system are shown in Figure 4.5.

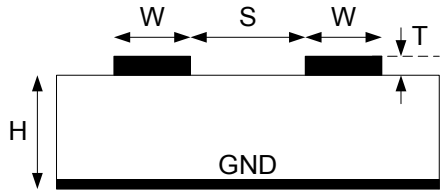

Figure 4.4: Cross section of coupled transmission lines

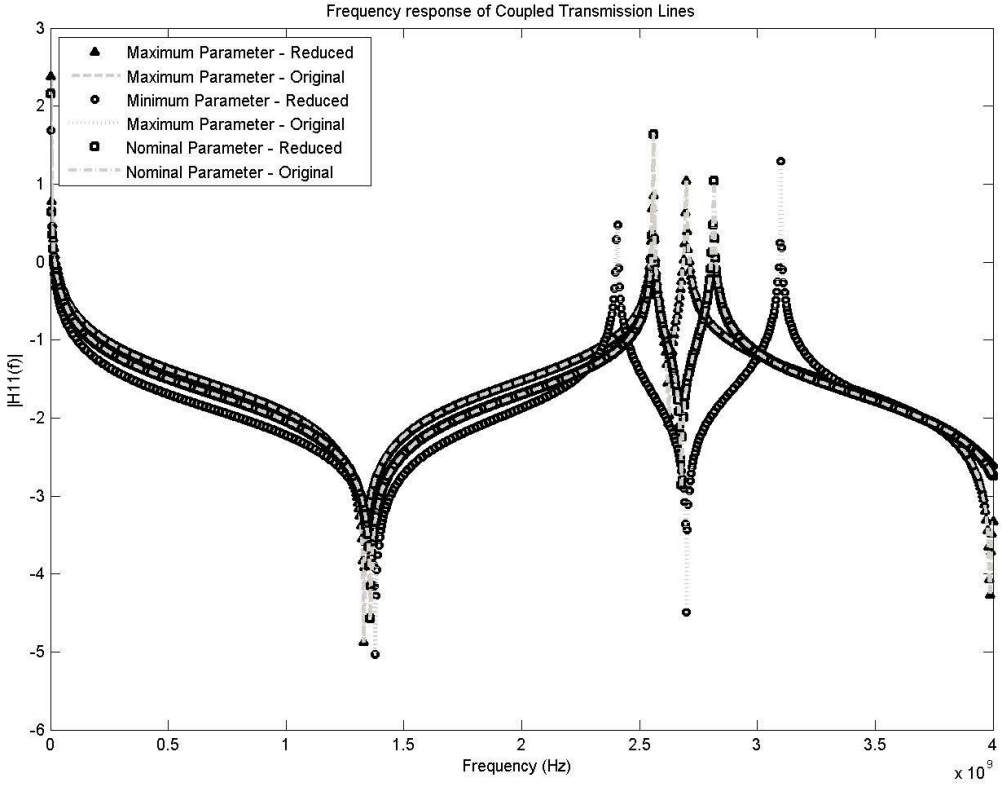

Figure 4.5: Responses of coupled transmission lines (Laguerre-SVD method)

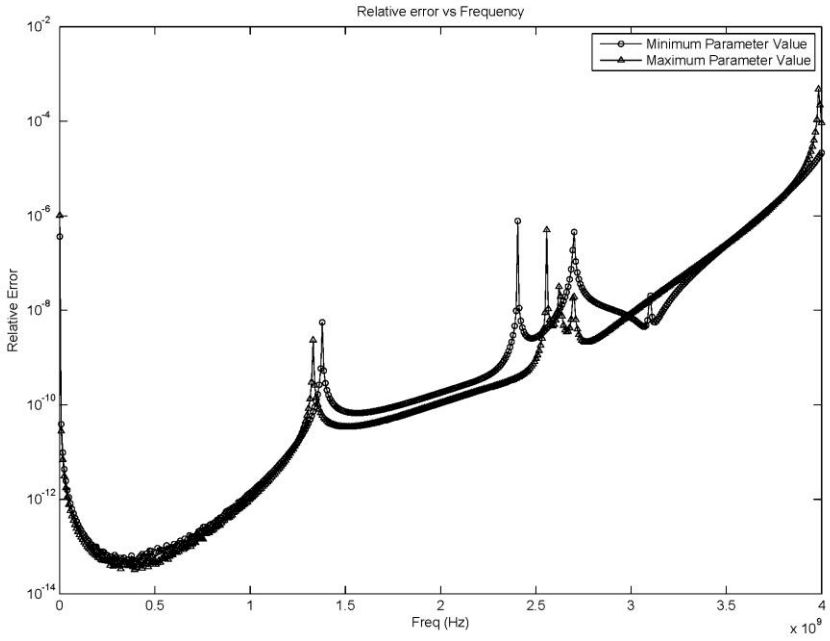

Figure 4.6: Relative errors of the responses (Laguerre-SVD method)

The responses of the reduced system match closely with the responses of the original system for the minimum (*W = 0.5* mm and *S = 1* mm), nominal (*W = 1.5* mm and *S = 2* mm) and maximum (*W = 2.5* mm and *S = 3* mm) values of the parameters sets. The degree of accuracy in performance is shown in Figure 4.6. The average error is below the order of 10^{-8}, however, it sharply rises as the frequency increases. The accuracy of performance not only depends on the number of matched moments but also on the efficiency of the interpolation method to generate the models of different elements, as discussed in Chapter 3.

In the final example, transmission lines of an arbitrary configuration are considered as shown in Figure 4.7. The choice of parameters and their variations are kept the same as that of the microstrip transmission line. The responses for the minimum, nominal and maximum values of the parameters sets are shown in Figure 4.8. The responses of both reduced and original

systems agree quite well. The average error for the responses shown in Figure 4.9 is below the order of 10^{-6}. However, like in the other cases, the relative error increases almost linearly with frequency, which may limit acceptable performance at higher frequencies.

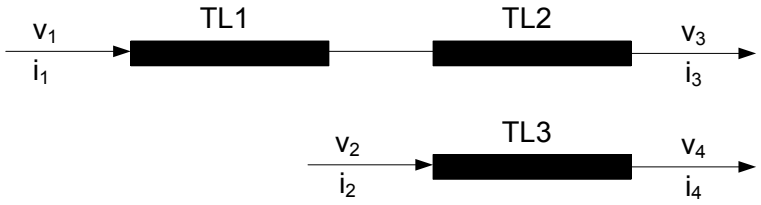

Figure 4.7: Transmission lines with an arbitrary configuration

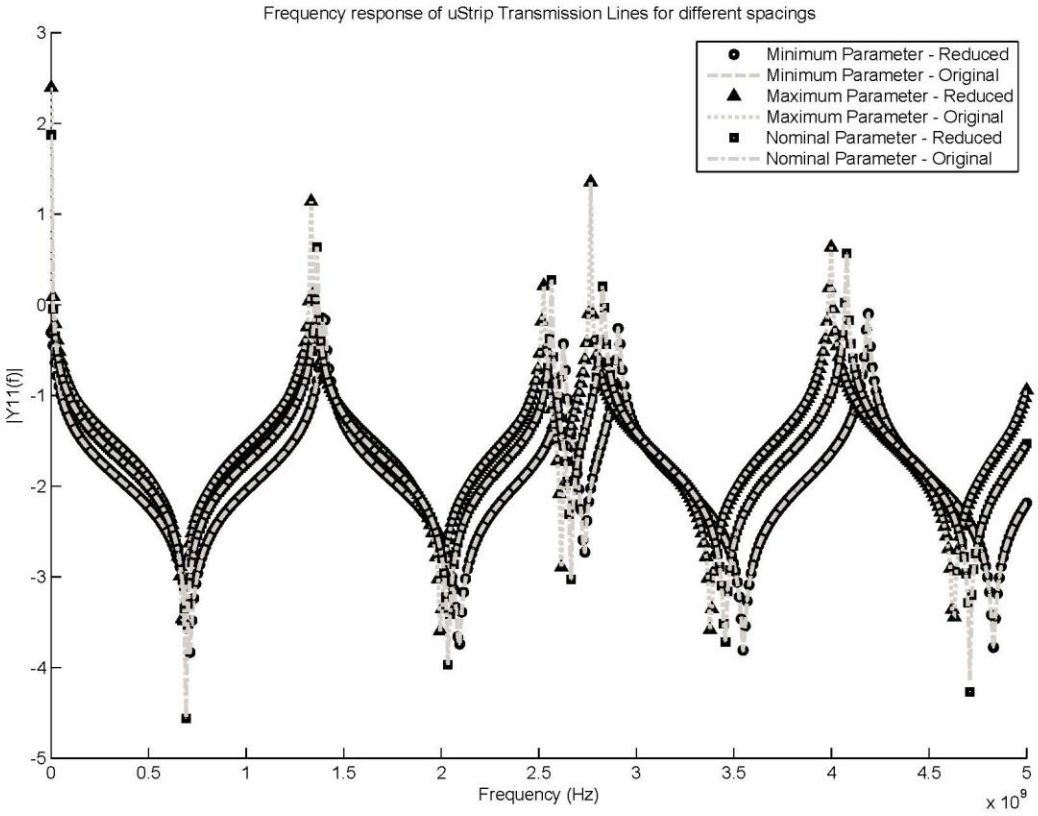

Figure 4.8: Responses of the system (Laguerre-SVD method)

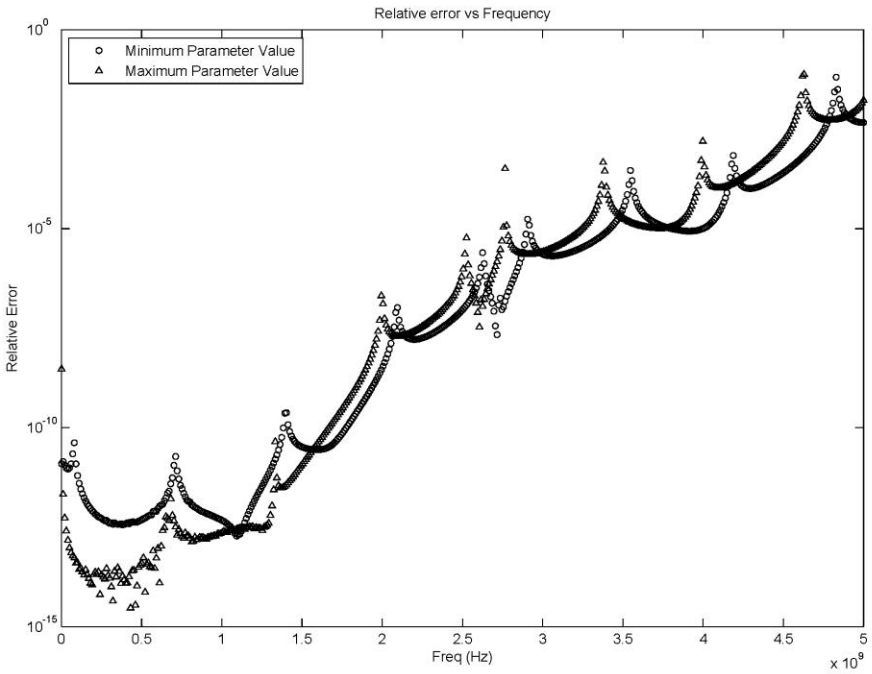

Figure 4.9: Relative errors of the responses (Laguerre-SVD method)

The computational cost of the model can be divided into three parts: (a) computation of the multivariate system and projection matrices, (b) SVD operation to obtain the projection matrix and (c) congruence transformation to obtain the reduced matrices and states. The total computational cost of this method depends on cost involved in all these steps. However, the computational cost of interpolation depends on the chosen interpolation scheme and may vary considerably depending on the selected scheme. Therefore, an efficient interpolation scheme will help to reduce the computational cost. The SVD operation to obtain the orthogonal matrix may increase the computational cost significantly for larger matrices. In such a case, the SVD can be replaced by modified Gram-Schmidt and Householder QR operations [18], [53], which are computationally cheaper [7].

The properties of the system matrices obtained from discretization, the multivariate interpolation scheme preserving positive definiteness [7] and the passivity preserving Leguerre-SVD MOR techniques used in this PMOR method. All of them guarantee the overall stability and passivity of this method. Also, the modified ordinary splines based interpolation technique used in [7] can preserve positive definiteness when applied to positive definite matrices. The method relies on a Krylov subspace based projection that eliminates the possibility of ill-conditioning. The evaluation of the model for the given design space is found to be numerically stable. This method, however, does not preserve the structure after reduction and scalability is not taken into consideration. A summary of the results obtained from different applications is listed in Table 4.1.

Table 4.1: Summary of results for Leguerre-SVD based PMOR method

Example	Order		Cost		Average Rel. Error	Ill-cond.	Passivity
	Org.	Red.	Org. (sec)	Red. (sec)			
TL1	401	28	9.1689	0.3257	~ 10^{-6}	No	Yes
TL2	402	32	15.2432	0.4135	~ 10^{-8}	No	Yes
TL3	422	40	20.5637	0.6251	~ 10^{-6}	No	Yes

4.3 Optimization based PMOR Method

In addition to conventional moment matching or balance truncation or interpolation based techniques to obtain the projection matrix, optimization techniques may present an alternate choice, especially, when the closed form expressions required for Taylor series are not available. Optimization can be achieved using different techniques. The method in [54] utilizes the recursive least square (RLS) optimization method. The optimal block vectors are used to construct the projection matrix, such that the system errors in the whole parameter space are minimized. This PMOR technique is characterized below using the applications presented in the previous section.

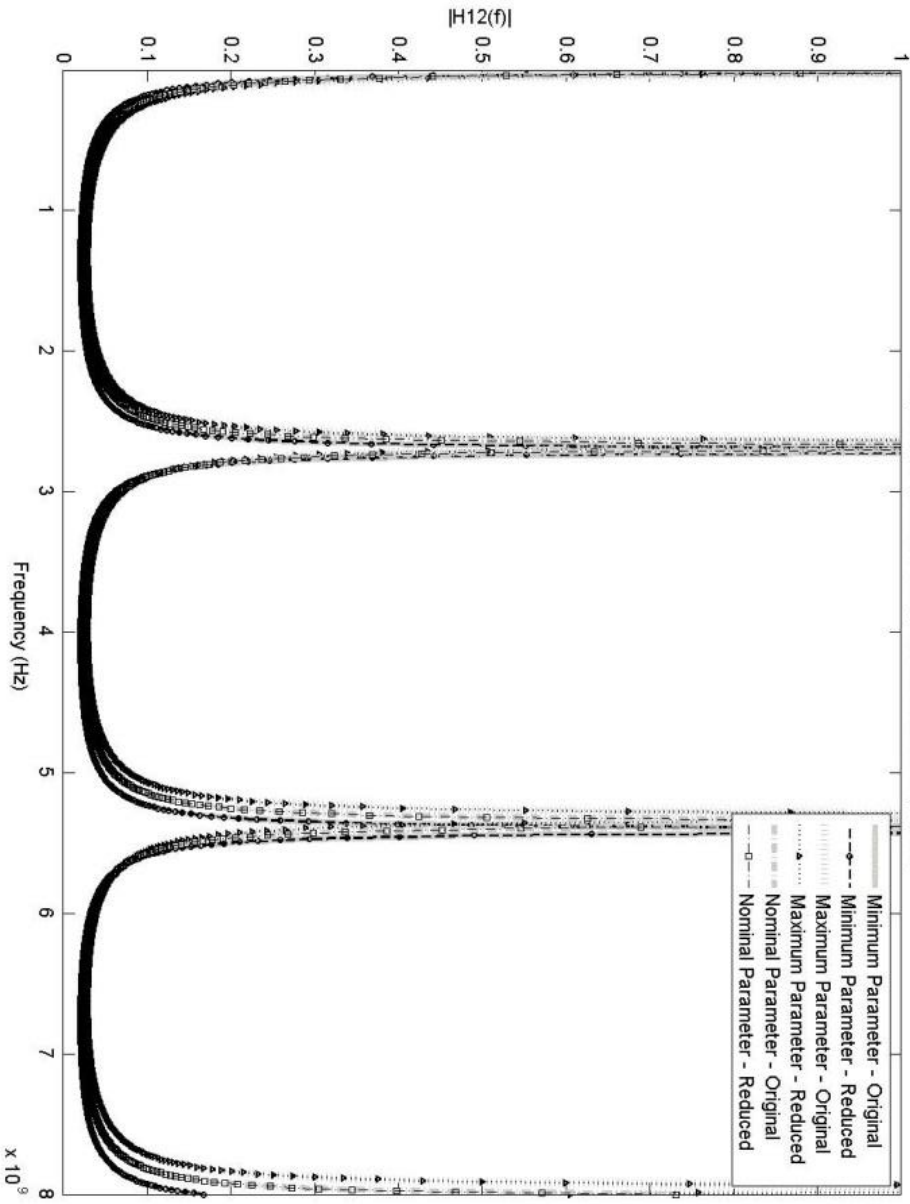

Figure 4.10: Responses of the system (Optimization based method)

Consider the lossy microstrip transmission line as shown in Figure 4.1. The selection of parameters and their ranges is the same as that presented in the previous section. The transfer function for a frequency range up to 8 GHz obtained from the simulation is shown in Figure 4.10.

The reduced system approximates the original system quite well up to the specified frequency range. The relative errors are plotted in Figure 4.11 for the entire range of frequency under consideration. The average error is approximately of the order of 10^{-4}. A notable change in the variation of the error is that it is somewhat periodic in nature, instead of a growing tendency of error as frequency increases. This property can make a method a better choice for high frequency, provided that the average error remains below the desired limit. However, it depends on how well the optimization can be performed as the complexity of the system increases. This method was found to be conditionally passive. The poles of the system are shown in Figure 4.12, which indicates that the system is stable.

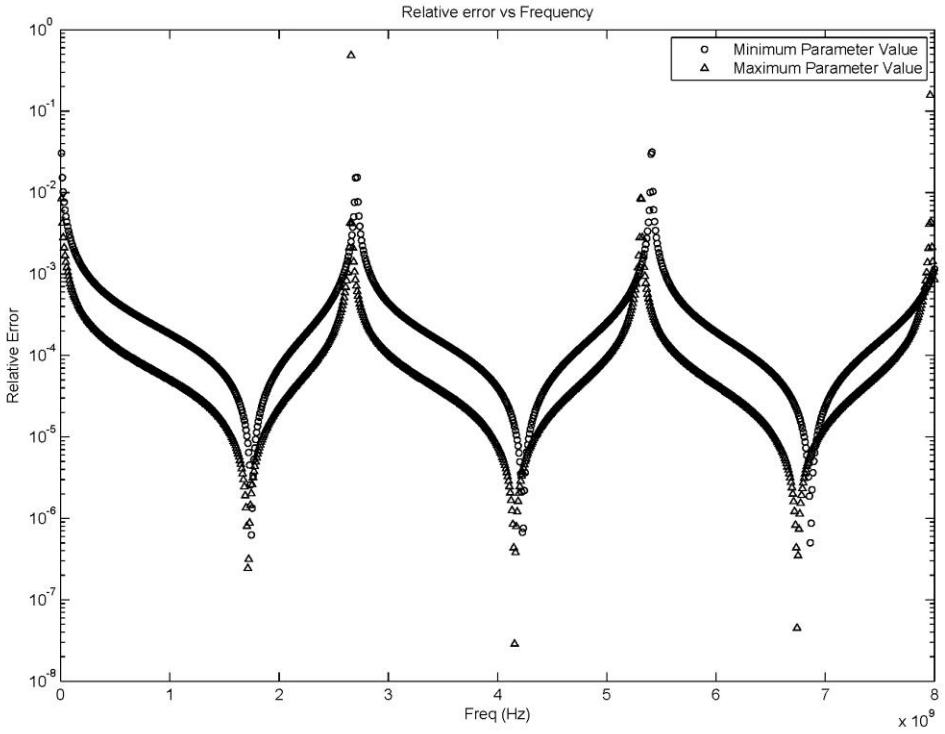

Figure 4.11: Relative errors of the responses (optimization based method)

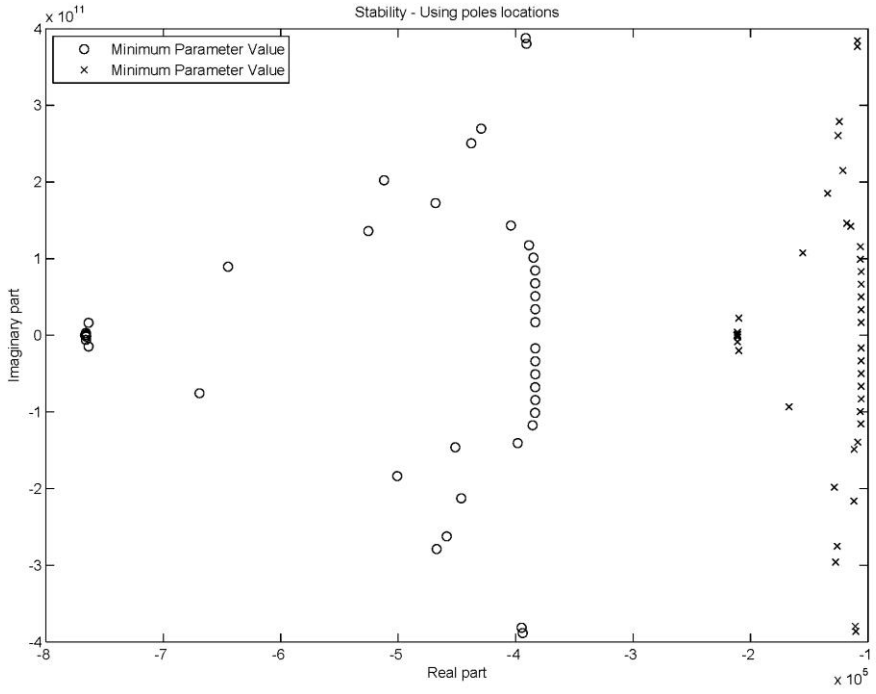

Figure 4.12: Poles of the system (Optimization based method)

The transfer function responses of the coupled transmission lines system are shown in Figure 4.13. The responses of the reduced system are in accordance with the responses of the original system for the entire frequency range. The relative errors are shown in Figure 4.14 and the average error increases approximately to the order of 10^{-2}, which is higher than that of the previous method and also that from the previous application. This is an indication that the optimization technique may require a greater effort to find an optimized solution as the complexity of the system increases. Also it is noticeable that the variation in the error starts deviating from periodic nature and exhibits the tendency of higher error with the increase in the frequency of operation. The plots of the poles of the system for the minimum and maximum sets of the parameters are shown in Figure 4.15. The plots indicate that the overall system is stable.

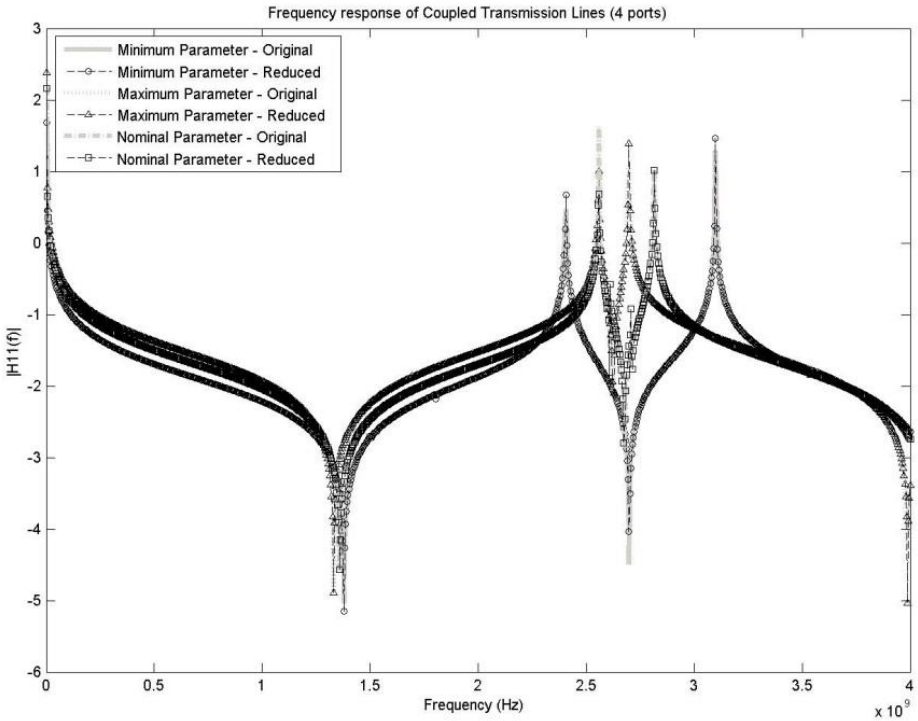

Figure 4.13: Responses of the system (Optimization based method)

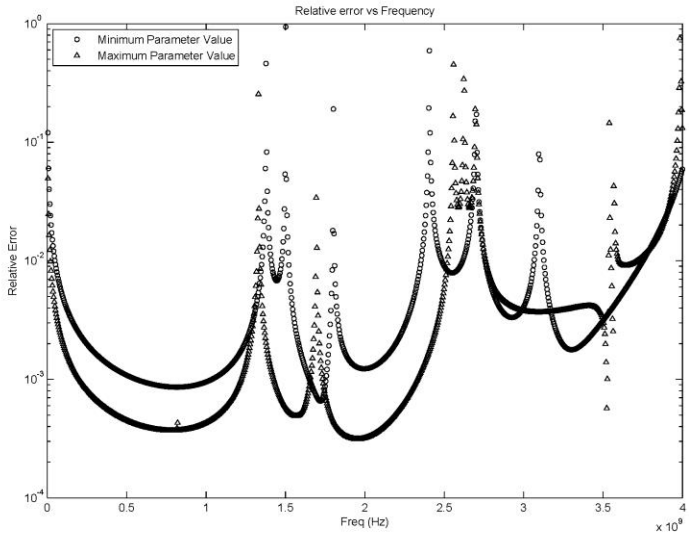

Figure 4.14: Relative errors of the responses (Optimization based method)

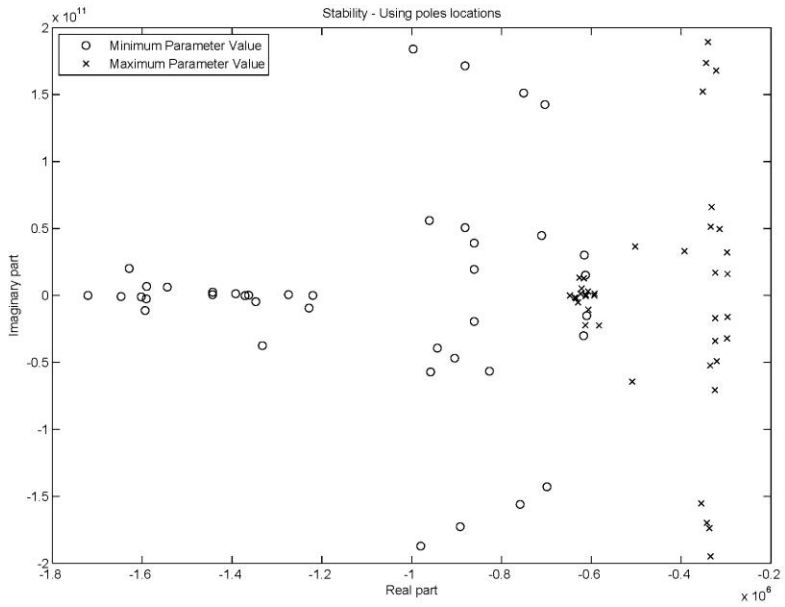

Figure 4.15: Poles of the system (Optimization based method)

Finally, the optimization based PMOR method is applied to the transmission lines system shown in Figure 4.7. The transfer function responses are shown in Figure 4.16. The order of the reduced system starts increasing as the complexity of the system grows. Additionally, the performance of the reduced system starts deviating from the original system at higher frequencies. This tendency of lower performance is also indicative from the relative errors shown in Figure 4.17. The average error for the minimum parameter set is more than the order of 10^{-1} while the average error is less than the order of 10^{-2} for the maximum set. However, at higher frequencies the errors may exceed the acceptable limit. The error is relatively higher for minimum set of the parameters than the maximum set, which is due to the effect of performance variation of the optimization process at different sets of parameters. The stability, however, is maintained within the operating range of the frequency as found from the plots of the poles in Figure 4.18.

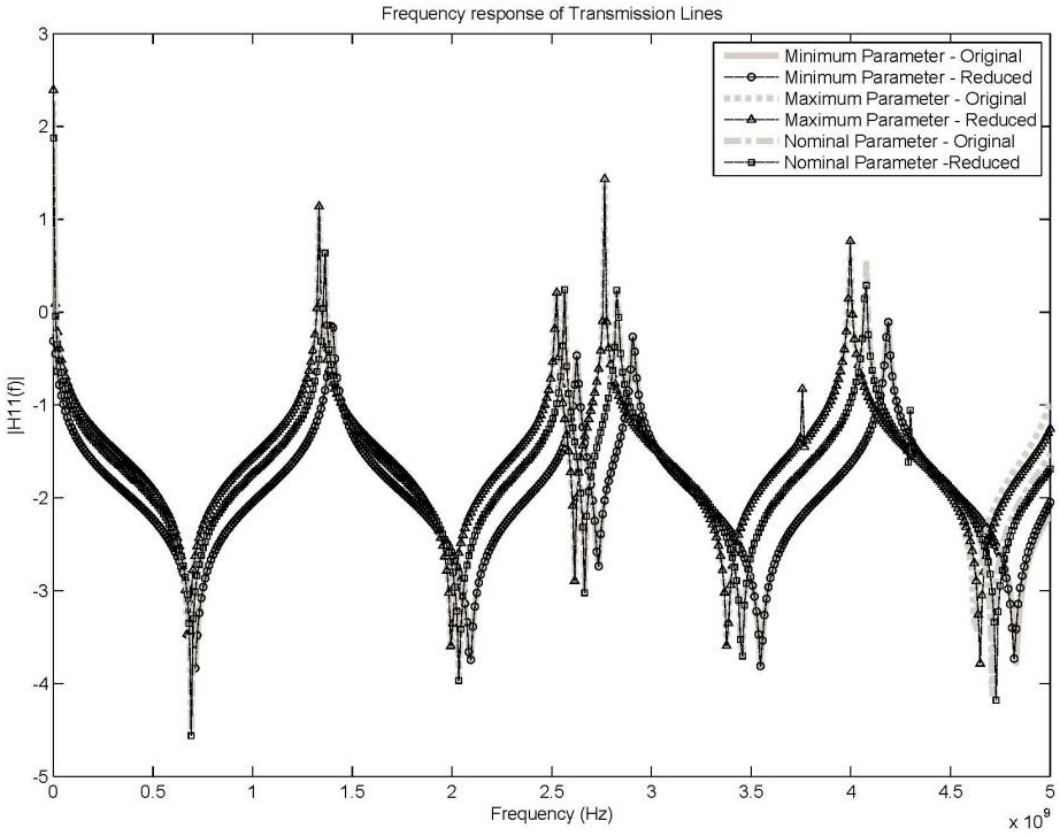

Figure 4.16: Responses of the system (Optimization based method)

Table 4.2 summarizes the results obtained from this method. It should be noted that the simulation time of the original system is the same as that presented when characterizing the previous PMOR method. This method is not scalable and does not preserve the structure of the system.

Table 4.2: Summary of results for Optimization based PMOR method

Example	Order		Cost		Average Rel. Error	Ill-cond.	Passivity
	Org.	Red.	Org. (sec)	Red. (sec)			
TL1	401	36	9.1689	0.4830	~ 10^{-4}	No	Yes
TL2	402	42	15.2432	0.6423	~ 10^{-2}	No	Yes
TL3	422	56	20.5637	0.7915	~ 10^{-1}	No	Yes

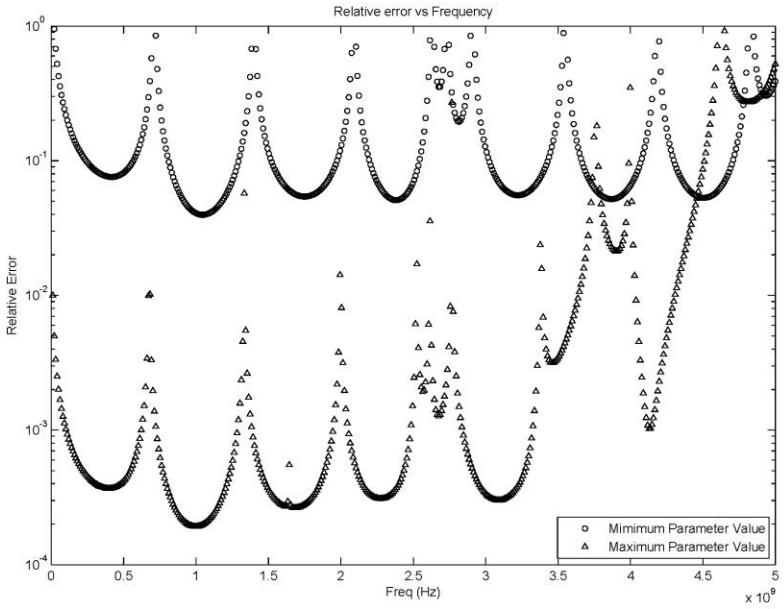

Figure 4.17: Relative errors of the responses (Optimization based method)

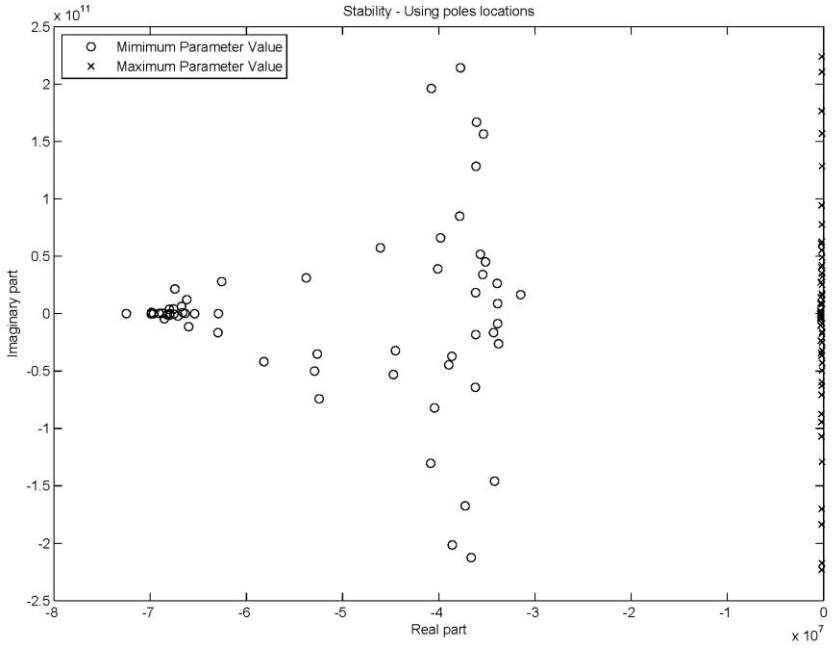

Figure 4.18: Poles of the system (Optimization based method)

4.4 Multi-parameter Moment-Matching PMOR Method

The multi-parameter moment matching technique is suitable for simple systems and it has limitations as the complexity of the system increases. The authors only considered resistance and capacitance of the interconnect model and did not include any inductance in the model. However, in this thesis, inductance is included in the interconnect model and found performance degradation, which the authors also anticipated. The model requires known closed form expressions of the system matrices because the moment matching technique is based on series expansion of the parameter-dependence. This PMOR technique is analyzed below with the example systems under consideration.

For the microstrip transmission line example of Figure 4.1, the parameters and their variations remain the same as before. The sensitivities of different circuit elements are considered up to second order for each individual parameter and first order cross term for different parameters. Figure 4.19 shows the frequency responses for different sets of parameters and the relative errors of the generated responses are shown in Figure 4.20.

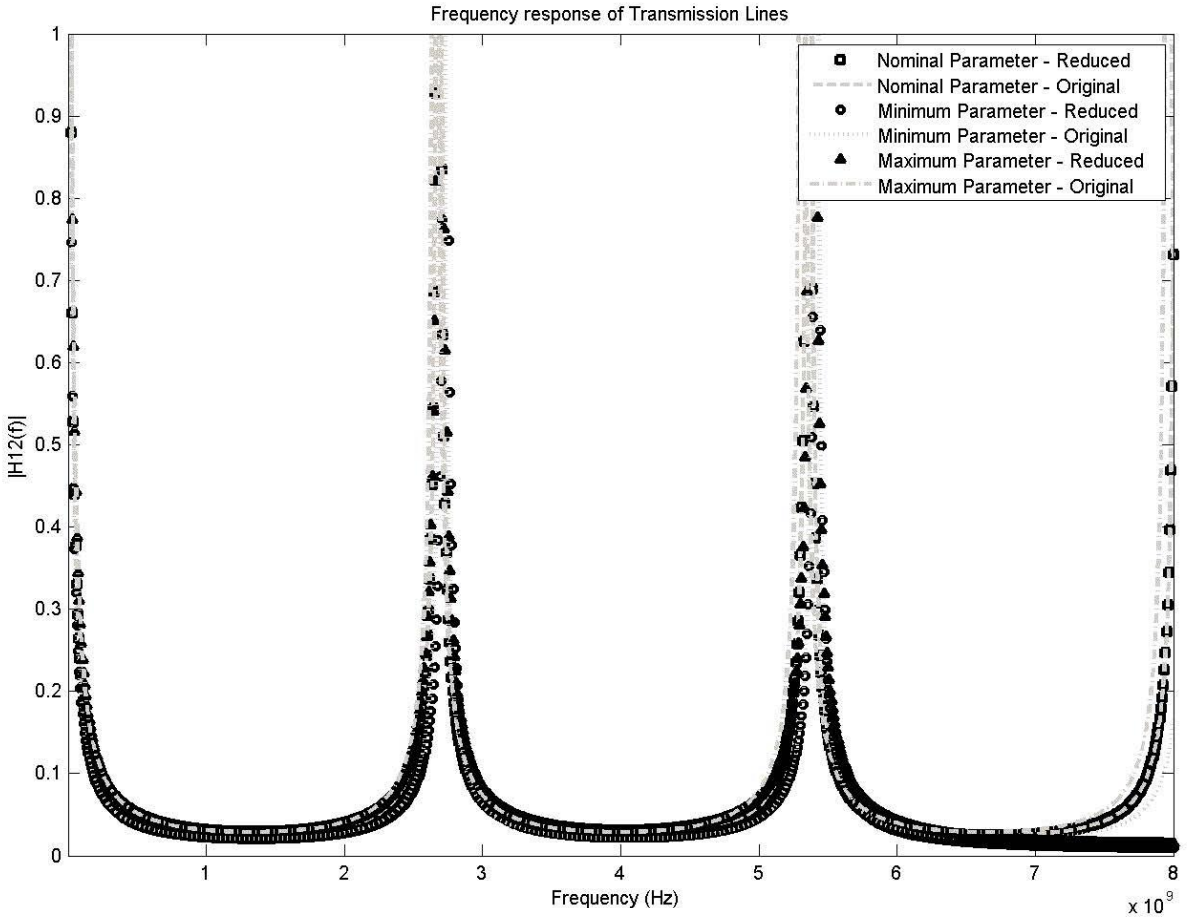

Figure 4.19: Responses of the system (MMM based method)

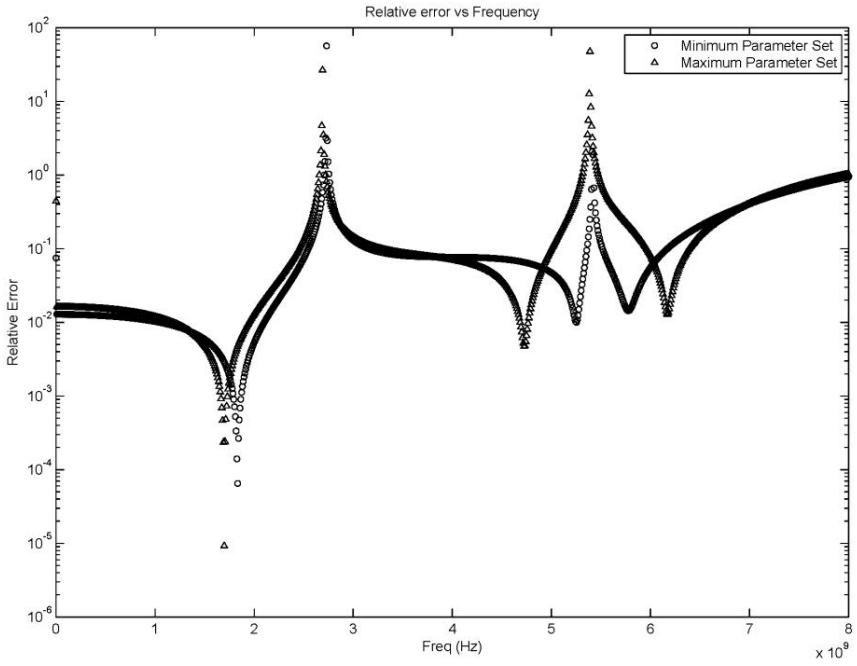

Figure 4.20: Relative errors of the responses (MMM based method)

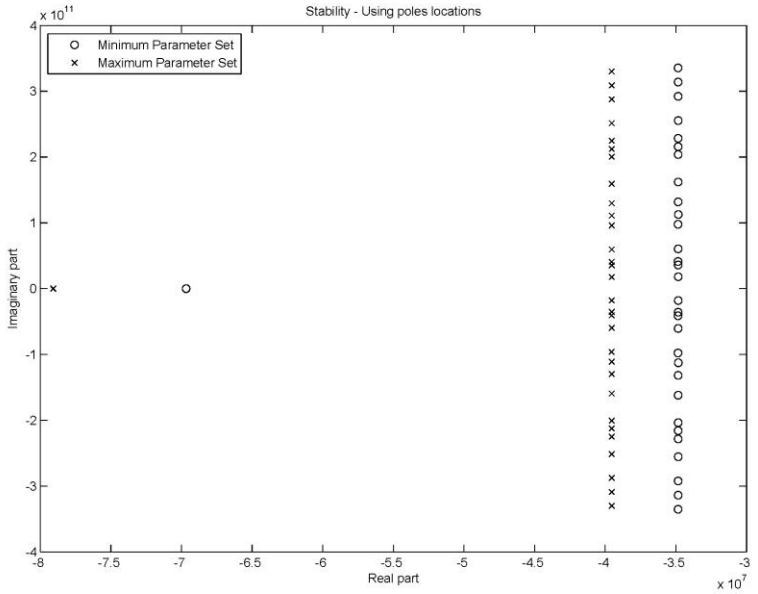

Figure 4.21: Poles of the system (MMM based method)

This method worked well at low frequencies. However, at higher frequencies its performance degraded rapidly and the error reached to an unacceptable level as found from Figure 4.20. The average error is approximately to the order of 10^{-1}. Also, the original responses obtained from Taylor series expansion deviate from the actual response due to the inaccuracy arising from such expansion. This method does not provide any guarantee regarding passivity of the system. Therefore, the stability of the system must be examined. The system remains stable as indicated from the plots of poles given in Figure 4.21.

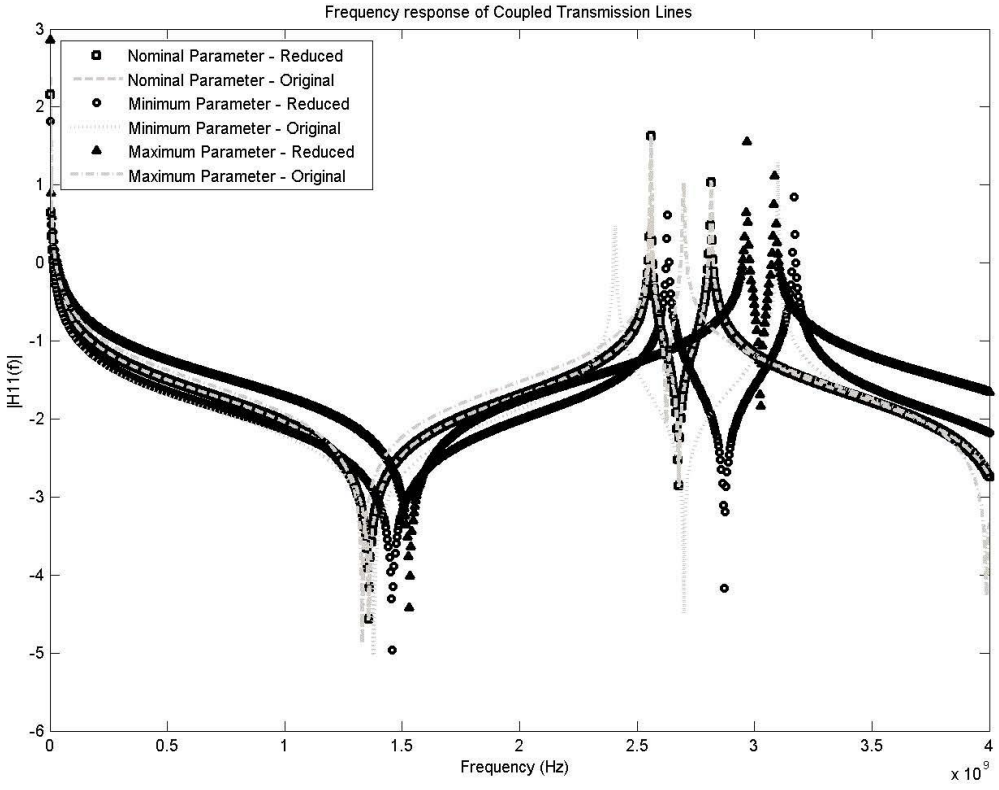

Figure 4.22: Responses of the system (MMM based method)

The coupled transmission lines of Figure 4.4 are considered next. The responses of the system are shown in Figure 4.22. It is notable that the performance degraded at a frequency

lower than that of the previous example. A reason for this degradation is the increasing complexity of the system. The moment matching technique used in this method is not efficient enough to preserve the moments well when the complexity of the system grows. This is also indicative from the observation that increasing the order of the reduced model does not improve the performance significantly. The relative errors are shown in Figure 4.23. The average error becomes higher than the order of 1 at higher frequencies and become unacceptable for relatively complex applications, especially, at higher frequencies. The system remains stable within the upper and lower bound of the parameter variation. However, there is no guarantee of stability because the method itself is not passive. The plots of poles of the system are shown in Figure 4.24, which ensured that the system under consideration is stable.

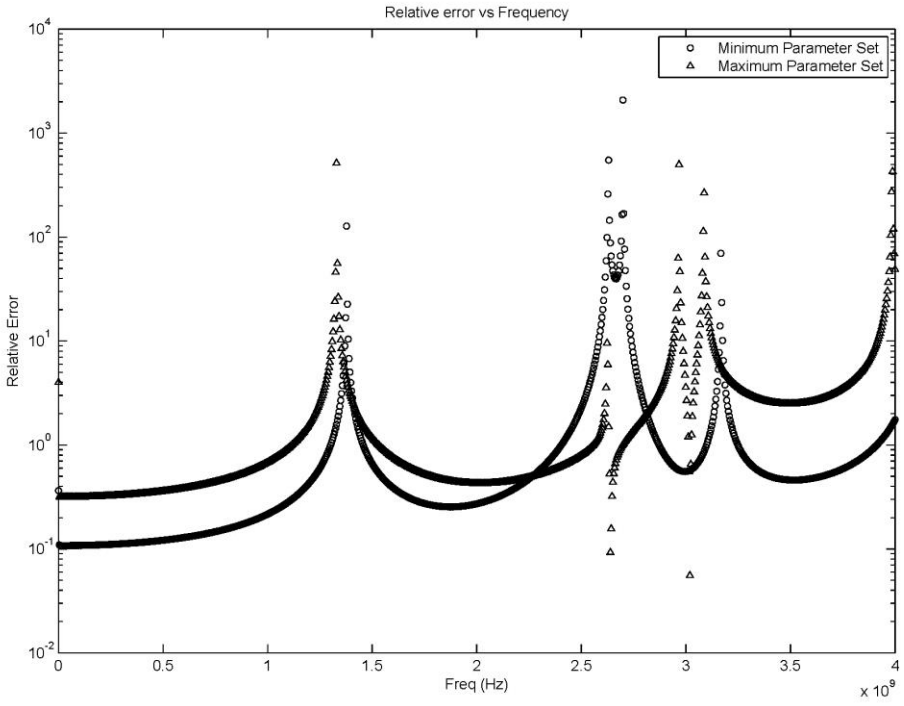

Figure 4.23: Relative errors of the responses (MMM based method)

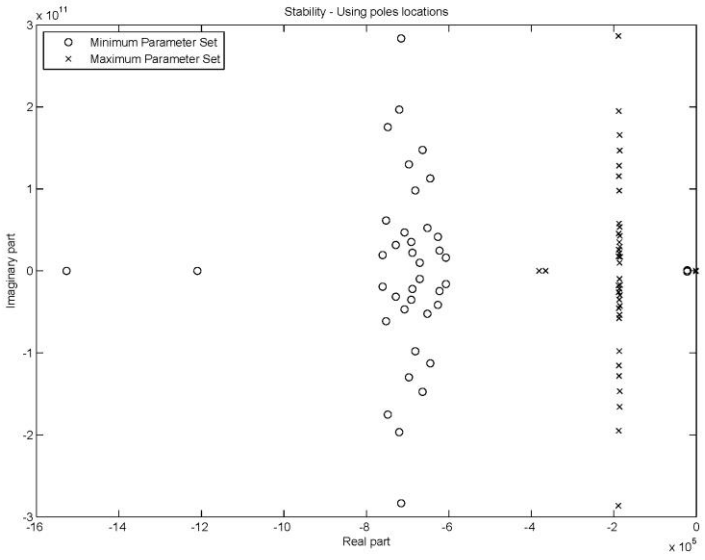

Figure 4.24: Poles of the system (MMM based method)

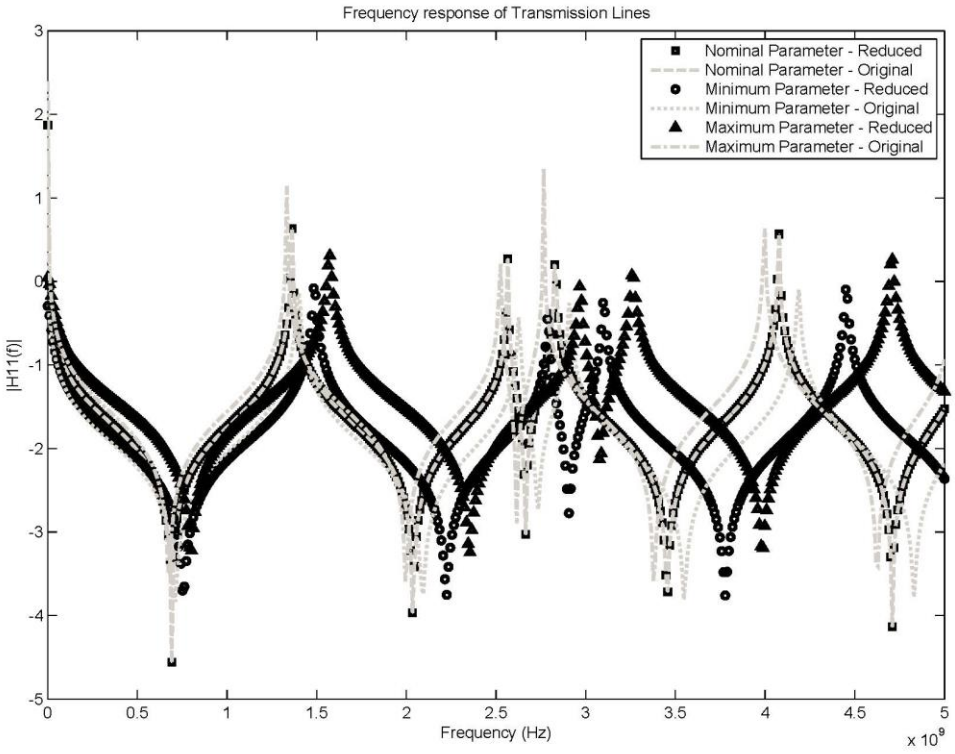

Figure 4.25: Responses of the system (MMM based method)

The responses of transmission lines of arbitrary configuration are shown Figure 4.25. The relative errors tend to increase, as expected, with higher complexity as shown in Figure 4.26. The order of the reduced system also increases notably in comparison to the previous systems. The reduced response also starts to deviate at sharp transitions in the response. This is mostly due to the use of Taylor series expansion, which utilizes only a single expansion point. The performance, however, can be improved by using Taylor series with multiple expansion points.

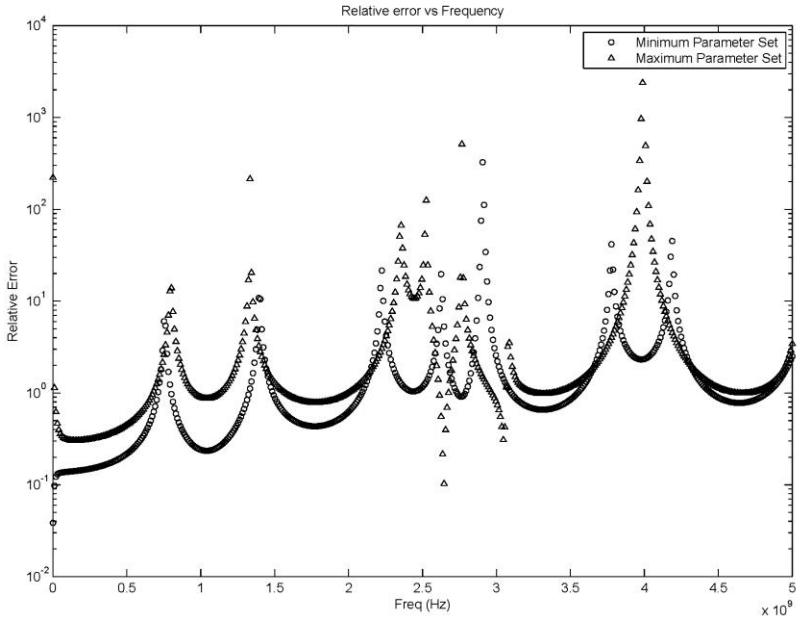

Figure 4.26: Relative errors of the responses (MMM based method)

The poles of the system are shown in Figure 4.27, which indicates that the system is stable. A summary of results for this method is listed in Table 4.3. The major disadvantage of this method is that it does not guarantee passivity, however, the systems were found to be stable. There was indication of ill-conditioning during model evaluation. Furthermore, it does not consider structure preservation or scalability of the model.

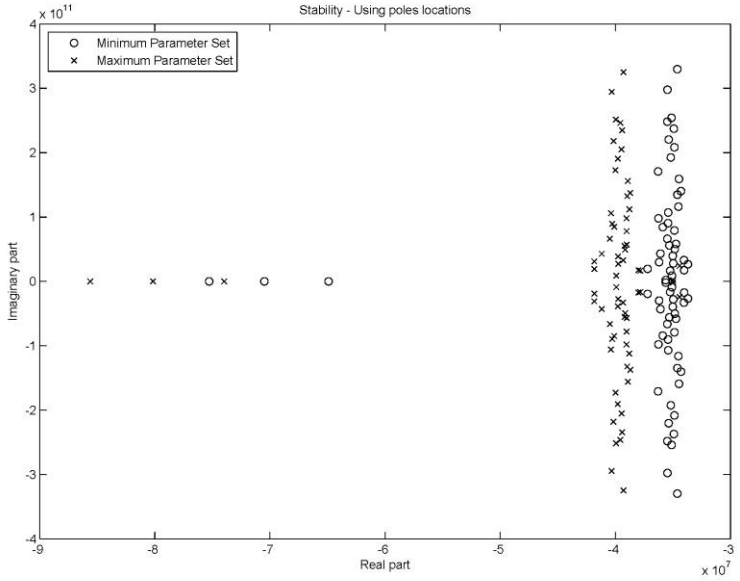

Figure 4.27: Poles of the system (MMM based method)

Table 4.3: Summary of results for MMM based PMOR method

Example	Order		Cost		Average Rel. Error	Ill-cond.	Passivity
	Org.	Red.	Org. (sec)	Red. (sec)			
TL1	401	32	9.1689	0.4126	~ 10^{-1}	Yes	No/Stable
TL2	402	40	15.2432	0.6261	~ 1	Yes	No/Stable
TL3	422	64	20.5637	0.9617	~ 1	Yes	No/Stable

4.5 SPARE PMOR Method

A scalable algorithm for passive, structure preserving, parameter-aware model order reduction (SPARE) is proposed in [10]. This technique also utilizes the closed form representations of system matrices and Taylor series expansions like the method discussed in the previous sub-section. However, this method can show an improvement in the accuracy of the response over the previous method, especially, for applications with smooth variation in responses. Moreover,

this method has additional advantages, such as passivity, scalability and preservation of structure.

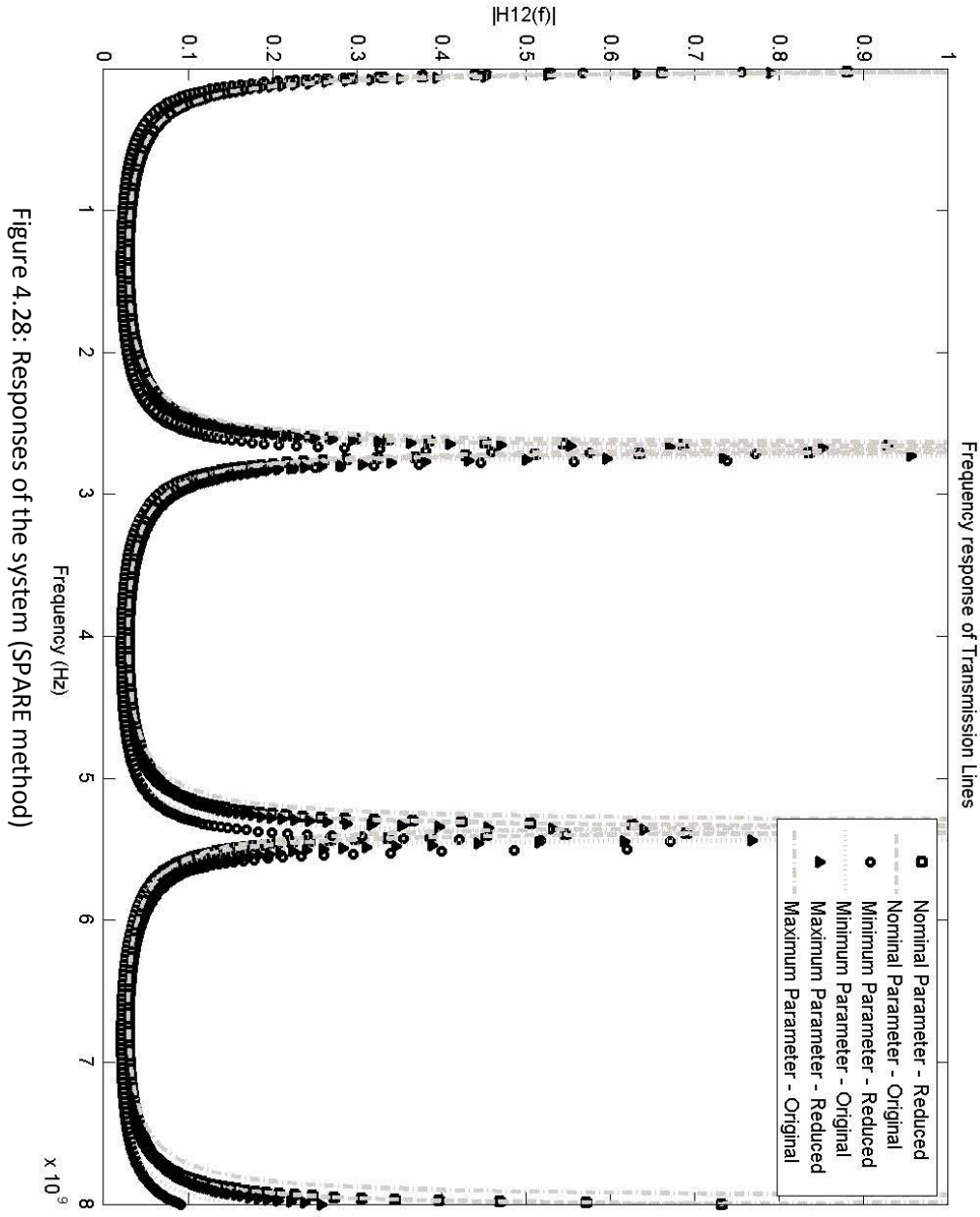

Figure 4.28: Responses of the system (SPARE method)

In general, as mentioned above, this method suffers from the same limitation arising from inaccuracy associated with a Taylor series expansion as discussed in the previous section. In addition, the deviation in the original response may arise from the truncation of the closed form expressions derived from methods like curve fitting techniques. This issue can be addressed to some extent by including higher orders in the closed form formulations. However, this introduces the additional cost of model construction. Also, the method deals with augmented matrices that may cause numerical stability problems. The performance of this method for the examples under consideration is presented below. The responses of a lossy microstrip transmission line are shown in Figure 4.28. It can be seen from the figure, the deviation in the responses due to the above issues starts to dominate when the variation in the responses is not smooth. Figure 4.29 shows the relative errors and the errors are approximately of the order of 10^{-2}.

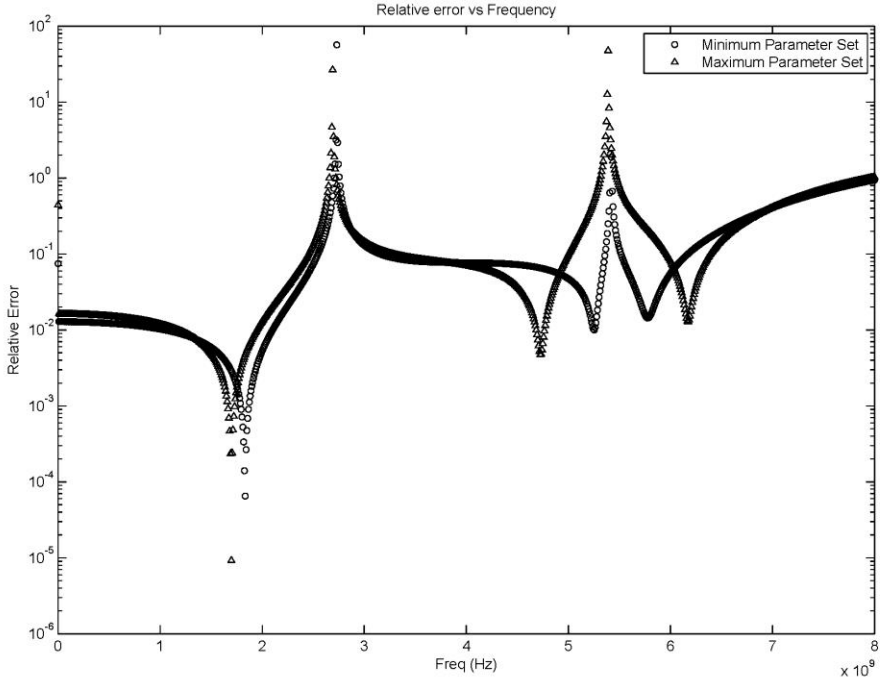

Figure 4.29: Relative errors of the responses (SPARE method)

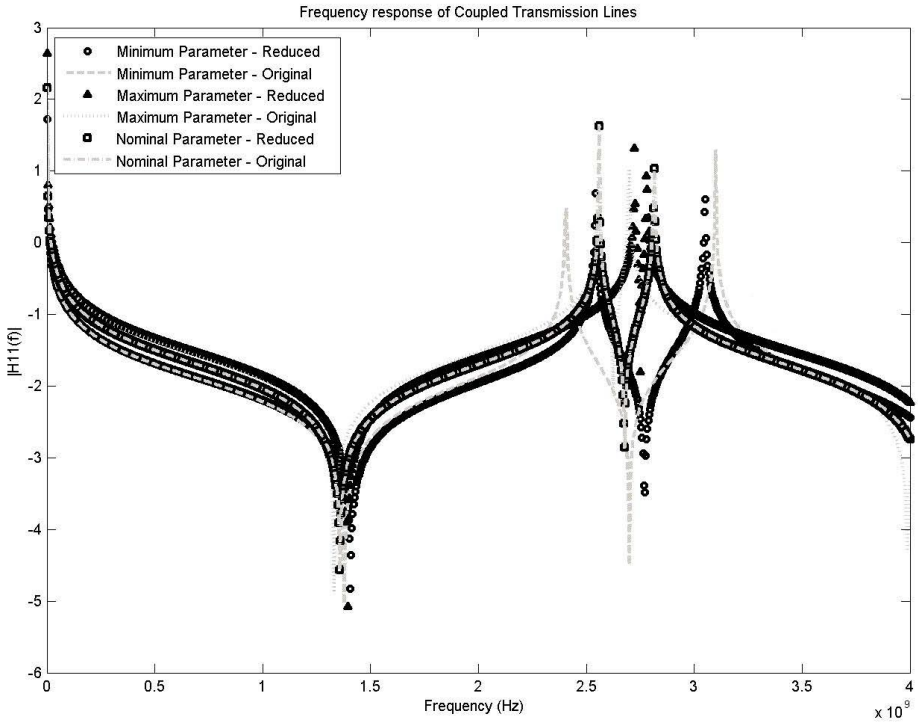

Figure 4.30: Responses of the system (SPARE method)

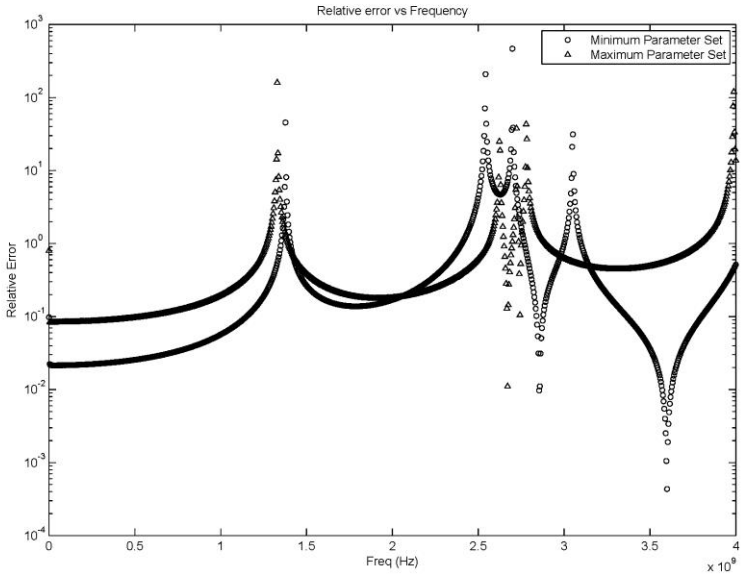

Figure 4.31: Relative errors of the responses (SPARE method)

The responses of the coupled transmission lines are shown in Figure 4.30 for the same variation in the parameters. The relative errors are shown in Figure 4.31, which indicates the tendency of increased errors as the complexity of the structure increases. The errors are approximately in the order of 10^{-1}.

For transmission lines of an arbitrary configuration, the responses are shown in Figure 4.32. The corresponding relative errors are shown in Figure 4.33. The results, again, indicate that the complexity of the structures may limit the performance. The relative errors, in this case, exceed the order of 10^{-1}.

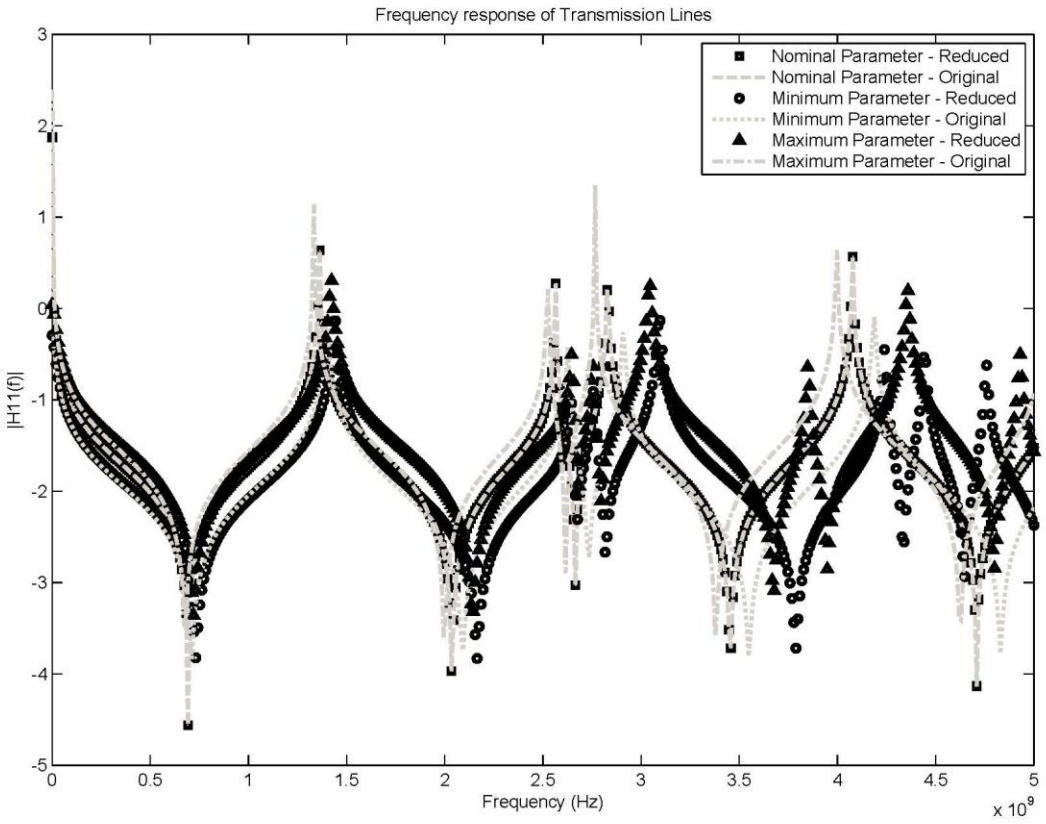

Figure 4.32: Responses of the system (SPARE method)

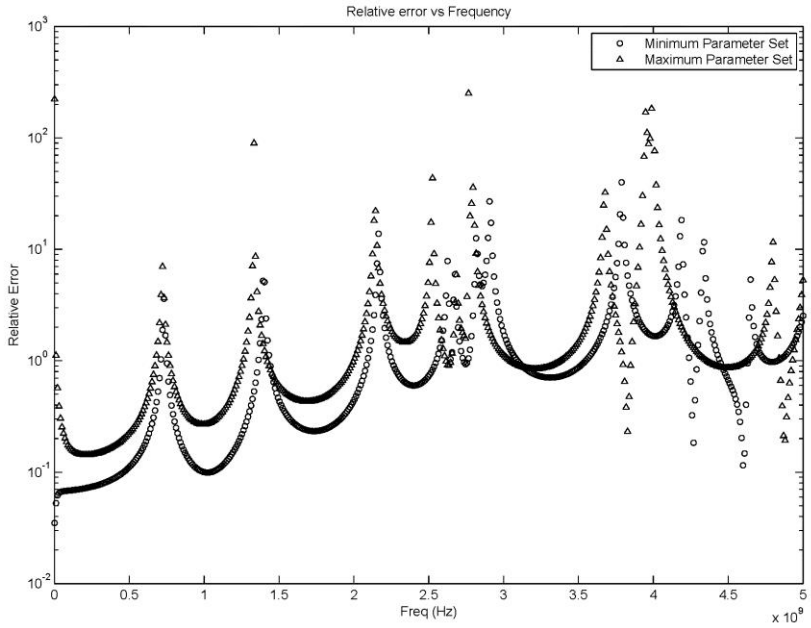

Figure 4.33: Relative errors of the responses (SPARE method)

The preservation of structure during the reduction process helps in improving the computational expense of the model. The block lower triangular matrices in the SPARE model can be exploited in a recursive manner. Thus the number of nominal transfer functions of reduced order that need to be solved for each frequency point can be decreased. For example, the transfer function of first order with respect to one parameter can be given as [10]

$$\hat{x}_{00}(s_i) = \left(\hat{G}_{00} + s_i\hat{C}_{00}\right)^{-1}\hat{B}_{00}$$

$$\hat{H}_{00}(s_i) = \hat{E}_{00}\hat{x}_{00}$$

$$\hat{H}_{10}(s_i) = \hat{E}_{10}\left(\hat{G}_{00} + s_i\hat{C}_{00}\right)^{-1}\left(\hat{G}_{10} + s_i\hat{C}_{10}\right)\hat{x}_{00} \qquad (4.2)$$

The above calculation requires two solutions of full block matrices and a matrix-vector multiplication. This may help to reduce the cost of using SPARE models in comparison to traditional full Taylor series models. The parameterized response can be obtained from the

linear combination of multiple transfer functions as given in (3.30). The computational cost of this operation is relatively cheap. As for passivity, the sufficient condition for passivity of an arbitrary system is that $B = L^T$, and C and G are positive semi-definite (PSD). SPARE complies with the first condition. The proof of the second condition is given in [10] for this method. This method also has the additional advantage of scalability and structure preservation of the model. However, it should be noted that dealing with the augmented system may lead to numerical instability if not handled carefully. The method does not work well when the variation in the response is not sufficiently smooth. Also, the augmentation method may counterbalance the overall improvement of the computational cost of the reduced system, as observed from the simulation. A summary of results for different applications is listed in Table 4.4. The order indicated in the system relates to the augmented system.

Table 4.4: Summary of results for SPARE PMOR method

Example	Order		Cost		Average Rel. Error	Ill-cond.	Passivity
	Org.	Red.	Org. (sec)	Red. (sec)			
TL1	966	160	9.1689	1.8236	~ 10^{-2}	Yes	Yes
TL2	972	168	15.2432	3.3373	~ 10^{-1}	Yes	Yes
TL3	1020	192	20.5637	5.1892	~ 10^{-1}	Yes	Yes

4.6 Comparison between Different Methods

The individual analysis of each method is presented in the above sections. Based on the above analyses, a comparison of the relative scopes and limitations associated with different methods is presented in this section. Some suggestions on possible improvements is discussed along with it. Table 4.5 shows the information accumulated from the above sections for all the PMOR algorithms that were characterized.

Table 4.5: The selected criteria and the results obtained for different PMOR methods

Criteria	Applications	L-SVD	Optimization	MMM	SPARE
CPU Time	TL1	0.3257	0.4830	0.4126	1.8236
	TL2	0.4135	0.6423	0.6261	3.3373
	TL3	0.6251	0.7915	0.9617	5.1892
Average error	TL1	$\sim 10^{-6}$	$\sim 10^{-4}$	$\sim 10^{-1}$	$\sim 10^{-2}$
	TL2	$\sim 10^{-8}$	$\sim 10^{-2}$	~ 1	$\sim 10^{-1}$
	TL3	$\sim 10^{-6}$	$\sim 10^{-1}$	~ 1	$\sim 10^{-1}$
Ill-condition	TL1	No	No	Yes	Yes
	TL2	No	No	Yes	Yes
	TL3	No	No	Yes	Yes
Passivity	TL1	Yes	Yes	No	Yes
	TL2	Yes	Yes	No	Yes
	TL3	Yes	Yes	No	Yes

It is important to note that the strengths and weaknesses of PMOR methods depend on the range of parameters values and the number of parameters taken into consideration. Moreover, the performances of PMOR methods can be significantly influenced by the types and complexities of the selected applications. Therefore, this comparison is based on the selected parameters and their ranges and it is derived from the observed performances of the selected applications. In reference to all criteria as listed in Table 4.5, it is clear that Leguerre-SVD PMOR method demonstrated significantly better performance in all cases. Therefore, this method can be recommended as the best for the specified criteria and for the selected applications under consideration. However, depending on the characteristics of a given application, the optimization technique and SPARE method may exhibit comparable performance. Moreover, as is clearly seen from Table 4.5, the moment matching method cannot be recommended for most applications because this method is not passive and is not accurate for practical usage.

In terms of computational cost, the performances of all the methods are quite similar except the SPARE method that demonstrated higher computational cost. The reason for this higher computational cost arises from the augmented matrices that can grow in size as the number of parameters increases and the increased number of sensitivity terms included in Taylor series as the complexity increases. However, it should be noted that this method is the only technique that is scalable and preserves the structure of the system. In addition, SPARE consumes more computational resources because the order of the reduced system depends on the number of sampled frequencies considered during the computation of the augmented projection matrix. The number of samples may increase substantially when the variation of the response of the system is not smooth. A possible improvement of this algorithm would be the use of an efficient sampling technique that determines the minimum number of samples, while capturing the samples corresponding to sharper variation in the responses. This may reduce the order of the reduced model significantly. A further area of improvement for this algorithm would be the possible introduction of sparsity in the augmented matrices by removing the sensitivity terms that contribute less to the overall system response.

In terms of accuracy, there were notable differences between the methods that were considered. The Laguerre-SVD based method provided the best accuracy overall. All methods based on Taylor series expansion exhibited inaccuracies that increased with increasing frequencies. Moreover, the sensitivity information required for Taylor-series based methods often used approximate closed-form expressions for the parameter dependence. This could be an additional source of error. Multipoint expansions can be used to mitigate the accuracy issues related to Taylor-series based methods. However, the CPU cost, in this case, may not be practical. Accuracy of the optimization-based technique depends on the effectiveness of the

error minimization technique and different techniques can be used instead of the suggested method to obtain better results.

All the techniques that were compared produced passive models by construction except the multi-parameter moment matching method. In terms of ill-conditioning both Leguerre-SVD and SPARE utilize Krylov subspace projection technique that ensures the construction of a well-conditioned system. However, it was observed that when large orders were used with SPARE, ill-conditioning did occur and this fact should be taken into consideration when choosing this technique for an application. The optimization based technique did not present any ill-conditioning issues while the multi-parameter moment matching technique exhibited several ill-conditioning issues for high orders.

4.7 Recommendations for Users of PMOR Techniques

As is evident from the comparison and analysis presented in the previous section, the Laguerre-SVD method was the best method in terms of overall performance and clearly seems to be the method of choice for several applications. The optimization-based technique also fared reasonably well and can be recommended for a wide variety of applications. However, it should be borne in mind that this technique is heavily dependent on the effectiveness of the error minimization technique. This technique is also a good choice when the number of parameters is high. The SPARE method can be recommended when the response of the system is smooth. The multi-parameter moment matching technique proved to be applicable only for simple systems with few parameters for relatively low frequencies of operation.

Chapter 5

CONCLUSIONS AND FUTURE WORK

5.1 Conclusions

In this thesis, several contemporary PMOR techniques are analyzed using common interconnect applications in order to characterize how they compare against each other. For this purpose, a set of criteria and metrics are established to measure the performance of each method. Each method is characterized individually and then all the methods are compared based on the metrics. During this analysis, the scopes and limitations of each method are investigated. Based on this comprehensive comparative study, some recommendations are presented for the consideration of users of PMOR techniques.

5.2 Future Work

- The study presented in this thesis was performed on systems that are relatively small. For complex applications, the size of the system might be relatively large and it would be an interesting effort to perform a similar analysis to that presented in this thesis to find out if other factors, such as time to construct the model become important from a computational point of view. Such an effort could either corroborate with the findings in this thesis or highlight the need to refine the comparative analysis further based on new information.
- The characteristics of some methods, such as interpolation, error minimization and curve fitting techniques are functions of complexities of large practical systems. The PMOR methods considered in this thesis can be implemented using a wide variety of techniques for interpolation, error minimization and curve fitting. Choosing different methods for each

of these techniques alters the performance of the particular PMOR method under consideration. An effort could be made to include the best choice of techniques to implement each PMOR method and perform the comparison of all PMOR methods. Moreover, the highest frequency of interest could be raised much further to include state-of-the-art applications that are currently under consideration in the research community. The inclusion of these issues may significantly affect the evaluation of different PMOR techniques.

- Some of the PMOR techniques considered in this thesis use Taylor based expansions and this has been a considerable limitation in regards to their performance. An alternative and more robust expansion, such as Padé, could be used instead of Taylor series in order to improve the performance of these methods. It should be noted that the alternative expansion should be compatible with model order reduction techniques. This would involve considerable theoretical work and might lead to more efficient PMOR techniques than what are currently available.

Bibliography

[1] L. T. Pillage and R. A. Rohrer, “Asymptotic waveform evaluation for timing analysis,” IEEE Trans. Computer-Aided Design, vol. 9, pp. 352–366, Apr. 1990.

[2] P. Feldmann and R.W. Freund, “Efficient linear circuit analysis by Padé approximation via the Lanczos process,” IEEE Trans. Computer-Aided Design, vol. 14, pp. 639–649, May 1995.

[3] R.W. Freund and P. Feldmann, “The SyMPVL algorithm and its applications to interconnect simulation,” in Numer. Anal. Manuscript. Murray Hill, NJ: Bell Labs., June 1997.

[4] D. L. Boley, “Krylov space methods on state-space control models,” Circuits Syst. Signal Processing, vol. 13, no. 6, pp. 733–758, 1994.

[5] E. Chiprout and M. Nakhla, “Analysis of interconnect networks using complex frequency hopping,” IEEE Trans. Computer-Aided Design, vol. 14, pp. 186–199, Feb. 1995.

[6] A. Odabasioglu, M. Celik, L. T. Pillage, “PRIMA: Passive reduced-order interconnect macromodeling algorithm”, IEEE Trans. Computer-Aided Design, pp. 645-654, Aug. 1998.

[7] F. Ferranti, G. Antonini, T Dhaene, L. Knockaert, A. E. Ruehli, “Physics-Based Passivity-Preserving Parameterized Model Order Reduction for PEEC Circuit Analysis,” IEEE Trans. On Components, Pack. And Manuf. Tech., vol. 1, no. 3, pp. 399–409, Mar. 2011.

[8] P. Gunupudi, R. Khazaka, M. Nakhla, T. Smy, and D. Celo, “Passive parameterized time-domain macromodels for high-speed transmission line networks,” IEEE Trans. Microw. Theory Tech., vol. 51, no. 12, pp. 2347–2354, Dec. 2003.

[9] L. Daniels, O. C. Siong, L. S. Chay, K. H. Lee, J. White, “A multiparameter Moment-Matching Model-Reduction Approach for Generating Geometrically Parameterized Interconnect

Performance Models," IEEE Trans. Computer-Aided Design, vol. 23, no. 5, pp. 678-693, May 2004.

[10] J. F. Villena, L. M. Silveria, "SPARE – a Scalable Algorithm for Passive, Structure Preserving, Parameter-Aware Model Order Reduction," IEEE Trans. Computer-Aided Design of Integrated Circuits and Systems, vol. 29, no. 6, pp. 925-938, May 2010.

[11] Y. Liu, L. T. Pileggi, and A. J. Strojwas, "Model order-reduction of RC(L) interconnect including variational analysis," in IEEE/ACM DAC, 1999, pp. 201–206.

[12] R. Achar, M.S. Nakhla, "Simulation of high-speed interconnects", Proc. of IEEE, pp. 693-728, vol. 89, no. 5, May 2005.

[13] R. Wang and O. Wing, "Transient analysis of dispersive VLSI interconnects terminated in nonlinear loads", IEEE Trans. Computer-Aided Design, vol. 11, pp. 1258-1277, Oct. 1992.

[14] W. T. Beyene and J. E. Schutt-Aine, "Accurate frequency-domain modeling and efficient simulation of high speed packaging interconnects", IEEE Trans. Microwave Theory Tech., pp. 1942-1947, Oct. 1997.

[15] T. L. Quarles, "The SPICE3 implementation guide", Univ. California, Barkleley, Tech. Rep., 1989.

[16] G. Wollenberg and A. Görisch, "Analysis of 3-D interconnect structures with PEEC using SPICE," IEEE Trans. on Electromagnetic Compatibility, vol. 41, no. 4, pp. 412–417, Nov. 1999.

[17] G. Antonini, D. Deschrijver, T. Dhaene, "Broadband Macromodels for Retarded Partial Element Equivalent Circuit (rPEEC) Method", IEEE Trans. on Electromagnetic Compatibility, pp. 35-48, vol. 49, no. 1, 2007.

[18] L. Knockaert and D. De Zutter, "Laguerre-SVD reduced order modeling," IEEE Trans. Microw. Theory Tech., vol. 48, no. 9, pp. 1469–1475, Sep. 2000.

[19] S. Kumashiro, R. A. Rohrer, and A. J. Strojwas, “Asymptotic waveform evaluation for transient analysis of 3-D interconnect structures,” IEEE Trans. Computer-Aided Design, vol. 12, no. 7, pp. 988–996, 1993.

[20] D. Xie and M. Nakhla, “Delay and crosstalk simulation of high speed VLSI interconnects with nonlinear terminations,” IEEE Trans. Computer-Aided Design, pp. 1798–1811, Nov. 1993.

[21] Q. Yu and E. S. Kuh, “Exact moment-matching model of transmission lines and application to interconnect delay estimation,” IEEE Trans. VLSI Syst., pp. 311–322, Jun. 1995.

[22] V. Raghavan, J. E. Bracken, and R. A. Rohrer, “AWESpice: A general tool for accurate and efficient simulation of interconnect problems,” in Proc. ACM/IEEE Design Automation Conf., June 1992, pp. 87–92.

[23] R. Griffith, E. Chiprout, Q. J. Zhang, and M. Nakhla, “A CAD framework for simulation and optimization of high-speed VLSI interconnections,” IEEE Trans. Circuits Syst., vol. 39, pp. 893–906, Nov. 1992.

[24] R. Sanaie, E. Chiprout, M. Nakhla, and Q. J. Zhang, “A fast method for frequency and time domain simulation of high-speed VLSI interconnects,” IEEE Trans. Microwave Theory Tech., vol. 42, pp. 2562–2571, Dec. 1994.

[25] W. C. Elmore, “The transient response of damped linear networks with particular regard to wide-band amplifiers,” J. Appl. Phys., pp. 55–63, Jan. 1948.

[26] J. Rubinstein, P. Penfield, and M. Horowitz, “Signal delay in RC trees,” IEEE Trans. Computer-Aided Design, pp. 202–211, July 1983.

[27] J. H. McCabe, “A formal extension of the Padé table to include two point Padé quotients,” J. Inst. Math. Applicat., vol. 15, pp. 363–372, 1975.

[28] T. Tang and M. Nakhla, “Analysis of high-speed VLSI interconnect using asymptotic waveform evaluation technique,” IEEE Trans. Computer-Aided Design, pp. 2107–2116, Mar. 1992.

[29] A. Odabasioglu, M. Celik, L. T. Pillage, “Practical considerations for passive reduction of RLC circuits”, in Proc. DAC, pp. 214-219, June 1999.

[30] J. R. Phillips, E. Chiprout, and D. D. Ling, “Efficient full-wave electromagnetic analysis via model-order reduction of fast integral transform,” in 33rd ACM/IEEE Design Automation Conf., Las Vegas, Nevada, June 1996, pp. 377-382.

[31] I. M. Elfadel and D. D. Ling, “A block rational Arnoldi algorithm for multiport passive model-order reduction of multiport RLC networks,” in Proc. ICCAD-97, Nov. 1997, pp. 66–71.

[32] L. M. Silviera, M. Kamen, I. Elfadel, and J. White, “A coordinate transformed Arnoldi algorithm for generating guaranteed stable reduced-order models for RLC circuits,” in Tech. Dig. ICCAD, Nov. 1996, pp. 2288–2294.

[33] L. M. Silviera, M. Kamen, and J. White, “Efficient reduced-order modeling of frequency-dependent coupling inductances associated with 3-D interconnect structures,” IEEE Trans. Comp., Packag., Manufact. Technol. A, pp. 283–288, May 1996.

[34] K. J. Kerns and A. T. Yang, “Preservation of passivity during RLC network reduction via split congruence transformations,” IEEE Trans. Computer-Aided Design, pp. 582–591, July 1998.

[35] P. Heydari and M. Pedram, “Model reduction of variable-geometry interconnects using variational spectrally-weighted balanced truncation,” in Proc. Int. Conf. Comput.-Aided Design, Nov. 2001, pp. 586–591.

[36] J. R. Phillips and L. M. Silveria, “Poor man’s TBR: A simple model reduction scheme,” IEEE Trans. Comput.-Aided Design, vol. 24, no. 1, pp. 43–55, Jan. 2005.

[37] Y. Li, Z. Bai, Y. Su, and X. Zeng, “Model order reduction of parameterized interconnect networks via a 2-D Arnoldi process,” IEEE Trans. Comput.-Aided Design, vol. 27, no. 9, pp. 1571–1582, Sep. 2008.

[38] Z. Zhu and J. Phillips, “Random sampling of moment graph: A stochastic krylov-reduction algorithm,” in Proc. Design, Autom. Test Eur. Conf. Exhibition, Apr. 2007, pp. 1502–1507.

[39] J. Phillips, “Variational interconnect analysis via PMTBR,” in Proc. Int. Conf. Comput.-Aided Design, Nov. 2004, pp. 872–879.

[40] A. E. Ruehli and A. C. Cangellaris, “Progress in the methodologies for the electrical modeling of interconnects and electronic packages,” Proc. IEEE, vol. 89, no. 5, pp. 740–771, May 2001.

[41] A. E. Ruehli, “Equivalent circuit models for 3-D multiconductor systems,” IEEE Trans. Microw. Theory Tech., vol. 22, no. 3, pp. 216–221, Mar. 1974.

[42] Xin Li, L. T. Pileggi, “Parameterized Interconnect Order Reduction with Explicit-and-Implicit Multi-Parameter Moment Matching for Inter/Intra-Die Variations,” IEEE, 2005.

[43] R. W. Freund, “Sprim: Structure-preserving reduced-order interconnect macro-modeling,” in Proc. Int. Conf. Comput.-Aided Design, Nov. 2004, pp. 80–87.

[44] H. Yu, L. He, and S. X. D. Tan, “Block structure preserving model order reduction,” in Proc. IEEE Behavioral Modeling Simulation Workshop, Sep. 2005, pp. 1–6.

[45] G. Wollenberg and A. Görisch, “Analysis of 3-D interconnect structures with PEEC using SPICE,” IEEE Trans. Electromagn. Compat., vol. 41, no. 4, pp. 412–417, Nov. 1999.

[46] G. Antonini and A. Orlandi, “A wavelet-based time-domain solution for PEEC circuits,” IEEE Trans. Circuits Syst.-I: Fundam. Theory Appl., vol. 47, no. 11, pp. 1634–1639, Nov. 2000.

[47] A. E. Ruehli, G. Antonini, J. Esch, J. Ekman, A. Mayo, and A. Orlandi, “Non-orthogonal PEEC formulation for time− and frequency-domain EM and circuit modeling,” IEEE Trans. Electromagn. Compat., vol. 45, no. 2, pp. 167–176, May 2003.

[48] G. Antonini, A. E. Ruehli, and C. Yang, “PEEC modeling of dispersive and lossy dielectrics,” IEEE Trans. Adv. Packag., vol. 31, no. 4, pp. 768–782, Nov. 2008.

[49] L. W. Nagel, “SPICE2: A computer program to simulate semiconductor circuits,” Dept. Elect. Eng. Comput. Sci., Univ. California, Berkeley, Tech. Rep. UCB/ERL M520, May 1975.

[50] G. Antonini, A. E. Ruehli, and C. Yang, “PEEC modeling of dispersive and lossy dielectrics,” IEEE Trans. Adv. Packag., vol. 31, no. 4, pp. 768–782, Nov. 2008.

[51] A. E. Ruehli and H. Heeb, “Circuit models for 3-D geometries including dielectrics,” IEEE Trans. Microw. Theory Tech., vol. 40, no. 7, pp. 1507–1516, Jul. 1992.

[52] J. de Geest, T. Dhaene, N. Faché, and D. de Zutter, “Adaptive CAD model building algorithm for general planar microwave structures,” IEEE Trans. Microw. Theory Tech., vol. 47, no. 9, pp. 1801–1809, Sep. 1999.

[53] G. H. Golub and C. F. Van Loan, Matrix Computation. Baltimore, MD: The Johns Hopkins Univ. Press, 1996.

[54] Z. Zhang, I. M. Elfadel, and L. Daniel, “Model Order Reduction of Fully Parameterized Systems by Recursive Least Square Optimization”, IEEE, 2011.

[55] J. R. Phillips, “Projection-based approaches for model reduction of weakly nonlinear, time-varying systems,” IEEE Trans. Computer Aided Design, vol. 22, no. 2, pp. 171–187, Feb. 2003.

[56] K. J. Kerns and A. T. Yang, “Preservation of passivity during RLC network reduction via split congruence transformations,” IEEE Trans. Computer-Aided Design, pp. 582–591, July 1998.

[57] Y. Bi, K. J. Kolk, D. Ioan, and N. Meijs, “Sensitivity computation of interconnect capacitances with respect geometric parameters,” in Proc. IEEE Int. Conf. Electr. Performance Electron Packag., Oct. 2008, pp. 209-212.

[58] T. El-Moselhy, I. Elfadel, and L. Daniel, “A capacitance solver for incremental variation-aware extraction,” in Proc. IEEE/Assoc. Comput. Machinery Int. Conf. Comput.-Aided Design, Nov. 2008, pp. 662-669.

[59] G. Ciuprina, D. loan, D. Niculae, J. F. Villena, P. Flores, and L. Silveria, “Parametric models based on sensitivity analysis for passive components,” Intelligent Computer Techniques in Applied Electromagnetic, Studies in Computational Intelligence, Berlin, Germany, Springer, vol. 119. 2008, pp. 231-239.